UNIVERSITY OF THESSALY

SCHOOL OF ENGINEERING

DEPARTMENT OF MECHANICAL ENGINEERING

Diploma thesis

New generation of batteries: Metal-air batteries

by

EIRINI KALAMPOKA

Supervisor: Prof. Panagiotis Tsiakaras

Submitted to fulfill part of the requirements for the acquirement of the Diploma of Mechanical Engineer

Volos, 2023

ΠΑΝΕΠΙΣΤΗΜΙΟ ΘΕΣΣΑΛΙΑΣ

ΠΟΛΥΤΕΧΝΙΚΗ ΣΧΟΛΗ

ΤΜΗΜΑ ΜΗΧΑΝΟΛΟΓΩΝ ΜΗΧΑΝΙΚΩΝ

Διπλωματική εργασία

Νέα γενιά μπαταριών: Μπαταρίες μετάλλου-αέρα

υπό

ΕΙΡΗΝΗ ΚΑΛΑΜΠΟΚΑ

Επιβλέπων: Καθ. Παναγιώτης Τσιακάρας

Υπεβλήθη για την εκπλήρωση μέρους των απαιτήσεων για την απόκτηση του Διπλώματος Μηχανολόγου Μηχανικού

Βόλος, 2023

Approved by the Members of Examination Committee:

First Examiner (Supervisor)	Dr. Panagiotis Tsiakaras Professor Department of Mechanical Engineering University of Thessaly
Second Examiner	Dr. Angeliki Brouzgou Assistant professor Department of Energy System, Faculty of Technology University of Thessaly
Third Examiner	Dr. Georgios Charalampous Assistant professor Department of Mechanical Engineering University of Thessaly

ACKNOWLEDGEMENTS

First of all, I would like to express my sincere appreciation and gratitude to my supervisor Professor Dr. Panagiotis Tsiakaras for his valuable guidance, for placing his trust and support on me until the completion of the present diploma thesis. His guidance was of the utmost importance and had a great impact in the quality of the thesis. I therefore express to him a heartfelt thank you for the excellent cooperation we had in the preparation of this dissertation, for the valuable time he had to give me important information and explanations on the subject, but also for his willingness and help, which he never hesitated to give to me.

Moreover, I would like to thank the members of the committee Dr. Angeliki Brouzgou, Dr. Georgios Charalampous for dedicating time to read and evaluate my thesis.

Last but not least, I owe a big thank you to my parents, Nikos Kalampokas and Mirsini Agiakatsika, and to my three siblings Konstantina, Maria and Panagiotis for the encouragement and financial support they offered me throughout my studies from school to my graduation from the Department of Mechanical Engineering at the University of Thessaly. They have always been an invaluable support to me, like a beacon that is always there, lit to guide through the storms and stand proud when the sails are unfurled. Their love, their moral encouragement, and their teaching words are more important than any financial support. I dedicate it to them.

Eirini Kalampoka

ΕΥΧΑΡΙΣΤΙΕΣ

Πρώτα από όλα, θα ήθελα να εκφράσω την ειλικρινή μου εκτίμηση και ευγνωμοσύνη στον καθηγητή και επόπτη μου καθηγητή Παναγιώτη Τσιακάρα για την πολύτιμη καθοδήγηση του, την εμπιστοσύνη και την υποστήριξη του μέχρι την ολοκλήρωσης της παρούσας διπλωματικής εργασίας. Η καθοδήγηση του ήταν υψίστης σημασίας και επηρέασε σημαντικά την ποιότητα της διπλωματικής εργασίας. Του εκφράζω λοιπόν, ένα εγκάρδιο ευχαριστώ για την άριστη συνεργασία που είχαμε στα πλαίσια εκπόνησης αυτής της εργασίας, για τον πολύτιμο χρόνο που διέθεσε για να μου δώσει σημαντικά στοιχεία και εξηγήσεις πάνω στο θέμα, αλλά και για την προθυμία του και τη βοήθεια, που ποτέ δε δίστασε να μου δώσει.

Επιπρόσθετα, θα ήθελα να ευχαριστήσω τα μέλη της επιτροπής καθηγητές κα Αγγελική Μπρούζγου και κο Γεώργιο Χαραλάμπους για το χρόνο τους να διαβάσουν και να αξιολογήσουν την διπλωματική μου εργασία.

Τέλος, οφείλω ένα μεγάλο ευχαριστώ στους γονείς μου, Νίκο Καλαμποκά και Μυρσίνη Αγιακάτσικα και στα τρία μου αδέρφια (Κωνσταντίνα, Μαρία και Παναγιώτη) για την ενθάρρυνση και την οικονομική υποστήριξη που μου πρόσφεραν καθ' όλη την διάρκεια των σπουδών μου από το σχολείο μέχρι και την αποφοίτηση μου από το τμήμα των Μηχανολόγων Μηχανικών στο Πολυτεχνείο του Βόλου. Υπήρξαν πάντα ανεκτίμητο στήριγμα για μένα σαν ένα φάρο που είναι πάντα εκεί αναμμένος για να καθοδηγεί στις φουρτούνες και να στέκεται περήφανος όταν ανοίγονται τα πανιά. Η αγάπη τους ,η ηθική τους ενθάρρυνση και τα διδακτικά τους λόγια είναι πιο σημαντικά από κάθε οικονομική υποστήριξη. Τους την αφιερώνω.

Ειρήνη Καλαμποκά

ABSTRACT

The purpose of this dissertation is about to refer at the published research that has already taken place in the scientists' committee and is in connection with the new generation battery, metal-air battery. More specifically, the significance is emphasized, as are the issues that must be solved in order for it to appear on the market.

Pervasive throughout the thesis are the implications of the energy crisis, showing the imperative for readers/consumers to replace the currently widely used lithium-ion battery with a metal-air one.The vast majority of this battery is used in consumer electronics and electrical vehicles. Recently, metal-air battery attracted a paramount attention as it can work in an open-air atmosphere and use not only metal components, as the traditional batteries use, but also the oxygen which exists in the environment. Scientists have found out that the new generation of batteries are metal-air batteries and those are the most promising to replace the lithium-ion battery. Therefore, the first chapter introduces the definition of energy and the phenomenon of the energy crisis today. Then, the second chapter mentions the theoretical background of electrochemical devices, such as the Nernst equation and Faraday's laws, as well as the working principles of some electrochemical devices, such as the fuel cell and the supercapacitor. In the third chapter, some rechargeable and non-rechargeable batteries that exist are analyzed, and in the fourth chapter, the working principle of a metal-air battery is thoroughly analyzed. The next two chapters delve into the non-rechargeable and rechargeable metal-air battery, respectively. In the seventh chapter, the working principle of the well-known lithium-ion battery is examined, and in the eighth it is compared with the metal-air battery. Finally, the ninth chapter presents the progress that has taken place in the cathode and in general in the design of the metal-air battery, the classification of the cell structure, the applications and the technical barriers of the cathode, anode and electrolyte.

Keywords: metal-air batteries, sustainable battery technology, energy storage, non-rechargeable batteries

ΠΕΛΙΛΗΨΗ

Ο σκοπός της παρούσας διπλωματικής εργασίας είναι να αναφερθεί στη δημοσιευμένη έρευνα που έχει ήδη λάβει χώρα στην επιτροπή επιστημόνων και σχετίζονται με τη μπαταρία νέας γενιάς και ειδικά με μπαταρία μετάλλου-αέρα. Πιο συγκεκριμένα, επισημαίνονται η σημαντικότητα αλλά και τα προβλήματα που πρέπει να αντιμετωπιστούν, έτσι ώστε να εμφανιστεί στην αγορά.

Διάχυτη είναι σε όλη την διατριβή είναι οι επιπτώσεις της ενεργειακής κρίσης, δείχνοντας την επιτακτική ανάγκη οι αναγνώστες-καταναλωτές να προβούν στην αλλαγής της μπαταρίας ιόντων λιθίου που έχει σήμερα ευρύτατη εφαρμογή με μια μετάλλου-αέρα. Η συντριπτική πλειοψηφία αυτής της μπαταρίας χρησιμοποιείται σε ηλεκτρονικά είδη ευρείας κατανάλωσης και ηλεκτρικά οχήματα. Πρόσφατα, η μπαταρία μετάλλου-αέρα τράβηξε ύψιστη προσοχή καθώς μπορεί να λειτουργήσει όχι μόνο με μεταλλικά εξαρτήματα, όπως χρησιμοποιούν οι παραδοσιακές μπαταρίες, αλλά με χρήση οξυγόνου που υπάρχει στο περιβάλλον. Οι επιστήμονες ανακάλυψαν ότι η νέα γενιά μπαταριών είναι μπαταρίες μετάλλου-αέρα και είναι οι πιο υποσχόμενες για την αντικατάσταση της μπαταρίας ιόντων λιθίου. Ως εκ τούτου, στο πρώτο κεφάλαιο εισάγονται ο ορισμός της ενέργειας και το φαινόμενο της ενεργειακής κρίσης σήμερα. Στη συνέχεια, στο δεύτερο κεφάλαιο παρατίθεται το θεωρητικό υπόβαθρο των ηλεκτροχημικών συσκευών, όπως η εξίσωση Nernst και οι νόμοι του Faraday, καθώς και η αρχή λειτουργίας κάποιων ηλεκτροχημικών συσκευών όπως η κυψελίδα καυσίμου και ο υπερπυκνωτης. Στο τρίτο κεφάλαιο, αναλύονται μερικές επαναφορτιζόμενες και μη επαναφορτιζόμενες μπαταρίες που υφίστανται και στο τέταρτο κεφάλαιο, αναλύεται διεξοδικά η αρχή λειτουργίας μιας μπαταρίας μετάλλου-αέρα. Τα δυο επόμενα κεφάλαιο εμβαθύνουν στην μη-επαναφορτιζόμενη και επαναφορτιζόμενη μπαταρία μετάλλου-αέρα αντιστοίχως. Στο έβδομο κεφάλαιο, εξετάζεται η αρχή λειτουργίας της ευρέως γνωστής μπαταρίας λιθίου-ιόντος και στο όγδοο συγκρίνεται εκείνη με την μπαταρία μετάλλου-αέρα. Τέλος στον ένατο κεφάλαιο, παρουσιάζεται η πρόοδος που έχει λάβει χώρα στην κάθοδο και γενικότερα στο σχεδιασμό της μπαταρίας μετάλλου-αέρα, η ταξινόμηση της δομής της κυψελίδας, οι εφαρμογές και τα τεχνικά εμπόδια καθόδου, ανόδου και ηλεκτρολύτη.

Λέξεις-κλειδιά: μπαταρίες μετάλλου-αέρα, βιώσιμη τεχνολογία μπαταριών, αποθήκευση ενέργειας, μη επαναφορτιζόμενες μπαταρίες

Contents

List of figures

Acronyms

AABs Al-air Battery

AGE alkaline gel electrolyte

APG αlkyl polyglycolide

CTAB cetyltrimethyl ammonium bromide

EDS energy dispersive X-ray spectroscopy

GDL gas diffusion layer

HER hydrogen evolution reaction

Li-ion lithium-ion

MABs Metal-air batteries

NiMH nickel-metal hydride

NMR nuclear magnetic resonance

PAA polyacrylic acid

PAM polyacrylamide

ORR oxygen reduction reaction

SEI solid electrolyte interphase

CHAPTER 1

Introduction

According to Britannica [**1**], energy, in physics, is the ability for doing a work. It may exist in potential, kinetic, thermal, chemical, nuclear, or other various forms. Energy is one of the most valuable things in the world. It is essential to all living organisms and all process that occur in the whole Earth. Man's life is indissolubly connected with energy. From prehistoric times, with the discovering of fire, until now energy is a commodity which plays a significant role in daily reality and in national economy. Therefore, it is not an overstatement to assume that energy is the heart of economy and technology.

Although the need for energy has risen dramatically as the global economy continues to grow. Greenhouse effect, water and air pollution make the energy generation more demanding. Unfortunately, non-renewable energy supplies such as coal, oil, and natural gas are limited on the planet. Fossil fuels contributed 81% of global energy demand in 2017, while between 7% and 17% of energy consumption worldwide in 2050 is predicted to be spent in overcoming effects of climate change. Significant expansion of electrification in the energy sector, particularly in transportation, is expected to be needed to meet the objective of limiting global temperature increase to 1.5 ◦C compared with pre-industrial levels **[**2]**.** Hence, researchers and politicians are becoming more interested in energy storage as also people become more aware of the environmental consequences of relying on fossil fuels and long-term durability of electricity networks around the world. As a result, new energy gadget development is critical for a sustainable civilization.

The world has never needed so many batteries to power the sustainable technologies of today and tomorrow. As global demand for batteries accelerates as well as renewable energy storage systems and consumer electronic devices, performance requirements, such as increased energy density and autonomy, fast charging, and safety, are rising significantly and are more and more demanding the creation of unique range of innovative materials to successfully power the challenges of energy transition. Tomorrow's demand for battery metals is unlikely to be met by primary mining alone, so the industry needs a new solution. This thesis is referred to the preview of the chargeable and non- rechargeable batteries as a form of a sustainable energy technology.

CHAPTER 2

Theoretical background

In today's world, clean energy technologies, such as energy storage and conversion, play the most significant role in human society's sustainable growth and are becoming the most vital factors in overcoming fossil fuel exhaustion and global pollution. Electrochemical technologies are regarded as the most viable, ecologically beneficial, and long-term clean energy solutions. Electrochemical energy technologies like secondary (or rechargeable) batteries and fuel cells have been created and they are being utilized or will be employed in a variety of critical applications, including transportation, stationary power, and portable/micro power. With increasing demand for these electrochemical energy, devices' energy, and power densities in a variety of new application areas, more research and development are required to overcome challenges such as cost and durability, which are regarded as major barriers to their application and commercialization. In the market, sophisticated electrochemical cells and cell components are easily available to aid us with our high technological skills. Suitable electrolytic cells are commercially available and may be coupled with other essential processing units to build fully integrated and compact batch or continuous production systems. The electrochemical phenomenon is crucial in supplying critical materials and technology that contribute greatly to the area of relevance in national security and human well-being. Furthermore, humans are also bio electrochemical machines that transform sun energy stored in food into muscular power via an electrochemical process [3].

2.1 History

The experiments of Galvani and Volta at the turn of the nineteenth century are mainly connected with the discovery of electrochemical phenomena. In 1791, Luigi Galvani accidently sent a current through the leg of a frog and saw the convulsive reaction. Following investigations with different metal strips proved the galvanic concept. Although there is indirect evidence that Parthian copper-iron cylinders manufactured 2000 years ago were early batteries, the battery is commonly assigned to Alessandro Volta, who built a "pile" of alternating disks of silver and zinc separated by salt-soaked fabric. Volta's investigations, as well as those of Nicholson and Carlisle, who electrolyzed water for the first time in 1800, demonstrated the link between chemical and electrical processes. Faraday's laws, published in 1830, provided quantitative knowledge of the links involving chemical reaction and electrical charge. Around the same time, the notion of electrodeposition was discovered. Even though the fuel cell is commonly associated with space-age technology, it was developed over 150 years ago. Sir David Grove created the first fuel cell out of platinum strips immersed in "acidulated water," and he is also recognized for initiating the first fuel-cell testing program: "A shock was provided which could be felt by five people

joining hands, and which was severe if received by a single person." Due to the high cost of hydrogen, the early fuel cells were unable to compete with batteries, and commercial development was halted. Many innovative fuel-cell technologies have since been developed, but serious development efforts began only with the thrust of the space program. The development of fuel cells for terrestrial applications is still in its early stages [4,5].

Many essential processes and electrochemical devices that are still in use today were developed in the second half of the nineteenth century. Electrochemical methods for generating aluminum and chlorine were developed and quickly came to dominate both sectors. During this time, the common zinc battery, the dry cell, and the lead-acid battery were all invented.

In the 1920s, significant efforts to quantify the design of electrochemical processes started. To describe an electrodeposit's homogeneity, the term "throwing power" was developed. The 1940s saw the development of techniques for modeling the range of reaction rates (current distribution) on an electrode surface. The mathematical resemblance between the equations defining the current distribution and those employed in the domains of electrostatics, hydrodynamics, and heat conduction was noticed by a number of researchers. Subsequently, applicable solutions were converted into electrochemical analogs. A vast class of problems had their approximate solutions provided by these early simulations, although electrode kinetics and mass transfer effects were not strictly taken into consideration. Early on, organizations led by Norbert Ibl in Switzerland and Charles Tobias in the United States developed novel methods for analyzing and measuring electrochemical processes. This was the beginning of the formal synthesis of electrochemistry with engineering principles, which started in the 1950s. In generalized design equations, the impacts of hydrodynamics, gas evolution, and electrode shape were precisely quantified. Nowadays, sophisticated electrochemical process models are accessible and computer simulation may be used to find solutions to practical issues [6,7].

2.2 Fundamentals in electrochemical science: Electrochemical thermodynamics and kinetics

An electrochemical cell is made up of two electrodes and an electrolyte through which ions are carried. To ensure the charge transfer process's continuation, the electrodes must be able to carry electrons across an external circuit. Figure 1 depicts a schematic diagram for a Li-ion battery. In this instance, electrical energy is applied to the electrodes. An electrolytic cell is a driven device, whereas a galvanic cell produces energy. Under steady-state circumstances, chemical species are separated into one electrode (cathode) and oxidized at the other (anode). A short-circuited galvanic cell can be used to mimic corrosion processes. In corroding systems, an electrode (typically a metal) is oxidized, but no useful work is generated [8].

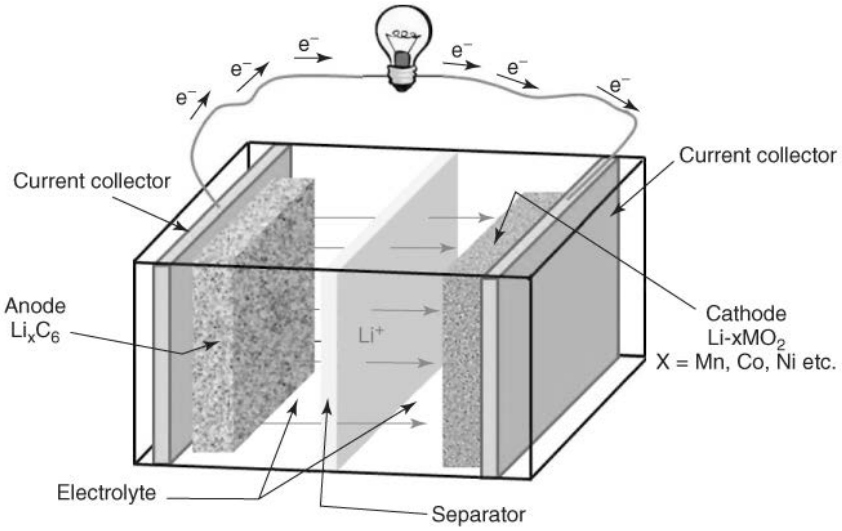

Figure 1 Schematic diagram representing Li-ion battery. Ions in the electrolyte and electrons in the external circuit carry charge, from [8].

When a passage of free electrons is formed and is continually travelling, an electric circuit is produced. "Current" is the continuous flow of free electrons via a conductor in a circuit. It is frequently described as a flow, like the movement of a liquid through a hollow pipe. Voltage is the driving force behind the movement of electrons within a circuit. A specific measurement of potential energy, called voltage, is always relative to two other places. When we talk about a circuit having a given level of voltage, we are measuring the amount of potential energy needed to transfer electrons from one location in the circuit to another. Voltage has no significance until two specific points are mentioned. In the case of a straightforward electric circuit, Ohm's law relates resistance (R), voltage (V), and current (I) (V=IR) [8].

2.2.1 Faraday's law

Faraday's principles are used in electrochemical systems where electrochemical changes take place at the surface of electrodes. Faraday's equations of electrolysis are numerical correlations based on electrochemical studies by Michael Faraday that were published in 1834.

1. According to Faraday's first law of electrolysis, the mass of a material changed at an electrode during electrolysis is exactly proportional to the amount of electricity transmitted at that electrode. An electrical charge is referred to as an "amount of electricity," and it is commonly measured in coulombs.
2. According to Faraday's second law of electrolysis states that the mass of an elemental material transformed at an electrode is precisely proportional to the element's equivalent weight for a given amount of power (electric charge). A substance's equivalent weight is calculated by dividing its molar mass by an integer that relies on the reaction the substance underwent.

Faraday's laws [1, 2] may be expressed mathematically as:

$$m = (\frac{Q}{F})(\frac{M}{z}) \quad (1)$$

where M is the material's molar mass, m is the mass of the substance in grams freed at the electrode, Q is the total electric charge carried through the substance, F is the Faraday constant (96 485 C mol^{-1}), and z is the number of electrons transmitted per ion (the valency number of ions of the substance).

In basic cases of constant current electrolysis, Q = I × t. Therefore, $m = (\frac{Ix\,t}{F})(\frac{M}{z})$ and with the combination of the number of moles (n=$\frac{m}{M}$). Finally,

$$n = (\frac{Ix\,t}{F})(\frac{1}{z}) \quad (2)$$

In the more sophisticated scenario of fluctuating electrical current, the total charge Q is the integrated electric current I(τ) across time: $Q = \int_0^t Id\tau$

It should be noted that the current here is a function of time, whereas t is the total electrolysis time. It is crucial to remember that transitory currents might cause deviations from Faraday's laws. This is true when charge is used in addition to electro reactions, which accumulate near interfaces Non faradaic transient currents are another name for such transient currents [8].

2.2.2 The Nernst Equation

Alessandro Volta invented the voltaic cell in 1799, which was the first electrochemical cell made up of two metal discs – zinc and copper – called electrodes and linked by cardboard soaked in sulfuric acid or saltwater brine as an electrolyte. Those were the first storage and electrochemical energy conversion experiments, and numerous others on batteries and fuel cells are now being developed. In 1836, John Frederic Daniell created a galvanic cell with two distinct compartments (called half-cells) where semi-reactions, oxidation (in the anode) and reduction occur (in the cathode). The anode and cathode are made up of two metallic plates, zinc in a zinc sulfate solution (1.0 mol L^{-1}) and copper in a copper sulfate solution (1.0 mol L^{-1}). An ionic conductor known as a salt bridge connects these two chambers. Figure 2 shows a schematic illustration of the Daniell galvanic cell, followed by the halves and total reactions that occur in the cell.

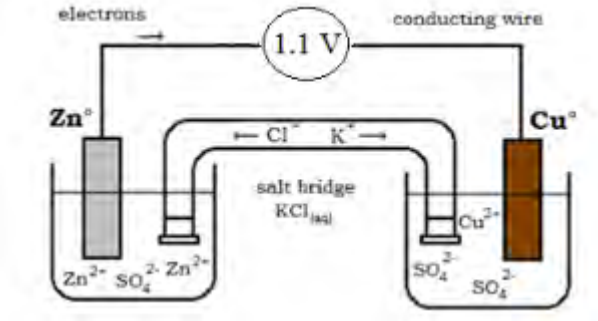

Figure 2 Schematic representation of Daniell galvanic cell, from [9].

Anode semi-reaction $Zn^0 \rightarrow Zn^{2+} + 2e^-$ $E^0 = 0{,}76V$ (3)

Cathodic semi-reaction $Cu^{2+} + 2e^- \rightarrow Cu^0$ $E^0 = 0{,}34V$ (4)

Overall reaction $Zn^0 + Cu^{2+} \rightarrow Zn^{2+} + Cu^0$ $E^0 = 1{,}10V$ (5)

The electrodes' standard potential (E°) values are as follows: At 25 °C and 1 atm pressure, copper (couple (Cu^{2+}/Cu)) reduction = 0.34 V and zinc (couple (Zn^{2+}/Zn)) reduction = 0.76 V, both relative to hydrogen potential.

Boulabiar et al. (2004) reported on a historical review of the Daniell cell teaching, and George F. Martins did a lengthy explanation of why it works (1990). Buckbee et al. (1969) explored the temperature dependency of the Daniel cell's standard cell potential, E°; they discovered that E° dropped as the temperature climbed and devised a quadratic equation that demonstrated E changed as a function of temperature.

The cell potential represents the electrical work that the cell is capable of performing. The temperature dependency of cell potential is also applied to other galvanic cells, such as Li-ion batteries and nickel-metal hydride batteries as described by Li et al. for Na-FeCl_2 ZEBRA advanced Battery. Furthermore, Austin et al. (2018) conducted research on the density function theory (DFT), the precision of which permitted the extraction of energy from a zinc/copper voltaic cell and the Daniell cell. Because the entire electrochemical system exhibits spontaneous and exothermic reactions, the system heats up while functioning [9].

Walther Hermann Nernst (1864–1941), a German chemist, have worked in numerous scientific fields including physical chemistry, solid state physics, photochemistry, solution theory, and the relationship between thermodynamics and electrochemistry, which includes the Nernst equation, which he discovered in 1887. His research in theoretical and experimental disciplines, as well as the development of the Nernst heat theorem, known as the third law of thermodynamics, all contributed to the creation of modern physical chemistry. In 1920, he was given the Nobel Prize in Chemistry, marking over a century in this year of 2023. The Nernst equation has various applications, including oxidation-reduction titration, pH dependency redox couple determination, and calculation of equilibrium constants, among others [9].

At the universities of Zurich, Berlin, and Graz, W.H. Nernst learned mathematics and physics under Ludwig Boltzmann and Albert von Ettinghausen. Later, at Würzburg (1887), he earned his Ph.D. under the supervision of physicist Friedrich Kohlrausch. After working in Leipzig for a while, he became a professor of physics and chemistry at the universities of Göttingen (1891-1905), where he founded the Institute of Chemistry, Physics, and Electrochemistry (1895), and Berlin, where he was also the director of the Physical-technical Institute of Physical Chemistry (1905-1925). He was named President of the Institute of Berlin-Charlottenburg (1922-1933), and from then on, he concentrated on acoustics and astrophysics research [7].

W.H. Nernst discovered an equation that connects the electromotive force of an electrochemical cell (electrode potential) to solution concentrations and temperature. In summary, the electrochemical cell potential is governed by cathodic and anodic electrodes, where each reduction semi reaction and

oxidation semi reaction occur, as stated in equations 3 and 4, and on the global electrochemical reaction, as shown in equation 5. For reversible transformation, the maximum electrical work (We) is equal to the Gibbs free energy change (G), or We,max = G. The following relationship yields the standard free energy change, ΔG°, and the G of any reaction:

$$\Delta G = \Delta G^0 + RT \ln Q \quad (6)$$

where, Q is the reaction's law of mass action The galvanic cell also requires a natural global electrochemical reaction for a redox reaction. Therefore, the thermodynamic variation of Gibbs (G) is negative for a positive cell potential, as described by equation 7:

$$\Delta G = -nFE; \; G^0 = -nFE^0 \quad (7)$$

where, E° denotes the standard cell potential and E denotes the cell potential for an electrochemical system; F denotes the Faraday constant, F = 96485 C mol^{-1}; and n denotes the number of electrons transported in mol. From equations (6) and (7) :

$$-nFE = -nFE^0 - RT \ln Q \quad (8)$$

This equation can be modified to get the Nernst (9):

$$E = E^0 - \frac{RT}{nF} \ln Q \quad (9)$$

The universal gas constant is R = 8.314 J $mol^{-1}K^{-1}$; the Faraday constant is F = 96485 C mol^{-1}; n is the number of electrons exchanged in mol; T is the absolute Kelvin scale temperature (T = 298.15 K); and Q is the reaction quotient.

The Nernst equation is a quantitative relationship that allows the calculation of the cell potential, E, in various ion concentrations of a unit; thus, the cell potential can be easily calculated by the Nernst equation and applied to a Daniell galvanic cell at 25 ºC; additionally, the Daniell cell potential is E=E° at standard conditions, i.e., ions in unitary concentration, because the second part of the Nernst equation becomes zero. Furthermore, thermodynamic functions may be acquired through electrochemical experiments [10].

2.2.3 Kinetics

The intrinsic electrode kinetics or mass transport processes regulate the pace at which an electrochemical process proceeds. If reactants are abundantly accessible at an electrode surface, mass-transport restrictions do not dictate the overall rate; we will analyze this scenario in this section, where slow kinetics drives the rate.

Many ideas in conventional chemical kinetics have analogs in electrode kinetics. The reactants, including both sorts of systems, must overcome energy barriers in order to produce products, and raising the temperature increases the possibility that this obstacle can be overcome. The significant distinction in electrochemical systems is that the reaction rate can be increased by raising the potential difference at the electrode surface. Indeed, one important benefit of electrochemical processes is that a 1 V rise in

overpotential may boost the reaction rate by a factor of 10^8. A temperature rise of several hundred degrees centigrade is required in a typical chemical reaction to achieve an equal change.

The potential difference created across a layer directly near the electrode surface influences electrode kinetics. As the electrode is polarized, charges accumulate on its surface, and a comparable charge distribution of the opposite sign accumulates in the solution approximately 10 A from the electrode surface. The double layer refers to these two distinct charge zones. Helmholtz's original idea for the double layer, suggested in 1879, was a parallel-plate capacitor. Because the distance between the parallel layers of charge is so short, even a slight potential difference of 100 mV across the double layer results in a massive electric field intensity of more than 10^6 V cm^{-1}. Although more precise models of the double layer have been developed since then, the overall notion of electrode kinetics being impacted by the strong field near to the electrode surface remains relevant [6,10].

A net current flowing through an electrode indicates that the electrode is no longer in equilibrium and that there is some over potential at the electrode-electrolyte interface. Because the over potential represents a source of heat generation as well as a source of energy loss, a quantitative model of the link between current density and over potential is necessary in design calculations. Unfortunately, mechanistic investigations into the current-over potential connection would follow from a thorough understanding of the electrode reaction mechanism; unfortunately, mechanistic investigations are difficult even for the simplest reactions. Furthermore, electrode surface preparation, microstructure, contamination, and other variables all have a major effect on kinetic measurements. As a result, a current-over potential relationship is often obtained experimentally, and the data is frequently fitted to conventional models [6,10].

The Butler-Volmer equation represents a rather generic model.

$$\frac{i}{i_0} = exp(\frac{a_a F}{RT} n_s) - \exp(-\frac{a_c F}{RT} n_s) \quad (10)$$

where i_0 denotes the exchange current density, a_α the anodic transfer coefficient, and a_c the cathodic transfer coefficient Experiment data may be used to calculate the exchange-current density and transfer coefficients. Transfer coefficients generally vary between 0.2 and 2; exchange-current density varies greatly, ranging between 10^{-14} and 10^{-1} A cm^{-2}. For near-room temperature copper deposition from aqueous electrolyte, i_0 = 0.001 A cm^{-2}, a_c= 0.5, and a_α = 1.5, and the Butler-Volmer equation becomes

$$\frac{i}{10^{-3}} = exp(58.06 n_s) - \exp(-19.35 n_s) \quad (11)$$

Figure 3 depicts a plot of this relationship. The curve is not symmetric at the origin because the transfer coefficients are not equal. Most industrial processes operate at current densities of more than 50 mA cm^{-2}. The overpotential is rather large in this range, and one of the variables in the Butler-Volmer equation can be ignored. The anodic overpotential is often positive, while the cathodic over potential is

typically negative. If the anodic over potential is large, the second part in the Butler-Volmer equation can be ignored:

$$\frac{i}{i_0} = exp(\frac{a_a F}{RT} n_s) \qquad \text{or} \qquad n_s = \frac{RT}{a_a F} \ln \frac{i}{i_0}$$

Express using common logarithms:

$$n_s = 2.3 \frac{RT}{a_a F} \log \frac{i}{i_0} \tag{12}$$

This is known as the Tafel equation, and it is frequently used in design applications. The pre-logarithmic term is on the order of 100 mV (that is, the over potential increases by 100 mV for every factor of ten increments in current density).

Typically, the exponential components in the Butler-Volmer equation are tiny and linearizable, resulting in

$$i = \frac{(a_a + a_c) i_0 F n_s}{RT} \tag{13}$$

While not technically valid at large current densities, the linear approximation is widely used as an engineering estimation. If the fluctuations in current density in a cell are minimal, this technique is justifiable.

Because the exchange-current density ranges so widely, its value is used to assess the slowness of reaction kinetics. An electrode system with a high exchange-current density is regarded as reversible, whereas one with a low exchange-current density is deemed irreversible. Table 1 contains typical values. Figure 4 depicts the importance of exchange-current density in determining surface over potential. When the exchange-current density is 10^{-3} A cm^{-2} and the current density is 100 mA cm^{-2}, the surface overpotential is 500 mV and 1500 mV when $i_0 = 10^{-12}$ A cm^{-2}, respectively. This finding is extremely significant for electrochemical energy conversion devices. According to Table 1, most hydrocarbon oxidations and oxygen reductions are rather irreversible. In general, noble metal surfaces have the maximum exchange-current density. Because these reactions are irreversible, no viable system for producing energy by direct electrochemical oxidation of hydrocarbons has been developed [6,10].

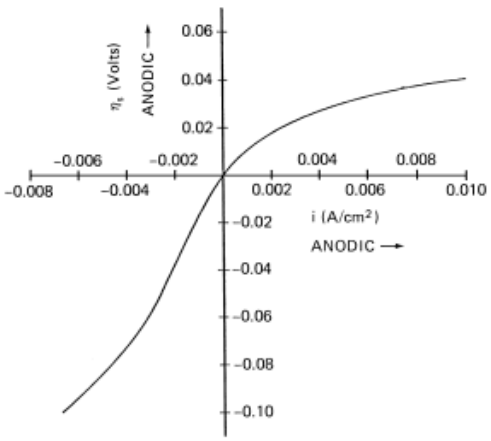

Figure 3 Current density–over potential curve for the Cu/CuSO4 system at 25◦C. The exchange-current density is 0.001 A cm^{-2}, αa = 1.5, and αc = 0.5 from [6].

Table 1 Approximate Values of Exchange-Current Densities, from [6].

Reaction	Electrode material	Temperature (ºC)	i_0
Copper deposition	Cu	25	10^{-3}
Ethylene oxidation	Pt	80	10^{-13}
Oxygen reduction	Au	25	10^{-12}
Hydrogen oxidation	Hg	25	10^{-13}

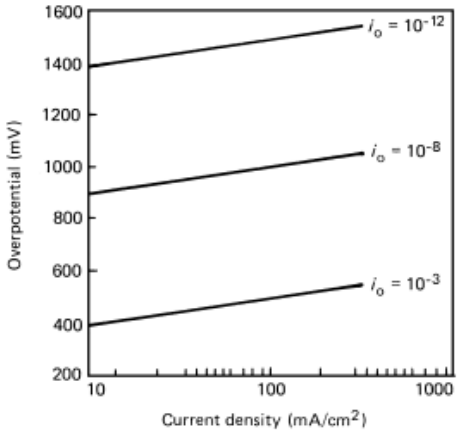

Figure 4 When the Tafel slope is 100 mV/decade, the over potential versus current density is shown. At a given current density, low exchange-current density causes large increases in over potential, from [6].

2.3 Electrochemical devices for energy conversion and storage

The need to free modern society from its reliance on fossil fuels is made more pressing by the growing human population; global warming caused by the combustion of fossil fuels; the rising cost of extraction and distribution of fossil fuels; and an uneven distribution of finite fossil-fuel stores, which continues to lead to conflict between and within nations. Wind and solar energy are ubiquitous and can be transformed locally into electrical energy, but they are diffuse and changeable across daily and seasonal time scales; the electrical energy from these sources must be focused and stored for use on diurnal and seasonal time scales of energy demand. Nature stores solar energy in the form of hydropower and biomass; our concern is to concentrate the electrical energy obtained from solar and wind energy into both portable and stationary stored energy that is efficiently and rapidly capable of converting back into electrical energy without polluting the environment.

Energy is most readily stored as chemical energy; fossil fuels reflect the long-term storage of solar energy as chemical energy. Combustion converts fossil-fuel energy into heat, resulting in harmful gas emissions. On the other hand, electrochemical technologies enable the conversion of electrical and chemical energy on a minute or less time scale, without the release of any hazardous gases, and may even be more efficient than a heat engine. The current objective is to develop an electrochemical technology capable of securely storing and recovering electrical energy at a rate and cost competitive with the efficiency of well-established fossil-fuel systems [11].

Rechargeable batteries, fuel cells, and supercapacitors are electrochemical devices that have been at the forefront of contemporary research into creating efficient, eco-friendly technologies. As we have

mentioned, an electrochemical cell consists of two halves, one of which includes the oxidation half-reaction and the other the reduction half-reaction. The functioning of an electrochemical cell is straightforward and consistent across all electrochemical devices. The anode undergoes oxidation, which produces electrons and ions. Electrons go across an external circuit and collide with ions on the cathode side, where the reduction reaction takes place. Typically, the reduction reaction is the process's rate-limiting step. Electron mobility generates the desired electrical voltage (electric energy) [12].

Basic quantities required for characterization, operation, and comparison of various electrochemical devices, as well as parameters needed to evaluate and investigate the electrochemical devices, are discussed below.

The energy density of an electrochemical devise is the amount of energy it holds in relation to its weight. Watt-hour per kilogram (Wh kg^{-1}) is the most common unit of measurement. A watt-hour is a unit of electrical energy that is equal to one watt used for one hour. Power density, rather than storage capacity, is a measure of how rapidly energy can be delivered. Because energy density and power density are frequently mistaken, it is critical to grasp the distinction between the two [3]. For example, a high energy density battery has a longer battery lifetime in comparison to its size. A high energy density battery, on the other hand, may offer the same amount of energy in a smaller footprint than a low energy density battery. This considerably broadens the range of battery uses. Forklift batteries may weigh hundreds of pounds in an industrial or warehouse setting. A lightweight battery for trucks has several advantages in terms of safety and handling. If a battery's energy density is too high, it may pose a safety risk. The probability of a thermal event grows as more active material is packed into a cell [13].

The total quantity of energy in a system per unit volume is described as energy density [13]. Specifically, energy density is the amount of energy that can be condensed in a device in relation to its mass (Wh kg^{-1}) or volume (Wh L^{-1}) and can be estimated from the potential and capacitance of the electrochemical device [14]. A high energy density electrochemical device can store energy in a smaller amount of mass, resulting in lower cost, more flexible electrochemical devices, and extremely low battery weight of batteries.

The Coulomb efficiency is commonly used to define the released capacity of a battery. It is the ratio between the discharge capacity after a full charge and the charging capacity of the same cycle. It is often a bit less than one. The discharge efficiency of the battery is impacted by electrolyte breakdown, material aging, ambient temperature, and varying charge-discharge current rates [15]. Cycle life is the number of charges and discharges that an electrochemical device can withstand before reaching a particular limit, which is often fixed at 80% of its initial capacity. The life cycles of a device are affected by the depth to which the discharge occurs (depth of discharge, DOD), as a greater depth of discharge reduces life cycles, the pace at which charging and discharging occurs, and the temperature at which the device functions. The proportion of battery capacity that has been discharged (DOD%) is given in maximum capacity [16].

When describing batteries, discharge current is sometimes represented as a C-rate to normalize versus battery capacity, which can vary greatly amongst batteries. A C-rate is a measure of how quickly a battery is depleted in comparison to its maximum capacity. A 1C rate indicates that the discharge current will completely deplete the battery in one hour. This amounts to a discharge current of 100 amps for a battery having a capacity of 100 amp-hours. This battery's 5C rate is 500 amps, while its C/2 rate is 50 amps. An E-rate, on the other hand, describes the discharge power. A 1E rate is the discharge power required to completely drain a battery in one hour [16].

2.3.1 Fuel cells

Fuel cells are electrochemical devices that use redox reactions to transform the chemical energy of the fuel into electrical energy. In its most basic form, a fuel cell consists of an electrolyte surrounded by both the anode and cathode electrodes, two porous electrodes, and an external connection for the passage of electrons. An oxidant gas, often air or pure oxygen, is delivered to the cathode, and hydrogen-rich gases, or even pure hydrogen, are given to the anode. The electrolyte separates the anode from the cathode and is made up of different components that impede electron passage. At the cathode, where oxygen is reduced, protons and oxygen are combined with the electrons that are moving through the external circuit to supply electrical energy. This is how H_2O, a reaction's byproduct, is created [17,18]. In **figure 5** a simple fuel cell is shown.

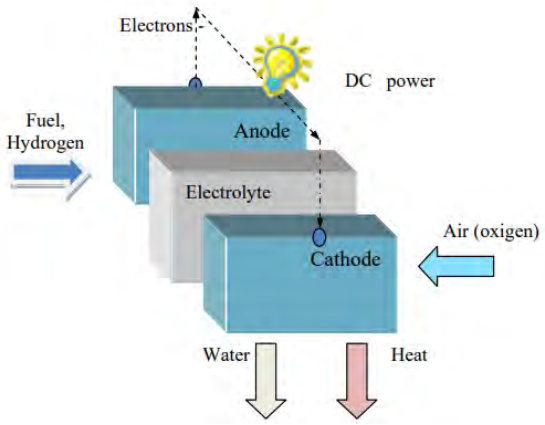

Figure 5 Basic principle of Fuel Cells, from [19].

There are several benefits to fuel cells. Regulations to minimize urban pollution, for instance, have boosted interest in affordable electrical power sources with acceptable dependability, longevity, and performance, with fuel cells receiving more attention for this reason. For automotive applications, proton exchange membrane (PEM) fuel cells in particular are being researched. Additionally, compared to combustion engines, which attain efficiencies ranging from 30% to 40%, fuel cells operate with total efficiencies of up to 60%. There are also fuel cell versions with little to no emissions.

Actually, there are several fuel cell technologies on the market, and each of them is distinguished by its operating temperature range, the fuels it can burn, the kind of catalyst it uses, and its energy conversion

efficiency ratio. The following are the most prevalent technologies on the market (Table 2): Polymeric Electrolyte Membrane Fuel Cells (PEMFC), Direct Methanol Fuel Cells (DMFC), Alkaline Fuel Cells (AFC), Phosphoric Acid Fuel Cell (PAFC), Molten Carbonate Fuel Cell (MCFC), Solid Oxide Fuel Cell (SOFC),

Table 2 The Different types of fuel cells that have been realized and they are currently in use and development, from [19].

	TEMPERATURE (ºC)	ELECTROLYTE	APPLICATION	REALISED POWER
AFC	<100	KOH	Transportation Space, Military Energy storage systems	5-150 kW
PEMFC	60-120	Nafion membrane	Transportation Space, Military Energy storage systems	5-250 kW
DMFC	60-120	Nafion membrane	Transportation Space, Military Energy storage systems	<5 kW
PAFC	160-220	H_3PO_4 immobilizedin SiC matrix	Combined heat and power for decentralized stationary power systems	50kW-11MW
SOFC	800-100	YSZ (yttria stabilized zirconia)	Transportation and stationary decentralized systems using combined heat and power (trains, boats, …)	100-250 kW

Direct alcohol fuel cells (DAFCs) have lately attracted interest and scientific curiosity due to their simplicity and high-power density. However, as DAFCs matured, various challenges with their performance improvement arose, and research for answers is currently ongoing. Low alcohol electro-oxidation kinetics (a), alcohol crossover (b), and electrode delamination (c) are responsible for the short lifespan and poor cell function are as follows [20]:

2.3.2 Electrolyzers

An electrolyzer is a device designed to directly perform electrolysis. A number of simple electrolysis cells are connected to create an electrolyzer. The contact between one metal (an electron conductor or electrode) and one electrolyte is the essential part of an electrolysis cell (an ionic conductor). Electrons cannot reside freely in the electrolyte because they are a highly reactive species. As a result, redox chemical changes occur on the electrolyte side of the interface as a result of the charge (electron) transfer process at the interface, which is powered by an external power source. Face-to-face with the first metal/electrolyte, a second one is offered to collect/supply electrons and balance charges. The electrodes where oxidation and reduction occur are called the anode and cathode, respectively. An electrolysis cell is essentially an electrochemical chain comprised of three separate phases: an anode, an electrolyte, and a second electron conductor. This is the simplest and most common kind of electrolysis cell (cathode). Because it is better suited for the design of large systems, planar geometry is favored over cylindrical geometry in electrolysis technological advancements (which is more frequently encountered in electrochemical generators).

From a thermodynamic perspective, an electrolyzer may be viewed as a mechanism that transforms electrical energy into chemical energy. An "electricity-driven chemical process" is how electrolysis is sometimes described. This indicates that the chemical change is not a natural process [21].However,

because the opposite reaction frequently occurs spontaneously, it is essential to stop the chemical compounds created at the anode and cathode during electrolysis from recombining on their own. Due to chemicals may be quickly transferred from one electrode to the next by diffusion or convection, liquid electrolytes are ineffective separators. Since solids are more effective, a charge-conducting membrane is often added between the anode and the cathode.

The way an electrolyzer works is the exact opposite of how a fuel cell works. In contrast to how oxygen and hydrogen react in fuel cells to create energy and water, electricity is used to break down water into oxygen and hydrogen. Three categories of electrolyzers exist: proton exchange membrane (PEM), alkaline and solid oxide.

PEM

There is no liquid electrolyte in a PEM water electrolysis cell. The following responses occur:

Anode: $H_20 \rightarrow \frac{1}{2}O_2 + 2H^+ + 2e^-$ (14)

Cathode: $2H^+ + 2e^- \rightarrow H_2$ (15)

Overall reaction $H_20 \rightarrow O_2 + H_2$ (16)

Electric current is employed in "SPE-cells" to split liquid water into gaseous oxygen and protons (anodic reaction, Eq. (14). Solvated protons travel to the cathode, where they are decreased into molecular hydrogen and liquid water is discharged (cathodic process, Eq. (15)). (electro-osmosis drag). A thin (0.2 mm thick) membrane of proton-conduction polymer electrolyte separates the anode and cathode. These cells are extremely compact and efficient. Current collectors are constructed of sintered titanium particles arranged in a hexagonal, tightly packed particle lattice.

The PEM water electrolysis technique is an efficient process up to 85% have been recorded at the laboratory scale at 1 A cm^{-2}(derived from the greater heating value of hydrogen). The biggest disadvantage is that this is a costly technology. The replacement of platinum-family catalysts and the high cost of SPE remain difficult concerns. Recent developments have been made at the cathodes of PEM cells [22, 21].

Platinum (Pt)-based materials are widely recognized to be the most effective catalysts for the reaction of hydrogen evolution in both acid and alkaline solutions [23]. Because PEM electrolyzers need an acidic medium, the reaction at the anode of the electrocatalysts is limited to noble metal and noble metal oxide catalysts, which are the most advanced OER electrocatalysts in acidic media. This necessity, however, results in a significant cost for the cell. Currently, efforts are concentrating on Pt-based electrocatalysts, such as alloys created utilizing innovative synthesis processes, Pt combinations with metal oxides, core-shell architectures, and surface-modified Pt/C catalysts to improve CO tolerance and stability [24].

As a liquid electrolyte in alkaline water electrolysis process, an aqueous solution of potassium hydroxide is employed. The following half-cell reactions happen:

Anode $2OH^- \rightarrow H_2O + \frac{1}{2}O_2 + 2e^-$ (17)

Cathode $2H_2O + 2e^- \rightarrow H_2 + 2OH^-$ (18)

Overall reaction $H_2O \rightarrow H_2 + \frac{1}{2}O_2$ (19)

In a traditional alkaline electrolyzer, hydrogen is produced at the cathode and oxygen is produced at the anode. At the cathode of an alkaline cell, water molecules are decreased into molecular hydrogen and hydroxyl ions. Hydroxyl ions are oxidized into molecular oxygen as they travel through the electrolyte to the anode. Alkaline water electrolysis in industry is a developed technique. Several megawatts (MW) industrial electrolyzers (such as those produced by Hydroquebec in Canada or Norsk-Hydro in Norway) can be used to produce hydrogen on a large scale.

The fact that hydrogen from water (ΔH^o = +285 kJmol^{-1}) takes more energy than hydrogen from methane (+160 kJ mol^{-1}) limits applications. Some changes are still conceivable in terms of the procedure. In an attempt to find other electrocatalysts, like transition metal macrocycles [16], and to construct alternative diaphragms have been described in the open literature. The challenges affect the system's lifespan and maintenance expenses.

Electricity is utilized in a high-temperature water electrolysis cell to split water molecules into gaseous hydrogen and oxygen via the half-cell processes listed below:

Anode $O^{2-} \rightarrow \frac{1}{2}O_2 + 2e^-$ (20)

Cathode $H_2O + 2e^- \rightarrow H_2 + O^{2-}$ (21)

Overall reaction $H_2O \rightarrow H_2 + \frac{1}{2}O_2$ (22)

An oxide-ion-conducting ceramic, commonly an yttrium-stabilized ZrO_2 membrane, serves as the electrolyte. Tsiakaras et al. investigated the catalytic and electrocatalytic behavior of the $La_{0.6}Sr_{0.4}Co_{0.8}Fe_{0.2}0_3$ (LSCF) perovskite placed on yttria-stabilized zirconia (YSZ), as well as the oxidative coupling of CH_4 on polycrystalline Ag films coated on YSZ at temperatures ranging from 720 to 850°C [25]. The research of the electrical properties of nano-sized powders at a wide range of temperatures and oxygen partial pressures reveals that the 0.5$Ce_{0.8}Sm_{0.2}O_{2-\delta}$-0.5Ba$Ce_{0.8}Sm_{0.2}O_{3-\delta}$ material has relatively good CO_2 stability, an acceptable total conductivity value, and the lowest contribution of electron conductivity in both oxidizing and reducing atmospheres [26]. Some studies have also been conducted on Ba$Ce_{1-x}Gd_xO_{3-\delta}$ (BCG) type ceramics when impacted by sintering additives such as Cu [27]. The membrane serves a dual purpose in PEM technology. It initially functions as a solid electrolyte, transporting electric charges from one electrode to the other, and then as a separator, preventing reaction and product recombination. The cathodic chamber is filled with water vapor. The main benefits of the high temperature process are (i) lower energy consumption (3 kWh Nm^{-3} H_2 at 900ºC versus 4 kWh Nm^{-3} H_2 at 80ºC) due to a lower G and better kinetics; (ii) lower costs as no electrocatalyst is needed at such temperatures; and (iii) the technique is well suitable for the centralized production of large

amounts of hydrogen using the high temperature heat released by nuclear reactors. On the negative side, the primary downsides include lower cell component lifespan due to high operating temperatures: material deterioration (phase change, reducing ionic conductivity) in connection to temperature and heat cycling, and gas tightness. The components of solid oxide water electrolysis (SOWE) cell are (i) stainless steel bipolar plates and (ii) manganite-coated stabilized zirconia as the solid electrolyte [21].

2.3.3 Electrochemical supercapacitors

Supercapacitors (SCs) offer a high-power density and a long lifespan. Materials and chemistries have advanced, and substantial research has been conducted to overcome supercapacitors management issues. Supercapacitors' potential engineering uses are constantly being investigated. Supercapacitors are critical in sustaining a system's voltage during higher loads in everything from portable equipment to electric automobiles. Supercapacitors are typically made up of two porous electrodes with a large surface area, an electrolyte, and a very thin separator. Electrolytes are either solid-state or organic aqueous in nature, depending on the requirements and application.

An electrolyte containing a combination of positive and negative charge carriers exists between the two plates. When a voltage source is connected, an opposite polarity charge layer is generated on both sides, resulting in an electric double-layer, as seen in Figure 6, giving rise to the name "double layer capacitor." It should be noted that no electrochemical reaction occurs during the discharge/charge. Supercapacitors are classified into three forms based on the process by which the charge is stored: electrochemical double layer capacitors (EDLC, Electric Double Layer Capacitor); Pseudo capacitors; and hybrid supercapacitors [28].

A basic EDLC (Electric Double Layer Capacitor) may be created by immersing two electrodes in an electrolyte (for instance, two carbon rods in salt water). The **figure 6** shows a straightforward schematic representation of the EDLC. After the circuit opens, the trend continues, showing that energy has been saved.

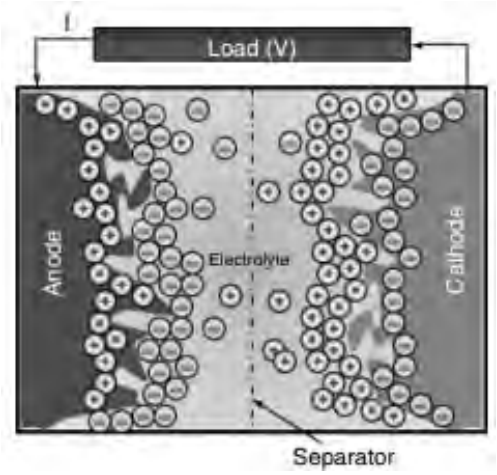

Figure 6 Schematic diagram representing double-layer supercapacitor, from [21].

The greater level of the electrodes is a crucial component that enables such a large capacity. Activated carbon is the electrode material most frequently employed (AC). Also mentioned in the literature as electrode materials for EDLCs are various confinement-based materials such as carbon nanotubes (CNTs) and graphene [29], which have a huge specific surface area and a porous structure.

Pseudo-capacitor devices are made of materials that, owing to thermodynamic considerations, conduct Faradaic oxidation and reduction reactions at specified potentials during charging and discharging [21]. The charge storage method is based on redox processes that occur on or near the electrode's surface and are characterized by high reversibility and rapidity [30]. The charge processes that occur between the electrode and electrolyte might also entail adsorption or intercalation (doping/dedoping) of the electrolyte, depending on the material design and structure. The expansion of the charge created beyond the prescribed potential is characterized by repulsive interactions between these species at the surface or inside the material structure itself, resulting in a broader voltage working window for viable applications. The importance of pseudo capacitive materials is largely recognized by their increased capacitance relative to EDLC (10–100 times the capacitance) due to electron transfer reactions that occur during charging, which contrasts with the electrostatic process defined by a process in which no Faradaic reactions occur [21].

Transition-metal oxides (RuO_2, MnO_2, etc.) and ECP (polyaniline (PANI), polypyrrole (PPy), and poly(3,4-ethylenedioxythiophene) and its derivatives) are the most frequently utilized materials for capacitor use as pseudo-capacitors. Transition-metal oxides have been shown to have large capacitances, with MnO_2 obtaining 698 F g^{-1} via a sol-gel technique and hydrous RuO_2 achieving 600-1000 F g^{-1} . However, the use of transition metals as electrodes is frequently limited due to their low conductivity and electroactive area (MnO_2 irreversibility and dissolution as a negative electrode) . Although RuO_2 performs admirably as a pure electrode material, its high cost and toxicity render it unsuitable for extensive commercial application. ECPs are employed as alternative pseudo capacitive materials since they are cheap and simple to make by in situ oxidation or electro polymerization. Specific capacitance values for PPy, PANI, and poly(3,4-ethylenedioxythiophene) have been reported to range from 150 to 400 , 115 to 420 , and 60 to 250 F g^{-1}. When doped, these materials have a reasonably high capacitance and decent conductivity, but they often have poor stability due to the mechanical stress of swelling and shrinking during doping and dedoping. Because of these disadvantages, pseudo-capacitors are widely combined with carbon materials to compensate for their poor mechanical and electrical characteristics [21].

Since hybrid capacitors combine a carbon electrode with an ECP, metal-oxide composite, or battery electrode, they often use both pseudo capacitive and EDLC processes for charging and discharging. Despite the fact that both of these methods have previously been investigated, the emphasis for these devices is on intercalation within the metal oxide or conducting polymer structure and short diffusion paths for electrolyte

diffusion within the pores of carbon materials . In order to boost the energy storage of electrochemical devices, much work has been put into the design of hybrid capacitors that utilize lithium-ion intercalation through the use of a lithium-ion electrolyte as well as through lithium predoping of the electrode. The latter characteristic has been shown to be especially helpful for high cycle rates that impede ion diffusion and effectively intercalate Li-ions required to produce a capacitive charge. By comparing long and short aligned titania nanotubes, Wang et al. discovered the inverse relationship between tube length and transport capacity. Both the anode and cathode porosities were taken into account to maintain a high-power density for the hybrid capacitor [330].

2.3.4 Ion batteries (Li+, Na+)

2.4.4.1 Lithium-ion battery Li+ (LIBs)

Lithium-ion batteries' main functional elements are anode, cathode, and electrolyte [27]. Instead of using metallic lithium as the anodic substance in a lithium-ion cell, intercalated lithium compounds (Li in porous carbon or graphite) are used. The cathode is made of a layered oxide, such as lithium cobalt oxide, a polyanion, such as lithium iron phosphate, or a spinel, such as lithium manganese oxide. Pure lithium is a highly reactive industrial substance that has a niche use. Lithium hydroxide is created through a strong reaction with water, which also releases hydrogen gas. Nonaqueous electrolytes are therefore necessary for LIBs. As the electrolyte, a typical mixture of non-aqueous organic carbonates, such as ethylene carbonate or diethyl carbonate, is used. This mixture typically contains a complex of lithium ions, such as lithium hexafluorophosphate ($LiPF_6$), lithium hexafluoroarsenate monohydrate (LiAsF_6), lithium perchlorate (LiClO_4), lithium tetrafluoroborate. Lithium ions that travel through the separator diaphragm and nonaqueous electrolyte from the negative electrode to the positive electrode during discharge also migrate back during charging.

Anodic half reaction: $xLi^+ + xe^- + 6C \rightarrow Li_xC_6$ (23)

Cathodic half reaction:$LiCoO_2 \leftrightarrow Li_{1-x}CoO_2 + xLi^+ + xe^-$ (24)

Li-poly batteries are becoming more popular throughout the world in radio-controlled vehicles and aircraft, airsoft guns, PDAs, and laptop computers. Examples include the Apple MacBook family, the Kindle from Amazon, the ThinkPad X300 from Lenovo, the OQO series of palmtops from HP, and Dell products powered by D-Bay batteries [21].

2.4.4.2 Sodium-ion battery Na+ (SIBs)

Lithium-ion batteries have dominated the rechargeable energy industry for the past 20 years (LIBs). The attractiveness of LIBs is made up of their high energy density, extended cycle stability, and well-understood electrochemistry. Due to the high demand for electric, hybrid, and plug-in cars globally, lithium-ion batteries are highly sought-after in the transportation industry [31]. For large-scale storage of

renewable energy, LIBs satisfy the requirements for high conversion efficiency and energy density in the grid energy storage sector [32]. Additionally, the consumer electronics industry is seeing a surge in demand for comparable-sized batteries without sacrificing performance due to rapidly developing advances in smaller and lighter gadgets.

Lithium is unfortunately scarce, which is a problem. The amount of lithium present on Earth is thought to be less than 20 parts per million (ppm). Lithium's availability declines to unsustainable low levels if it is continuously extracted from natural sources. This suggests that in order to satisfy rising customer demand, future LIBs could require supporting technologies. Therefore, it's critical to carefully evaluate the long-term economic, political, and societal effects of this lithium preoccupation over the world.

Due to electrochemical similarities, the sodium ion battery (SIB) has been proposed as an alternative to the LIB. Contrasting lithium, sodium is inexpensive and abundant, with natural sodium being nearly a thousand times more common than lithium. It can also be found in salt water and deposits in the earth's crust. The last ten years have seen a surge in interest in sodium-ion battery development due to these clear advantages [33].

Similar to LIBs, SIBs feature an organic electrolyte, a porous separator, and a cathode-anode electrode pair. Related to the layered lithium metal oxide (LiMO) cathode and carbon anode of LIBs, this pairing in SIBs generally comprises of a layered sodium metal oxide (NaMO) cathode and carbonaceous anode. Both use the same electrolyte, which is a combination of organic solvents and metal salt that has been dissolved (1 M). In order to prevent shorting and encourage isotropic ion transport, the porous separator typically a polymeric barrier provides electrode separation.

Take into account that complete cells, which have a certain combination of cathode and anode material, are what commercial rechargeable batteries are made of. A half-cell, in contrast, replaces the counter electrode with a reservoir of lithium or sodium foil and is used to study the performance of a particular cathode or anode material.

Energy is added to the battery during the charge cycle, which moves electrons from the cathode to the anode. The breakdown of sodium atoms at the cathode into a positive sodium ion and a negative electron causes them to deintercalate from the NaMO structure (26). While negative electrons move via an external circuit, positive sodium ions are driven by an applied electric potential to move through the ionically conductive electrolyte in the direction of the anode. As the ions intercalate the anode's interlayer gap, an electron and a sodium ion combine once more to create a stable sodium atom (26). These processes are reversed upon discharge, resulting in the release of stored energy.

$$Na \rightarrow Na^{+} + e^{-} \quad (25)$$

$$Na^{+} + e^{-} \rightarrow Na \quad (26)$$

The main problem with SIB is sodium's incompatibility with conventional intercalation substances. The sodium cation is significantly heavier (23.00u vs. 6.94u) and has a radius that is 1.02 $\dot{A}$ more than the lithium cation (0.76 $\dot{A}$). The slower sodium diffusion rates with LIB intercalation materials are a result of this physical difference. However, because of weaker solvation shells and a lower charge-to-radius ratio, their enormous size enables a 20% decrease in overall binding energy for sodium cations [34].

However, SIBs have one practical benefit over LIBs: aluminum may be used to manufacture current collectors at a low cost. Cathodes in LIBs are constructed of aluminum, whereas anodes are built of more costly, denser copper. Because sodium cannot alloy with aluminum, aluminum may be used to create anodes in SIBs, reducing or eliminating the possibility of corrosion [34].

2.3.5 Metal batteries

The need for energy has grown dramatically as the world economy continues to expand. The traditional non-renewable energy sources on Earth, such as coal, oil, and natural gas, are unfortunately few. Therefore, the creation of new energy technologies is crucial for a sustainable civilization. Among the best possibilities to address the demand for energy storage are cutting-edge biofuel batteries, supercapacitors, and metal-air batteries. Due to their ability to function in an outside environment, MABs have recently received a lot of attention. Metal anodes and an air cathode make up MABs. The MAB cathode harnesses oxygen from the surrounding air to significantly reduce battery weight, which has unheard-of benefits for many applications. MABs are less expensive than other batteries, notably lithium-ion batteries, which now hold the majority of the market share. This is because the anode can be manufactured from inexpensive metals like Al, Zn, and Fe, and the cathode supply, oxygen from air, is readily available. Theoretical energy density is a key factor in assessing the performance of different battery configurations. MABs are appealing not just as compact power generators for portable electronics and electric vehicles, but as compelling power transfer stations or energy storage devices to handle energy flow among renewable energy generators, like wind turbines and photovoltaic panels, electric grids, and end-users. Since oxygen is used as an oxidant in the cathode during the discharge period and is directly supplied from the atmosphere, MABs have a much greater energy density. Iron-air batteries (FABs) have the lowest theoretical energy density and cell voltage, whereas lithium-air batteries (LABs) have the highest theoretical energy density (5928 Wh kg^{-1}) and highest cell potential (nominally 2.96 V) (nominally 1.28 V). Due to financial and security concerns, research is also focusing on Al, Zn, and Fe-air batteries [35].

CHAPTER 3

Batteries

A battery includes an anode, a cathode, an electrolyte, a separator, and an external case. The primary distinction between battery and fuel cell systems is that fuel cells require fuel from an outside source, whereas batteries, being closed systems, do not. One more difference is the materials employed as electrodes and electrolytes, which influence the system's particular properties. The separators are made of polymeric materials, paper, or paperboard, while the outer shell is composed of steel, polymeric materials, or paperboard. In general, electrodes and electrolytes vary depending on the use of the battery [36].

There are two main kinds of batteries for domestic use: primary cells that are only used once and secondary cells that can be recharged. The most popular main cells are zinc-carbon and alkaline-manganese. Alkaline-manganese batteries are made of a steel case in contact with carbon and MnO_2 as the cathode and a brass rod in contact with powdered zinc as the anode. KOH paste is used as the alkaline electrolyte. A carbon rod in direct interaction with carbon, MnO_2 as the cathode, and a zinc case serving as the anode are the typical components of zinc-carbon batteries. As an electrolyte, NH_4Cl and ZnCl_2 paste is used. A stainless-steel jacket is used to retrieve the zinc electrode from the cylindrical cell, which also typically has a separator made of plastic or paperboard and an asphalt seal.

NiCd, which has been used commercially since 1950, was regarded as one of the most dangerous disposal methods. The anode is commonly made of NiOH, while the electrolyte is a combination of LiOH_2 and KOH [37]. Lithium, on the other hand, includes no hazardous elements and as the lightest of the other metals chosen, has the highest energy content, allowing it to have a high electrochemical potential. However, if the metallic lithium is exposed to moisture as the batteries corrode, there is a risk of fire immersion. To utilize all the metallic lithium content, these batteries must be totally depleted.

G.N. Lewis took the first step toward realizing the potential of Li-ion in 1912, but it wasn't until the early 1970s that the first lithium-ion secondary batteries became commercially available. These batteries used TiS_2 as the cathode and Li metal as the anode [38]. The new rechargeable Li-ion battery hit the market in the 1990s. The technology of lithium-ion batteries is based on the fact that lithium is also the most electropositive metallic element. This battery type has been proven to be stable at over 500 cycles, can be made in many forms and sizes, and requires little maintenance compared to other batteries, while researchers aim to extend cycling life, boost safety, and reduce manufacturing costs. Li-ion batteries are utilized in high-end electronics, have just been introduced to the power tool sector, and are making inroads into the hybrid electric vehicle business, making them a real candidate for powering future electric vehicles [39].

There is a significant difference between primary and secondary lithium batteries when it comes to battery conservation. Primary cells have a cathode made of metallic lithium, whereas rechargeable batteries have a positive electrode made of Li_xMA_2 and a negative electrode made of graphite. $LiCoO_2$, $LiNiO_2$, and $LiMn_2O_4$ are some of the compounds employed at the cathode. An organic liquid containing dissolved molecules such as $LiClO_4$, $LiBF_4$, and $LiPF_6$ can be used as the electrolyte [40].

Nickel metal hydride (NiMH) batteries were created in 1989 and first marketed in Japan in 1990. NiMH batteries offer a high electrochemical capacity and are environmentally friendly. They work well in a wide range of temperatures, from 20 to 60 degrees Celsius, and have a lifespan of 500 to 1000 cycles. The positive electrode is made of a porous Ni plate that is activated with nickel hydroxide. The negative electrodes are made of a hydrogen storage alloy powder, such as Ni-Co or other random metal powder, on a metal-mesh substrate, with an inert insulating layer between them. In most cases, potassium hydroxide is utilized as an electrolyte. NiMH batteries are considered environmentally benign and may be used in many applications in place of NiCd batteries. Although, the production costs, are significantly higher than that of NiCd batteries [41].

Researchers are also very interested in flexible energy-storage devices because of their aesthetic adaptability and ease of integration with electronic gadgets of varied designs. These adaptable portable electronics will be extensively used and have an impact on lifestyles in the future. The accompanying flexible energy storage and conversion systems are needed to maintain an uninterrupted power supply for these flexible electronic goods, given the significant interest in flexible electronics. In recent years, work has been done to meet the aesthetic requirements of flexible electronics by developing high-performance flexible energy storage and conversion systems, such as flexible solar cells, flexible chemical batteries, and flexible supercapacitors. The lithium-ion battery is the most popular and well-known of the numerous kinds of flexible energy storage and conversion systems because of its comparatively high energy density. Even though the battery's performance has significantly increased since Sony debuted its first generation, the energy density is still insufficient to meet the energy needs of cutting-edge electronic devices. It goes without saying that the creation of compact, high-energy-density flexible energy storage and conversion devices is crucial for the advancement of flexible electronics.

Metal-air (metal-oxygen) batteries have been recognized as suitable candidates among the many energies storage and conversion systems because the exhausted material (oxygen) is stored outside the battery. This gives these systems a high energy density, enabling them to satisfy the needs of cutting-edge electronic devices. Metal-air batteries typically function in an open system and are based on the oxygen-reduction reaction (ORR) and oxygen-evolution reaction (OER), as opposed to the intercalation and conversion reactions of commercial lithium-ion batteries. Metal-air batteries can be classified as zinc-air, aluminum-air, lithium-air, potassium-air, sodium-air, and so forth, depending on the type of anode that is utilized. Lithium-air, potassium-air, and sodium-air batteries can work on a high-voltage platform because they are frequently

used in non-aqueous systems due to their severe sensitivity to water. The magnesium, aluminum, zinc, and iron anodes, in contrast to nonaqueous systems, are all compatible with aqueous electrolytes, have energy densities similar to lithium-air batteries, and have also been extensively studied; in this article, we refer to them as aqueous systems. It should be emphasized that in order to stop electrolyte leakage in the aqueous system, a hydrophobic protective layer is also required. Although there are a growing number of polytypes of metal-air batteries, the coin-type and Swagelok designs are the ones that are most frequently explored since they are inflexible and large and cannot take advantage of energy density [162,192,207,285].

Zinc air batteries are a potential battery technology that makes use of the presence of oxygen in the air as an oxidizing agent. As a result, they have a much better energy density than ordinary batteries. Where a solid fuel would ordinarily be required, zinc air batteries utilize the oxygen in the air to significantly reduce the bulk and volume of the battery required. Based on mass energy density, zinc air batteries can achieve two or three times the energy density of lithium-ion batteries now in use. As a result, considerable progress in volumetric energy density may be made, as zinc air batteries have the potential to increase by up to 50%.

Zinc's strong electro-positivity, environmental friendliness, and inexpensive cost make it a good material for energy storage. Zinc air batteries contain two electrodes: one solid zinc electrode that serves as the anode during discharge and one air-breathing electrode that allows air to enter the cell. A separator membrane separates the electrodes to prevent particle transmission from one to the other. The membrane can also be modified to prevent zinc ion and zinc hydroxide transport to the cell's cathode, which can cause short circuiting in cells that cycle often [42].

Among the several forms of batteries, the metal-air battery exhibits exceptional promise. This sort of battery employs oxygen from the surrounding environment as an active material on one of its electrodes. Because the active material does not need to be stored inside the battery, practically the whole area inside the battery may be used for the other electrode's active material. As a result, batteries with air electrodes have a larger capacity, both in terms of weight and volume. However, in order to benefit from the open space, the other electrode materials must fulfill specific conditions. Zinc, aluminum, lithium, and iron are among the promising choices [43].

For a wide range of reasons, aluminum as an anode is desirable. It has a low atomic mass and a high negative standard potential, and it can transport three electrons per atom. These properties result in a high theoretical energy density. Furthermore, there is a high supply of aluminum in nature and a low output of aluminum. The anode in an al-air battery stores 100% of the fuel [44]. It can also be released in saline, which is a solution of sodium chloride in water, as well as acidic and alkaline electrolytes. Al-air systems, on the other hand, offer an advantage over saline systems because of the increased conductivity and solubility of alkaline electrolytes. Aluminum corrodes significantly in alkaline solutions, resulting in fuel loss during standby and coulombic losses during discharge [45].

Li-air batteries are regarded as one of the most essential battery systems, contributing to a variety of applications due to their high theoretical energy densities. Li-air batteries vary from many primary and secondary batteries in that the active ingredients are pure lithium metal as the anode material, and oxygen from the surrounding air is not stored inside the cell but may be taken constantly from the environment. Because the active oxidant is ambient air, Li-air batteries are safer than commercial lithium-ion batteries. For this reason, Li-air batteries have gotten a lot of interest because they have a theoretical specific energy that is 5–10 times higher than traditional rechargeable Li–ion batteries that employ LiMn_2O_4 or LiCoO_2 as the positive electrode [46].

However, low current density, low charge-discharge efficiency, and insufficient cyclability are limiting issues for Li-air battery performance. All of these issues are caused largely by the pore structure of the air electrode and oxygen-li-ion interfacial interactions. In addition to these issues, the discharge li-air reaction is hampered by the insoluble lithium oxide discharge products, which can fill the cathode's active surface area and obstruct the route for other reactive species, blocking further reactions inside the cathode. It should also be highlighted that batteries with cobalt and nickel cathodes pose a health risk and have a severe environmental effect. This is due to the manufacture, processing, and use of these heavy metals, which cause environmental dangers during disposal and, eventually, global warming. To overcome these challenges, researchers are working to create novel components for the li-air cell, like new materials for the positive electrode, electrolyte, and catalyst [47]. However, lithium-air batteries have demonstrated extraordinarily high discharge capacity. Lithium supplies are limited and may run out in the near future. Sodium, in contrast, is the fourth most plentiful element on the planet and hence has the potential to be a lithium substitute. It is a widely available and low-cost element, making it a viable material for energy storage system applications [49]. Because the reaction mechanism of sodium is comparable to that of lithium, it is feasible to swap the anode materials without affecting the system design.

The cathode materials and architecture can have a substantial influence on the battery performance since the discharge products of sodium-air batteries are not soluble in the organic electrolyte but are instead deposited on the electrode similarly to lithium-air batteries [50]. Electrochemical rechargeable batteries or non-rechargeable batteries [51] are energy storage devices that accept electricity generated elsewhere and use it to generate electrochemical reactions at both electrodes before spontaneously releasing this energy downhill. In the commercial market, a variety of rechargeable batteries (including lead-acid, nickel cadmium (Ni-Cd), nickel metal hydride (Ni-MH), zinc-air, liquid redox, lithium ion (Li ion), and lithium-ion polymer batteries) are available (**Figure 7**); they come in various shapes and sizes with varying energy to weight and energy to volume ratios related to stabilize an electrical distribution network and can be utilized several times.

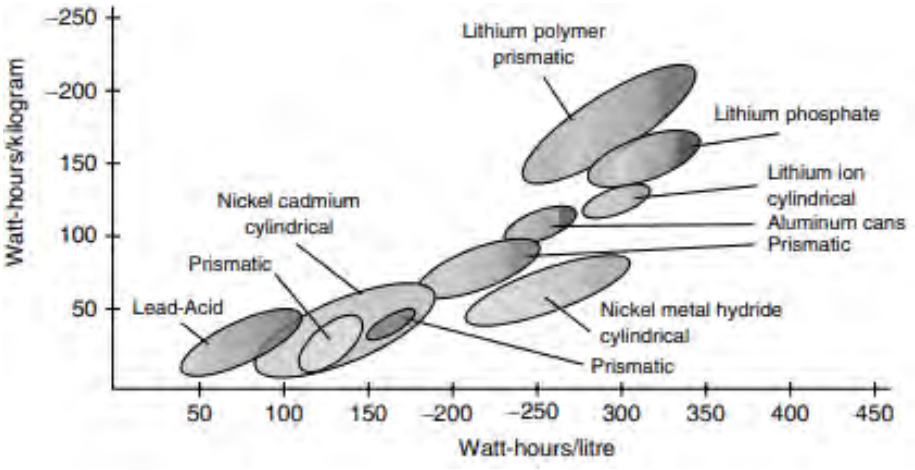

Figure 7. The energy to weight and energy to volume ratios of various battery types are assessed, from [21].

Batteries are effective at delivering high power levels, but they are limited in terms of the amount of energy they can store per unit weight (50–1000 W kg1) compared to fuel cells because they can only use up to 100% of the material on their plates, whereas fuel cells can turn 100% of the chemical fuel available into energy. So, when depth of discharge (DOD) reaches 90%, the majority of today's rechargeable batteries need to be cycled roughly 100 times; nonetheless, batteries that can withstand more than 1000 recharges while achieving a high DOD are also available. Additionally, systems capable of 50,000 recharges are doable at 40% DOD. Depending on how they are used, batteries have a different life cycle. Their use in applications like car starters, portable consumer electronics, light vehicles (like electric wheelchairs, golf carts, electric bikes, and electric forklifts), tools, and providing long-term power to internal artificial organs (heart pacemakers, hearing aids, etc.) has had a revolutionary impact on our way of life. Industrial rechargeable batteries are utilized in grid energy storage facilities for load leveling, where they are used to store electric energy for times of high demand. The technology to extend the lifespan of automobiles by decreasing their cost and weight is being driven by promising applications in hybrid cars and electric vehicles. Although the initial cost of rechargeable batteries is higher than that of disposable primary batteries, their overall cost of use and effect on the environment are less than those of disposable primary batteries, despite the fact that they are classified as pseudo-pollutant contributors due to electricity needed to charge them. Newer low self-discharge batteries maintain their charge for several months and may deliver charges of up to 70% of their stated capacity, in contrast to older rechargeable batteries that must be charged before use. Rechargeable batteries are typically charged using a battery charger that draws power from the AC mains, and charging times range from a few minutes (for quick chargers) to several hours. Rechargeable battery demand has increased due to the fact that it is expanding twice as quickly as that of non-rechargeable batteries. Although there is still no perfect battery, there is a good selection of batteries available for a variety of uses. In this dissertation we will focus on metal-air batteries their challenges and perspectives.

CHAPTER 4

Working principle of metal-air batteries

Scientists and governments are emphasizing more on energy storage. This is mainly occurred because humanity becomes more aware of the environmental consequences of dependency on fossil commodities as well as their reliability and the efficiency of electrical networks around the world. Energy storage can help to resolve the issue of wind and solar intermittent power; in some cases, it can respond quickly to significant demand changes. Energy storage becomes ever more popular. The efficiency of an energy storage facility is characterized by its ability to respond quickly to changes in demand, the total amount of energy that can be stored, and the rate at which energy is lost throughout the storage process [52]. For instance, wind turbines are globally well-known, but it is an erratic and unreliable system because they produce electricity only when it is windy. Therefore, it is hard to sustain a stable supply and demand balance with the renewable energy. So, energy storage is necessary.

Nowadays, the scientist's community provides us with a variety of energy storage devices. There are systems which store energy in different forms such as electrochemical, kinetic, pressure, potential, electromagnetic, chemical, and thermal [53]**.** Some typical examples are fuel cells and batteries. Those devices may also have the ability to increase supply for energy at peak times, including air conditioning, especially at the summertime. It is generally known when power stations are forced to increase productivity to meet power needs during peak hours, electricity prices rise. Storage of energy enhance energy system efficiency by permitting utilities to buy electricity during off-peak hours when energy is less expensive and sell it back to the system when energy demand is higher.

In the group of energy storage devices batteries are separated from the other due to their essential advantages. The main benefits are high efficiency and the variety of sizes. The development of batteries can be followed back to the 1800s, when physicist Alessandro Volta conceptualized its development. A battery is a device that runs through electrochemical reactions in a cell or cells connected in series. The primary purpose of a battery is to store energy in an electrochemical way. The electrochemical cell's three main components are: an anode, a negative electrode (where oxidation occurs); a cathode, a positive electrode (where reduction occurs); and an electrolyte, which helps ion transfer between the two electrodes. Batteries are divided into non-rechargeable and rechargeable ones. The first is called also primary batteries and it has been reported [54] that these are small, light, reasonably priced, and simple sources of power that are suitable for a wide range of portable equipment. They obtain their power from chemical reaction that is irreversible. For instance, most of alkaline batteries are primary. On the other hand, rechargeable batteries are named as secondary ones and they are capable of recharging and discharging several times, due to the reversible redox and the reversible reaction which occurred in them.

To give you an idea, lithium-ion (Li-ion), nickel-metal hydride (NiMH) and lead-acid batteries are some of the common rechargeable batteries.

Metal-air batteries (MABs) are a promising technology with applications ranging from portable devices to large-scale energy storage. They are both safer and they have a higher energy density than others. MABs attracted a paramount attention as it can work in an open-air atmosphere and use not only metal components, as the traditional batteries use, but also the oxygen which exists in the environment. This system includes three basic components: a metal anode, a porous air cathode, and an electrolyte that separates the two electrodes. The anode material of a metal-air battery is made up of metals such as lithium (Li), sodium (Na), iron (Fe), zinc (Zn), and other elements. Electrolytes come in a variety of forms [56], consisting of aqueous electrolytes, non-aqueous (aprotic), solid-state, and hybrid electrolytes.

Non-aqueous electrolytes are used by the anode which composes of lithium-air, sodium-air and potassium-air batteries which are extremely sensitive to water. On the other hand, aqueous electrolytes are for anodes made up of magnesium, aluminum, iron, or zinc. These aqueous systems need a hydrophobic protective layer to protect electrolyte leakage. On the anodic electrode of MABs, metal transforms into ions, whereas on the cathodic electrode, oxygen transforms into hydroxide ions. In contrast, metallic ions pass from the anode to the cathode in a typical ionic battery. The gas diffusion layer allows oxygen to diffuse into the MAB. In an aqueous electrolyte system, oxygen behaves differently than in a non-aqueous electrolyte medium [52], as is shown in **Figure 8**.

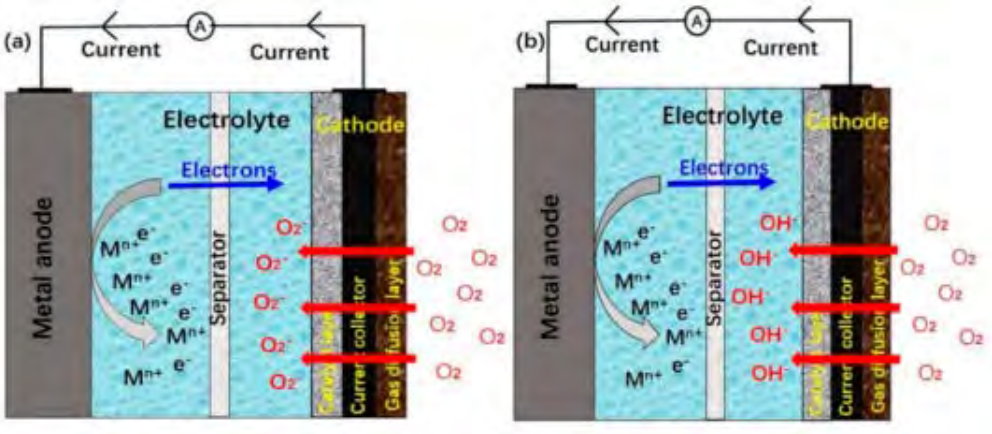

Figure 8 MABs' working principle for a) non-aqueous and b) aqueous electrolyte adapt from [35].

Electrons are created during the transformation of the metal into metallic ions, and the metallic ions then dissolve into the electrolyte. All these procedures are reversed during a charging operation. Table 3 lists the reaction formulas for a number of MABs.

Table 3 Cathode, anode, and overall reactions of metal-air batteries

Metal Anode	*Electrolyte*	*Anode Reaction*	*Cathode Reaction*	*Overall Reaction*	*Ref.*
General		$M \Leftrightarrow M^{n+} + ne^-$	$O_2 + 2H_2O + 4e^- \Leftrightarrow 4OH^-$		[35]
Iron (Fe)	*Alkaline Aqueous*	$Fe + 2OH^- \Leftrightarrow Fe(OH)_2 + 2e^-$	$O_2 + 2H_2O + 4e^- \Leftrightarrow 4OH^-$	$2O_2 + 3Fe \Leftrightarrow Fe_3O_4$	[57]
Aluminum (Al)	*Alkaline Aqueous*	$Al + 4OH^- \rightarrow Al(OH))_4 + 3e^-$	$O_2 + 2H_2O + 4e^- \rightarrow 4OH^-$	$3O_2 + 2Al \rightarrow Al_2O_3$	[58]
Zinc (Zn)	*Alkaline Aqueous*	$Zn + 4OH^- \Leftrightarrow Zn(OH)_4^{2-} + 2e^-$	$O_2 + 2H_2O + 4e^- \Leftrightarrow 4OH^-$	$O_2 + Zn \Leftrightarrow ZnO$	[59]
Lithium (Li)	***Non-Aqueous***	$\boldsymbol{Li \Leftrightarrow Li^+ + e^-}$	$\boldsymbol{O_2 + e^- \Leftrightarrow O_2^-}$ $\boldsymbol{O_2^- + Li^+2 \Leftrightarrow LiO_2}$ $\boldsymbol{LiO_2 + Li^+ + e^- \Leftrightarrow Li_2O_2}$	$\boldsymbol{O_2 + Li \Leftrightarrow Li_2O_2}$	**[60]**

4.1 MABs electrolyte

There are several types of electrolytes, including aqueous electrolytes, non-aqueous (aprotic), solid-state, and hybrid electrolytes as is shown in figure 9.

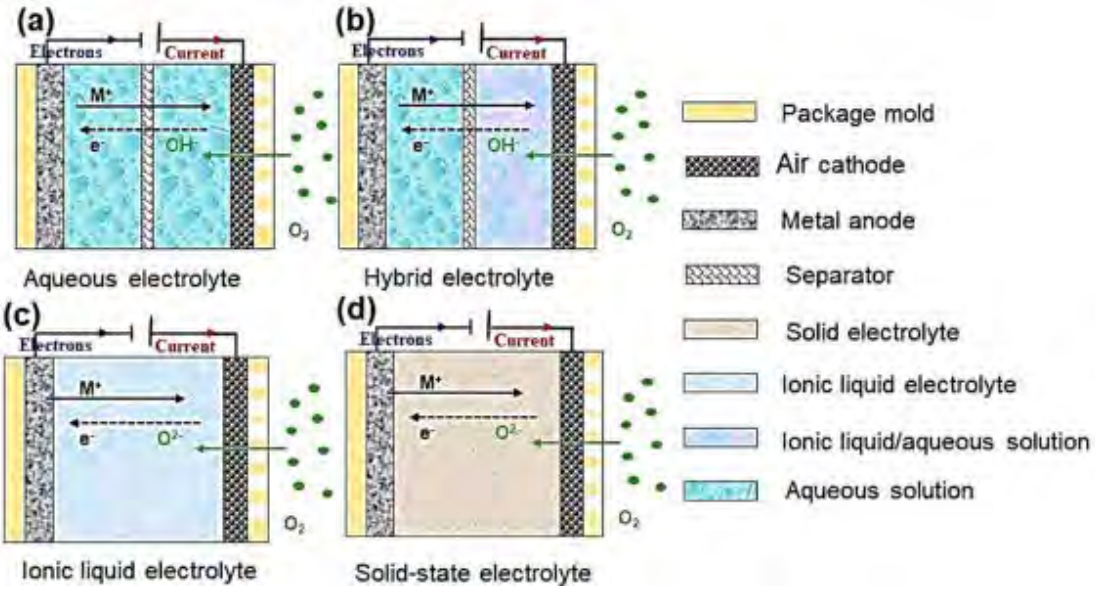

Figure 9 Different type of electrolytes at metal-air batteries [61].

4.1.1 Aqueous electrolyte

Ionic conductivity is high in aqueous electrolyte. It is also appealing for batteries with a high-power density. Water-based electrolytes are also non-flammable and inexpensive. Although, the aqueous electrolyte is more corrosive than an organic solution, it has a limited water thermodynamic electrochemical window. Its thermal use range is reduced because its performance at low temperatures is determined by the freezing point [52]. Based on the pH number, aqueous electrolytes can be divided into three categories, alkaline, neutral, and acidic.

An alkaline electrolyte solution with a pH value greater than 7 and less than or equal to 14 is the most commonly utilized electrolyte in aqueous-based MABs contrasted to an acidic electrolyte due to its better ORR, lower over potential, and faster reaction kinetics. When CO_2 from the air reacts with this electrolyte, however, it creates a carbonate that surrounds the cathode. Because it obstructs the pores of the positive electrode, a large amount of carbonate decreases the cathode's efficiency [61]. Furthermore, utilizing alkaline electrolytes that are too powerful is damaging to the environment. Aqueous alkaline electrolytes are commonly used in zinc-air and aluminum-air batteries. MABs with alkaline electrolytes have stronger oxygen electrocatalysis activity and metal corrosion resistance than those with neutral or acidic electrolytes.

The neutral solution has a pH of seven, and it has been shown to improve secondary Zn-air battery cycle stability and longevity; however, no simulation studies have examined the efficiency of neutral Zn-air batteries in a laboratory environment at this time. Neutral Zn-air batteries' pH stability is critical for cell activity. Furthermore, in a neutral salt solution, an aluminum alloy–air battery can discharge with greater activity and a lower corrosion rate than in an alkaline electrolyte **[**61**].**

The pH of the acidic solution is between 2 and 7. Due to the reduced battery efficiency caused by a large amount of H^+ in the solution reacting directly with metal, it is rarely included in aqueous-based MABs. The performance of an Al-Zn alloy anode is determined by various types of acids at the same pH, operating temperature, and concentration **[**61**].** The production of byproducts on the cathode and the dendrite formation on the anode were both prevented by the acidic solution. Some types of MABs, however, may experience corrosion as a result of this **[**62**].**

The metal electrode suffers from fundamental problems in an aqueous electrolyte, such as electrode corrosion, passivation, hydrogen evolution, and dendrite development. Different electrolyte additives and the design of the electrolyte material can minimize some of these difficulties and improve the performance of the metal electrode. In alkaline conditions, ZnO and polyethylene or ZnO and carboxymethyl cellulose (CMC) can be utilized. Zn^{2+}, In^{3+}, and Sn^{3+} are the additions for neutral saltwater solution. Furthermore, several aromatic carboxylic acids are beneficial in alkaline solutions and have similar benefits in acidic environments. In acidic solutions, the imidazole group N atoms can be applied.

4.1.2 Non-aqueous electrolyte

A significant benefit of non-aqueous MABs is the reduction of electrolyte leakage while maintaining thermal stability and resilience. They may also be able to solve the issues of electrolyte evaporation and gas crossover. Another benefit is that it permits MABs' energy density to be increased, as well as the construction of reusable and bendable electronics. It does, however, have the ability to increase the battery's resistance while reducing its capacity. Due to the poor wetting feature that limits the three-phase interface interaction, the solid-based electrolyte has more OH interfacial transporting resistance than the aqueous environment for MABs, although employing alkaline gel electrolyte (AGE) may minimize these

concerns [63,20]. In an ionic liquid electrolyte, there are two types of cations: (1) alkali metal ions in a chemical-free solvent and (2) big natural cations with inorganic or organic anions. The production of carbonate, which plugs the electrode pores and consumes the electrolyte, poses a problem for this type of electrolyte [61]. Low volatility, minimal flammability, and great ionic conductivity characterize ionic liquids. They can handle humidity in laboratories. RTILs (room temperature ionic liquids) are a type of salt that has a melting point of less than 100°C and is made up of large organic cations and organic/inorganic anions, among other things. As a result of the drying out problem, researchers have focused their efforts to RTILs as MAB electrolytes because they are very conductive, extremely nonvolatile, and can assist the electrochemistry of many metals [64]. RTILs are very costly. In MABs with metal electrodes that are unstable in water, such as Na and Li, the aprotic organic electrolyte is commonly utilized **[**64**].** The creation of a solid electrolyte interphase (SEI) at the anode's surface is aided by this. However, it raises worries about flammability, the environment, toxicity, and the economy. Furthermore, an organic electrolyte produces a discharge product that is nonconductive and insoluble, causing it to deposit in the air cathode pores and obstruct them [64,65]. The expense, undecomposed discharge products, and low efficiency of the round trip with organic electrolytes have all been examined, and a mixed electrolyte system has been developed to alleviate these difficulties [66].

4.1.3 Hybrid electrolyte

Hybrid electrolyte is combination of two different electrolytes, a solid electrolyte barrier and gas diffusion. In a hybrid battery system, the anode electrolyte is known as an anolyte, while the cathode electrolyte is recognized as a catholyte. A unique aqueous iron–air battery was constructed using an alkali metallic ion (Na^+ or Li^+) solid-state electrolyte (SSE) separator, which included alkaline anolyte and acidic catholyte. The alkali metallic ion behaves as an ionic transport mediator when the anode and cathode are exposed to oxidation-reduction processes (redox reactions) [20,67]. The schematic schematics for each cell in non-aqueous Na-O_2 batteries are displayed in Figure 10.

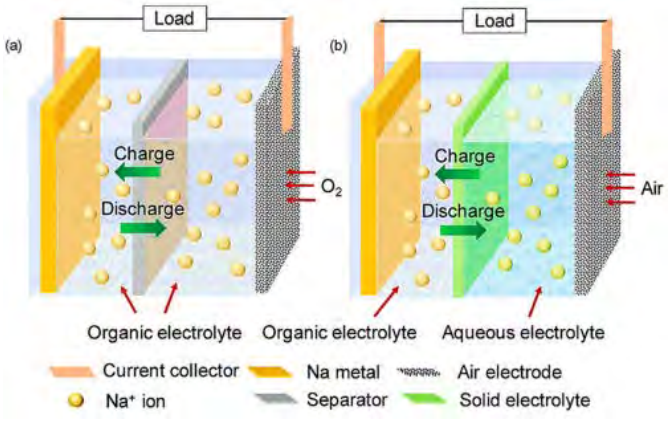

Figure 10 Working principle of a) non-aqueous Na-02 battery b) hybrid Na-air Battery, taken from [66].

4.1.4 Selecting electrolyte

Each type of electrolyte has benefits and drawbacks to consider. Electrolytes are often chosen by a trial-and-error approach based on rules of thumb relating various electrolyte features; as a result, time was wasted testing different electrolytes to achieve the desired performance. Figure 11 shows a link between the solvent reorganization energy and the ORR rate constant k and the oxygen diffusion coefficient D (O_2) in non-aqueous Li-O_2, Na-O_2, and K-O_2 cells. The study illustrates the fundamental correlations between the solvent and the salt in the membrane, as well as the influence these interactions have on the battery's overall performance. It has been found that as the size of the cation rises, the rate of ORR in the presence of alkali metal ions becomes more reliant on the salt anion used [61].

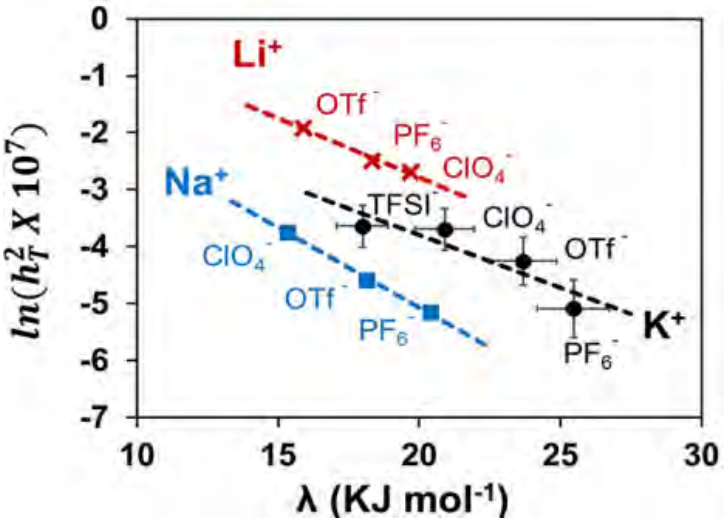

Figure 11 Correlation graph between solvent reorganization energy λ, the diffusion coefficient of oxygen and the ORR rate constant k, adapted from [61].

4.2 Cathode of MABs

Cathode is the third element of MABs, and the active material for the cathode is oxygen from the surrounding air, which is both free as well as abundant. It also does not require a large shell to hold it confined, increasing the device's energy density [68,69]. The cathode reactions are the oxygen reduction reaction (ORR) and the oxygen evolution reaction (OER), with ORR occurring during the discharge cycle and OER taking place during the charge cycle [66,70].

4.2.1 Air cathode components

A gas diffusion layer (GDL), a catalyst, and a current collector compose the air cathode, as shown in Figure 12. Air cathode has a significant impact on MAB characteristics; thus, it must be optimized by increasing ORR, minimizing carbonate and byproduct production, preventing from flooding in the air cathode, and electrolyte evaporation.

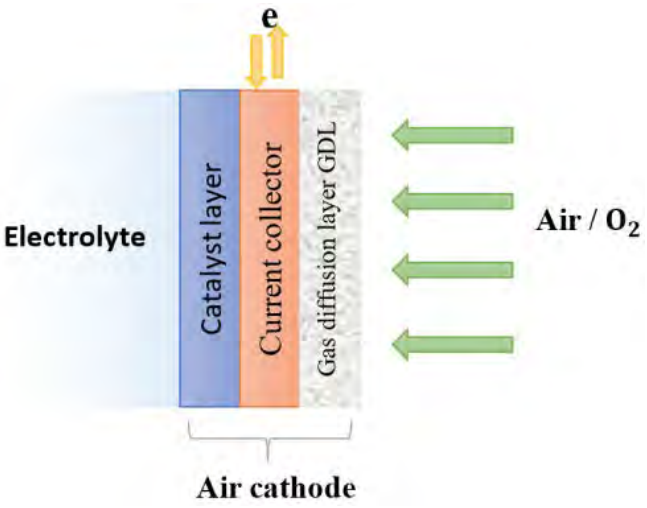

Figure 12 Air Cathode components of MABs, adapted from [52].

The gas diffusion layer (GDL) is responsible for a number of functions. It serves as a conduit for air between the catalyst layer and the air atmosphere, allowing oxygen to permeate the atmosphere or, in another way, absorbing air from the environment. It also prevents electrolyte from flowing out of the battery, prevents water from entering the battery, and supports the battery's catalyst layer. Hydrophobicity, lightness, thinness, and high porosity are all desirable qualities in GDL. This takes careful research ahead of time. Carbon or catalytic materials and hydrophobic binders such as polytetrafluoroethylene PTFE (Teflon) are widely used in gas diffusion layers, and the catalytic materials are frequently mixed with the binders before being placed or imprinted on current collectors [71].

The principal functions of current collector include connecting to external electronic systems to give a final circuit and transfer electrons between them. It can be composed of non-metal or metal, using porous foam-like metals including Ni-mesh, Cu, and stainless steel used for the metal current collector. Carbon cloth, conductive carbon paper, and graphitic fiber, on the other hand, are non-metal current collectors constructed of carbon-based materials [35,71].

The third factor that influences MAB properties is electrocatalysts. Because the natural kinetics of oxygen reactions are often sluggish, improving the kinetics of these reactions enhances the electrochemical efficiency of MABs while simultaneously minimizing over potentials, the bifunctional catalyst is essential to increase the OER and ORR. The catalyst layer can be separated into four groups: [62,72,73,74,75]

i. Transition metals and metal macrocyclic complex.
ii. Carbonaceous materials as doped carbons.
iii. Single, binary, and ternary metal oxides (e. g., MnO).
iv. Noble metals and their alloys such as platinum (Pt).

4.3 Oxygen electrochemical reactions in MABs

Because oxygen operates differently in aqueous and non-aqueous electrolytes (reaction paths are in Table 4), a number of catalysts was needed to correspond to different reaction processes. Both processes take place without the use of catalysts on an air cathode electrode; however, because the natural kinetics of oxygen are slow, the application of electrocatalysts can accelerate the reactions.

Table 4 Pathway reactions for the different electrolytes of metal-air batteries, adopted from [52].

Electrolyte		**Oxygen Reaction**	**Reaction Pathway**	
			Two-Step	**Four-Step**
	Alkaline	ORR	$O_2 + H_2O + 2e^- \longrightarrow O^+ + 2OH^-$ $O^+ + 2OH^- + H_2O + 2e^- \longrightarrow 4OH^-$	$O_2 + H_2O + e^- \longrightarrow OOH^+ + OH^-$ $OOH^+ + e^- \longrightarrow O^+ + OH^-$ $O^+ + H_2O + e^- \longrightarrow OH^+ + OH^-$ $OH^+ + e^- \longrightarrow OH^-$
Aq. MAB		OER		$OH^- \longrightarrow OH^+ + e^-$ $OH^+ + OH^- \longrightarrow O^+ + H_2O + 2e^-$ $O^+ + OH^- \longrightarrow OOH^+ + 2e^-$ $OOH^+ + OH^- \longrightarrow O_2 + H_2O + e^-$
	Acidic	ORR		$OH^- \longrightarrow OH^+ + e^-$ $OH^+ + OH^- \longrightarrow O^+ + H_2O + 2e^-$ $O^+ + OH^- \longrightarrow OOH^+ + 2e^-$ $OOH^+ + OH^- \longrightarrow O_2 + H_2O + e^-$
		OER		$H_2O \longrightarrow OH^+ + H^+ + e^-$ $OH^+ \longrightarrow O^+ + H^+ + e^-$ $O^+ + H_2O \longrightarrow OOH^+ + H^+ + e^-$ $OOH^+ \longrightarrow O_2 + H^+ + e^-$
Non-Aq. MAB		ORR		$O_2 + e^- \longrightarrow O_2^-$ $O_2^- + Li^+ \longrightarrow LiO_2$ $2LiO_2 \longrightarrow Li_2O_2 + O_2$
		OER		$Li_2O_2 \longrightarrow 2Li^+ + O_2 + 2e^-$

When oxygen is present, two reactions occur: the oxygen reduction reaction ORR and the oxygen evolution reaction OER.

This occurs throughout the MAB discharge process and includes several steps, the most essential of which are:

1) From the surrounding environment, oxygen diffuses into the catalyst's surface.
2) The catalyst's surface absorbs oxygen.
3) Through an external circuit, electrons from the anode are transported to oxygen molecules.
4) The oxygen bond weakens when the oxygen connection is interrupted.
5) The hydroxyl ion product is transported to the electrolyte after being removed from the catalyst's surface. In OER, all of these procedures may be reversed during the charging period.

Because the intermediates formed were quite stable after oxygen adsorption, either a four-step or a two-step method can be employed in the ORR and OER processes, respectively. The two-electron process produces superoxide, which is a reactive oxygen species [52].

$$O_2 + H_2O + 2e^- \rightarrow HO_2^- + OH^-$$

The hydroxide OH− produced in the four-electron process [52].

$$O_2 + 2H_2O + 4e^- \rightarrow 4OH^-$$

For high energy and power densities, the four-electron method is essential. To avoid carbonate ions building in the liquid electrolyte over time, alkaline media must be supplied clean air or use an O_2-permeable membrane [76].

4.4 Anode of MABs

There has been a great deal of research and improvement since the first metal-air battery, the zinc-air battery, was invented in 1878. Anodes in MABs can be made of a variety of metals, such as zinc, aluminum, iron, lithium, sodium, potassium, and magnesium. When it relates to anode electrodes, each metal has its own unique strengths and weaknesses. The anode's discharge capacity is defined by its chemical activity. Because of metal's high activity, a secondary reaction with other electrolyte components may develop, which cannot be controlled.

The use of oxygen from ambient air as a cathode source has the added benefit of significantly lowering the cost and weight of the MAB. Furthermore, the MAB's anode can be constructed of inexpensive materials. MABs can also be classified into primary batteries and secondary batteries according to whether they are rechargeable or not, which it depends on the metal of the anode.

CHAPTER 5

Non-rechargeable Metal-Air Battery

Al-air Battery (AABs)

Hulot [64] was the first to propose aluminum as a battery's component in 1855, using it as a cathode in conjunction with a zinc amalgam. Buff introduced aluminum as an anode material for the first time in 1857 [65]. He noticed an oxide layer forming on the surface of a polarized aluminum anode immersed in water. When the aluminum anode was combined with a carbon cathode in a nitric acid solution, a voltage of 1.377V was measured. In 1893, Brown obtained a patent for a galvanic battery that used an Al-Zn anode. The alloy, which included the same amounts of zinc and aluminum, offered "excellent economy in the prevention of the current." In 1962, Zaromb wrote the first article describing an AAB. His purpose was to minimize the weight of alkaline primary batteries by substituting aluminum for zinc. Zaromb recognized that all recent attempts to create a functional aluminum battery had failed because a passivating oxide layer would form or because the oxide layer would be soluble in extremely alkaline electrolytes, which would result in excessive corrosion rates. Pryor and coworkers' patents from 1965 to 1968 made significant claims about how alloying, mostly with tin but also with gallium, magnesium, bismuth, zirconium, zinc, manganese, copper, silver, nickel, iron, arsenic, antimony, cobalt, and boron, may increase Al anodic performance. The development of AABs for EV applications, telecommunications, and unmanned aerial vehicle (UAV) has occurred since Zaromb's discovery. UUV applications also employ aluminum-seawater batteries with aluminum alloy anodes comparable to those in AABs [2].

The Al–air battery has several distinguishing characteristics, including high energy density, light weight, good recyclability, environmental friendliness, and it is inexpensive. Furthermore, the electrolyte is also a non-aqueous, alkaline, salty solution. As a result, we will concentrate on Al–air batteries in this section [52]. Aqueous or ionic liquid electrolytes can be used with the main components of an AAB, aluminum anode, air-breathing cathode, and separator. In aqueous electrolytes, the cathode is the positive electrode where the oxygen reduction process (ORR) occurs, and the anode is the negative electrode where Al oxidation occurs. Because of the presence of aluminum in aqueous electrolytes, secondary (rechargeable) designs are not possible.

5.1 Anode material

5.1.1 Pure aluminum

Alkaline solutions are the most often used aqueous electrolytes because they have greater theoretical cell potential and attainable power compared to neutral or acidic solutions. Open circuit potentials in alkaline media, however, cause aluminum to corrode at high rates, and hydrogen is being created at greater positive potentials than for the creation of aluminum metal from aluminum ions in solution (showing rechargeability in aqueous systems to be impossible). High over potentials for anodic dissolution are produced as a result of the formation of passivating oxide or hydroxide surface layers [77]. These are shown in **figure 13** and the action of aluminum is represented by acid, neutral, and alkaline electrolytes in a Pourbaix diagram created following Pourbaix's normal conventions [78]. The Pourbaix graphic shows how alkaline electrolytes tend to have lower Al immunity than acidic or neutral solutions. The following is also displayed in Fig. 13(a) callouts: (i) the ability of protons to react with the boehmite (γ-ALOOH) surface layer to form Al^{3+} ions that can exist in acidic media; (ii) the passive nature of the alumina film in neutral solutions; and (iii) the ability of OH^- to react with the $Al(OH)_3$ surface layer to form $Al(OH)^-_4$ ions that can exist in alkaline solutions. It is interesting to note that, as a function of current density, neutral electrolytes corrode at a higher pace than acidic ones. According to Moon and Pyun [79], a proton is discharged under cathodic potential in acidic solutions, although the effect of this proton discharge in acidic solutions is negligible. This is seen by the comparatively flat acidic solution corrosion rate curve in figure 13(b). Under cathodic polarization, the water reduction suggested by equation $3H_2O + 3e^- \rightarrow 3OH^- + \frac{3}{2}H_2$ takes place in neutral and alkaline solutions. As a result, the reason corrosion increases with increasing cathodic polarization in the neutral solution is because water reduction gradually produces more hydroxide ions. Regardless of the applied current density, the alkaline solution's high concentration of hydrogen ions leads to an almost constant corrosion rate.

Error! Reference source not found.13(c) demonstrates that an alkaline solution achieves a larger negative open-circuit potential than an acidic or neutral solution. This introduces the idea of "activation," whereby the disruption of the passive oxide layer causes the aluminum surface to become more electrochemically active. In order to preserve a bare metal surface, Moon and Pyun used an electrode that allowed abrasion of the aluminum. According to figure 13(c), all solutions' increases in open-circuit potential over time show that reconstruction of oxide or hydroxide films does take place to some extent even in the absence of mechanical disruption. In an alkaline electrolyte, pure aluminum is most anodically active, although corrosion is severe. At 10^{-2} mA cm^{-2}cathodic current density**,** figure 13 (b) shows a factor of 25 increase in corrosion in alkaline over acid and neutral. According to Perrault [80], aluminum's open circuit potential in strongly alkaline solutions closely resembles the Nernst potential for

the oxidation of aluminum hydride to aluminate ions, suggesting that aluminum hydride on the metal's surface might serve as an intermediate in the dissolution reaction.

Aluminum hydride production was also proved by Despic and others [68,69], while Adhikari directly demonstrated its presence through secondary ion mass spectrometry. The existence of H-vacancies in the AlH_3 construct is thought to be functioning as a catalyst for pitting corrosion of the aluminum, and the ensuing nanoscale voids are thought to be the beginning locations for this process [77].

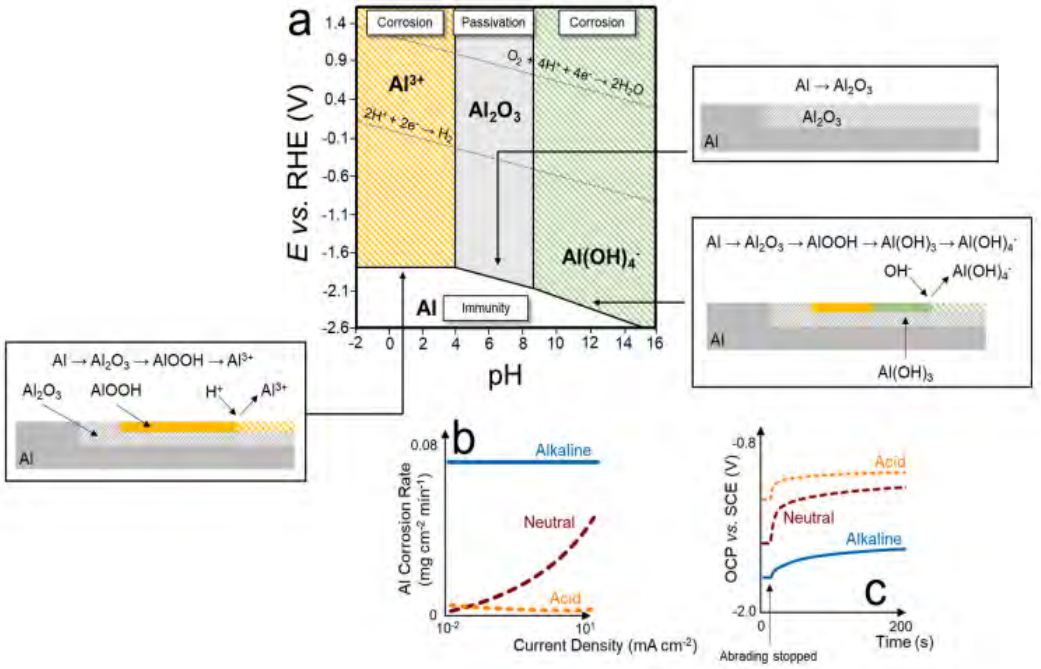

Figure 13 . (a) Pourbaix diagram for the aluminum-water system; (b) corrosion rates of pure aluminum as a function of applied cathodic current density at 20 ◦C in various aqueous solutions (inspired from Ref. [77]); (c) open circuit potential transients obtained after interrupting abrading action on pure aluminum specimen at 20 ◦C in de-aerated aqueous solutions (inspired from Ref. [77]).

Doche et al. [81] investigated the electrochemical behavior of 99.999 percent pure aluminum in 4 M NaOH in order to better understand the hydroxide layer. They and others proposed that Equation $Al(OH)_3 + OH^- \rightarrow Al(OH)_4^-$ results from three single-step electron transfers via hydroxide addition to produce solid $Al(OH)_3$, followed by additional hydroxide addition to produce $Al(OH)_4$. Adsorbed hydrogen atoms and intermediate oxidation products compete with one another on the aluminum surface as a result of the simultaneous occurrence of the hydrogen evolution process (HER). This technique helps to explain the erratic behavior that was noticed when aluminum was submerged in the electrolyte. The air-formed aluminum oxide layer dissolves quickly ($Al_2O_3 \rightarrow Al(OH)_4^-$). At first, a mixed potential of around 1.63V vs. Standard Hydrogen Electrode (SHE) is seen. The bare aluminum surface then quickly dissolves, producing both hydroxide ($Al(OH)_3$) and HER. At the end of the transient behavior, the $Al(OH)_3$ layer stabilizes, the oxide layer dissolving rate decreases, and the mixed potential shifts to 1.66 V vs. Standard Hydrogen Electrode (SHE). The formation/dissolution of passivating layers (Al_2O_3) and discharge product layers

$Al(OH)_3$ frequently causes cell voltages in the 1.2-1.6V range [82], which are much lower than the theoretical value of 2.35V [83]. In an effort to enhance the performance of pure aluminum, alloying metals to energize the anode surface while reducing corrosion has been considered.

5.1.2 Alloy aluminum

The ability to create a solid solution with aluminum, having a greater purity than aluminum, having a larger hydrogen over potential, and being soluble in alkaline electrolytes are all desired features of alloying metals. The Pryor patents [84–90] and other sources [91–93] examine a large number of alloying metals; nevertheless, this text covers work on the two most often researched elements— In, and Ga. When solid solutions are formed, diffusion of the alloying element into the solid aluminum structure is made easier by a melting temperature lower than that of aluminum. In a three-step surface segregation process, metals nobler than aluminum activate the aluminum, according to research by Reboul et al. [94]:

1. Aluminum disintegration caused by the galvanic pair,
2. Aluminum and alloying element(s) oxidation, releasing cations into the electrolyte,

i.e., $Al(M) \rightarrow xAl^{3+} + M^{n+} + ye^{-}$.

3. Reintroducing the cathodic cations produced in Step (1) to the anode surface, which promotes more anodic dissolution of aluminum by lowering the stability of the passive oxide film ($Al + M^{n+} \rightarrow Al^{3+} + M$)

Due to their greater hydrogen evolution reaction (HER) over potentials, surface segregation of the more noble alloying elements also somewhat inhibits aluminum corrosion. For a number of metals, Rüetschi and Delahay [95] found a correlation between hydrogen over potential and the potency of the metal-atomic hydrogen connection. They showed that over potential increased linearly with declining bond strength. When only solid solutions are existent in the alloy, the alloying elements' protective actions against the anodic dissolution of aluminum are often seen. The ingredients found to produce Al-alloys that are more active than pure aluminum include gallium, indium, and tin.

5.1.3 Aluminum-gallium alloys

Several electrochemical/morphological conditions can cause an Al-Ga anode to be activated, according to Tuck et al. [96]. In the case of low amounts of Ga, it happens after polarization below the Ga/GaO_3^{3-} reduction voltage (1.55 V vs. Standard Hydrogen Electrode (SHE)), implying that activation is triggered by gallium ion reduction to generate active gallium sites in their oxide films. Surface agglomeration caused activation at greater levels of Ga content. In both cases, Ga metal on the alloy surface cracked and thinned the Al_2O_3 oxide layer, enhancing Al diffusion and dissolution. Activation was restricted when surface gallium production was hampered, by back-diffusion of gallium into the aluminum matrix, or by decreasing Ga mobility by cooling below the gallium melting temperature. The authors came to the conclusion that there was a threshold amount of gallium surface coverage below

which the alloy would not activate. This critical threshold was discovered to be 3 g cm^{-2} in 4 M NaOH at 60 ºC, corresponding to a Ga concentration of more than 0.1 wt. percent in the alloy. Below this threshold, gallium levels in the alloy did not allow surface gallium concentrations to rupture the oxide layer, allowing aluminum transport and activation. Macdonald et al. [97] used Al-Ga alloys in a corrosion investigation at 50 ºC in 4 M KOH to evaluate AAB anodes. When gallium was added to aluminum, the open circuit potential moved by 120 mV in the cathodic direction, resulting in a 20-fold increase in corrosion rate compared to pure aluminum. Corrosion rates rose with time as a result of surface roughening in an alkaline environment. The effect of mechanical history on the corrosion rate of 0.5 wt. percent Ga-Al alloys was investigated using the degree of "cold-working," defined as the amount of pressing and rolling of alloy material prior to electrochemical testing. There was no clear relationship between corrosion rate and cold working. Annealing at 380 degrees Celsius for 2.5 hours resulted in greater corrosion rates than any cold-worked sample. The significant corrosion rates reported in all circumstances investigated suggest that binary Al-Ga alloys would not be acceptable as AAB anodes. Hunter [98] states that when Ga >0.26%, Al-Ga (here generated by heat-treatment at 600 ºC of cast bars after a water quench) functions as a super active alloy. Hunter defined aluminum activation as having several stages: (i) in alkaline electrolytes, the active state is unalloyed aluminum. (ii) a super active aluminum alloy, has a fairly low open circuit potential and greater activity.(iii), a hyperactive aluminum alloy, has an even lower open circuit potential and exceptionally high corrosion rates. Pitting corrosion was seen in Hunter's hyperactive alloys, with separate Ga-rich phases forming on these regions [98]. Aluminum dissolving was characterized by grain boundary attack and surface disintegration. Choi et al. [99] found a corrosion current of 91.25 mA cm^{-2} for a 0.47 wt. percent Ga alloy in 4 M NaOH, compared to 22 mA cm^{-2} for pure aluminum tested under the same circumstances. The alloy had been water-quenched after being annealed at 450 ºC for 2 hours. Gallium surface particles facilitating aluminum oxide dissolving were blamed for the severe corrosion observed. The sum of the studies suggests that Al-Ga binary alloys are inappropriate for use as AAB anodes and that corrosion rates keep rising with growing gallium content via the methods mentioned.

5.1.4 Aluminum-indium alloy

Macdonald et al. [100] discovered that corrosion in Al-In alloys at 50 ºC in 4 M KOH was substantially lower than in Al-Ga alloys, but still greater than in pure aluminum. Open circuit potentials were moved roughly 50 mV in the cathodic direction compared to pure aluminum and reported corrosion rates were 4-5 times higher than aluminum, with only a little fluctuation in corrosion rate when the Indium concentration was varied from 0.01 wt. percent Indium to 0.5 wt. percent Indium. The authors proposed that various alloying elements, including indium, had minimal critical concentrations for inhibiting corrosion and that the inhibitive impacts were saturated at the concentration levels utilized in their study.

Similarly, Hunter's [101] study of Al-In alloys revealed no clear relationship between galvanostatic corrosion current density and indium concentration at open circuit circumstances. It was hypothesized that specimen preparation just before testing may have contributed to the relatively random nature of the results, since the surfaces described were produced in a manner comparable to the Al-Ga samples but were not ground or polished prior to the experiment. Scamans et al. [102] investigated Al-In alloy behavior in 4 M NaOH, discovering exceptionally low corrosion currents for Al-In alloys, in contrast to Hunter [101] and Macdonald et al. [100]. This suggests that the material preparation (though not explicitly mentioned by Scamans et al. [102]) before testing may have an influence on its reactivity.

Several other studies have collected single data point information on Al-In alloy open circuit corrosion in alkaline liquids. Wilhelmsen et al. [103] measured a corrosion current density of 5.3 mA cm^{-2} in 4 M KOH at 60 ºC for an alloy containing 0.1 wt. percent Indium in aluminum, compared to 87 mA cm^{-2} for pure aluminum, a significantly lower figure than Macdonald et al. [100] and Hunter [101]. This might be due to the longer time span (18–20 h) used to calculate the corrosion rate, as opposed to around 1 h for previous studies. Surprisingly, the maximum corrosion was detected within the first hour of the Al-In alloy's contact with the electrolyte. El Abedin and Saleh [104] subjected an aluminum alloy with 0.77 wt.% in content to 4 M KOH at room temperature for 30 minutes and reported an aluminum test under the same circumstances. The alloy melt was cooled in air here, and cast samples were utilized for corrosion testing. Sun and Lu [106] employed vacuum melting and drop casting to create an alloy containing 0.5 wt.% In in Al. Prior to testing, samples were annealed at 580 ºC for 2 hours and water quenched. The specimens were exposed to 4 M NaOH for 1 hour at 25 degrees Celsius, and the evolved hydrogen was gathered to assess the corrosion rate. The alloy's corrosion current density was reported to be 7.06 mA cm^{-2} compared to 13.8 mA cm^{-2} for pure aluminum. The Al-In corrosion current densities addressed in this section are shown in **Figure 14**.

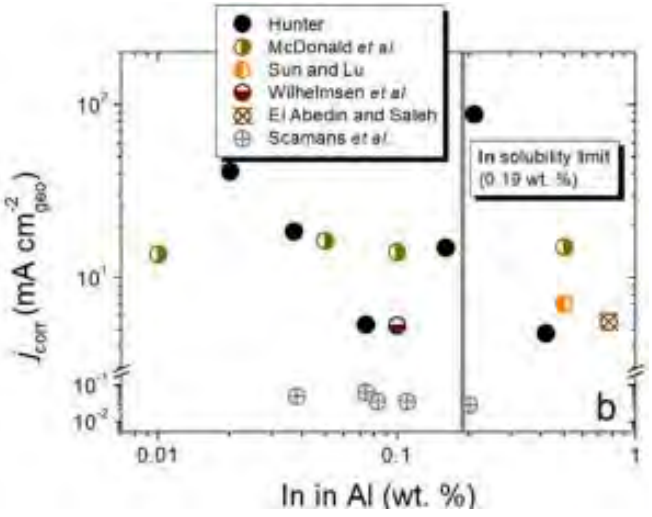

Figure 14 Corrosion current density as a function of indium concentration in binary Al–In alloys [77,100–102,104,106]; adopted from [77].

Apart from one data point obtained by Hunter [101], the corrosion rate appears to be essentially static with growing indium content above the solubility of indium in aluminum which is consistent with the saturation idea proposed by Macdonald et al. [100]. In addition to composition, the collective work implies that alloy preparation has an important influence on anode performance. If aluminum alloy anodes are eventually successful in accessing commercial markets, this will have an impact on the production techniques designed for them.

Zinc is also a suitable alloying component for the anode of an aluminum-air battery because it enhances the nominal cell voltage and reduces the rate of self-corrosion. According to a study, adding Zn to an Al 99.7% purity anode reduced its discharge performance due to the creation of a Zn oxidation coating. Additionally, indium (In) was applied to an aluminum-zinc anode to prevent this formation, which improved the discharge performance of Al–air systems by reducing the resistance of the zinc oxidation film via Inions. Furthermore, an Al-Zn-In alloy anode manufactured of advertising aluminum (99.7% purity) is less expensive than 4N aluminum (99.99 percent purity) [107].

5.2 Electrolyte

5.2.1 Aqueous electrolyte additive chemistry with aluminum and aluminum alloys

Surface phenomena in aluminum alloys are described as being dependent on transit of alloying elements; diffusion through solid matrices to and from the surface; and dissolution and deposition of species that are soluble in the electrolyte. In lieu of developing new alloys particularly intended to facilitate aluminum activation, one commonly investigated strategy for improving aluminum anode performance is to modify electrolyte chemistry with additives. The effective use of current commercial alloys may speed the adoption and usage of AAB-powered cars and equipment.

The notion of AAB improvement using electrolyte additions has been around since Zaromb [105] first announced the AAB design in 1962. Zaromb and colleagues evaluated inorganic (ZnO, KI, and amalgamating mercury species) and organic (ethanol, methanol, and a series of alkyldimethylbenzylammonium salts, referred to as "hyamines") additives in electrolytes, separately and in several mixtures, with aluminum anodes of 99%-99.99% purity in that work and another [55]. In general, when reduced corrosion was seen, it was frequently accompanied by greater anode polarization. With ZnO with mercury added to the electrolyte, good results were obtained. Zinc metal deposition from the solution reduced the corrosion rate, although the Zn deposits flaked off after a short time. The inclusion of mercury into an amalgam improved Zn adhesion while also increasing hydrogen evolution reaction (HER) overvoltage. The amalgam technique, on the other hand, was viewed as troublesome due to the usage of mercury as well as its strong reactivity with oxygen in the air oxygen. Without any further electrolyte inputs, hyamine compounds displayed lower Al corrosion rates. As alkaline electrolyte additions, the solubility species of elements often employed in AAB alloy anodes have

been thoroughly investigated. MacDonald and English [108] reported corrosion in aluminum specimens containingSnO_3^{2-} ,$(InOH)_3$,BiO_3^{3-},$Ga(OH)_4^-$,Mn_4^{2-} species alone or in binary combinations. In several circumstances, additions had a negative effect as compared to pure electrolyte. The inclusion of $(InOH)_3$exacerbated aluminum corrosion by roughly a factor of three and dissolving $Ga(OH)_3$ into the electrolyte resulted in the full loss of the aluminum specimen. With the single-component additive 0.001 M K_2MnO_4 , the greatest coulombic efficiency achieved was 99% at 200 mA cm^{-2} discharge current density. Corrosion rate was roughly one-third lower with this addition compared with electrolyte without additive. Although coulombic performance was 77% at a discharge current density of 200 mA cm^{-2} (Coulombic efficiency of pure aluminum under the same conditions was 89%), the addition of 0.01 M sodium stannate decreased corrosion compared to aluminum under open circuit conditions. Under discharge circumstances, however, solutions containing 0.01 M sodium stannate inhibited less efficiently than electrolytes containing 0.001 M sodium stannate. The authors hypothesized that aluminum dissolution undermined the surface-deposited tin to a greater extent at high stannate concentrations, resulting in tin surface layer decohesion. They came to the conclusion that using stannate as the only electrolyte additive was not appropriate for AAB applications. At higher discharge current densities, binary additive combinations performed best, with stannate/indium hydroxide additions attaining 96% coulombic efficiency at 400 mA cm^{-2}. Indium hydroxide assisted aluminum activation but did not significantly enhance cathodic current density under discharge circumstances (in the presence of stannate).

Doche and colleagues [109] investigated the performance of a single aluminum alloy [Al-0.1Sn-0.5 Mg] (values in weight percent) and three grades of pure aluminum (99.7%, 99.95%, and 99.99%) in alkaline electrolytes containing various concentrations of sodium stannate and hydroxide. The alloy has previously been tuned to function at 60 ºC in 8 M KOH containing 0.01 M sodium stannate for the Alu-power battery [110]. They saw significant corrosion in the 99.7% Al anodes right away. It proved unable to extract accurate electrochemical properties from the material, so further research with this grade of aluminum was discontinued. The remaining two Al grades, as well as the Alu-power alloy, were tested at 60 degrees Celsius in 4 M NaOH containing 0.05 M sodium stannate and 20 g L^{-1}aluminum hydroxide. In open circuit conditions, the alloy had the lowest corrosion current density (12.1 mA cm^{-2}), while the corrosion current density for the 99.95% Al anode was only 10% higher (13.5 mA cm^{-2} vs. 12.1 mA cm^{-2}) than for the 99.999% Al material. Coulombic performances were 96.8%, 95.6%, and 91.2% for the alloy, 99.999% Al, and 99.95% Al, respectively, at a discharge potential of 1.55 V (vs. Standard Hydrogen Electrode (SHE)). Based on the results of these tests, the performance of the 99.95% Al anode was considered satisfactory, considering that it was the least expensive material. The best conditions for the 99.95% alloy were then established using a two-level, three-factor (2^3) full factorial: electrolyte concentration (3 M-5 M NaOH), stannate concentration (0.02 M -0.08 M), and temperature (55 ºC-65 ºC).

Because aluminate by-products are routinely formed during cell operation, the aluminate content was kept constant at 20 g L^{-1}.

At 200 mA cm^{-2} current density, optimum operation at 65 ºC with 0.04 M stannate in 3 M NaOH resulted in an anode potential of 1.36 V vs. SHE. Coulombic performance was not specifically assessed, although it was predicted to be more than 95%.

Recent additive chemistry initiatives have assessed "green" organic, hybrid organic/inorganic, and other unique corrosion inhibitors. Motives include decreasing the toxicity of industrial materials and the simplicity and cost savings of adopting materials that do not require sophisticated chemical manufacture. Abdel-Gabar and colleagues [111] investigated two alkaline additives: a cationic surfactant (cetyl trimethyl ammonium bromide (CTAB)) and lupine seed extract. An alloy anode with the weight percentages of 0,687Al-0.171Fe-0.135Si-0.003Ti-0.001Cu-0.001Mn-0.001Ni-0.001Zn was used. For electrolytes with single-component additions, Tafel extrapolation and electrochemical impedance spectroscopy were employed to assess corrosion current density effects, whereas gasometry was used for single-and dual-component electrolyte combinations. Working with lupine seed oil revealed that altering additive content altered both cathodic and anodic polarization curves, demonstrating that rates of aluminum dissolution and hydrogen evolution were functions of lupine seed extract concentration. Corrosion current density reduced with increasing extract concentration (29.68 mA cm^{-2} in the absence of extract and 3.82 mA cm^{-2} for 4.464 g L^{-1} lupine seed extract). This impact was due to additive species adsorption on anodic and cathodic sites, which lowered the active Al surface area. Conductance tests were initially performed on the CTAB surfactant to identify the critical micelle concentration (1.8 x 10^{-4} M). CTAB addition had a qualitatively similar effect as lupine seed extract, with the exception that a steadily decreasing corrosion current density with increasing CTAB addition was observed only up to the critical micelle concentration (12.44 mA cm^{-2} in the absence of CTAB and 5.50 mA cm^{-2} CTAB at the critical concentration). For CTAB concentrations larger than the critical micelle concentration, there was a modest increase in corrosion current density. CTAB reduced hydrogen development by 13.7% compared to pure alkaline electrolyte in gasometry studies, whereas lupine seed extract reduced observed hydrogen generation by 62.7%. There was no synergy shown when the two additions were combined, as an electrolyte containing both functioned similarly (69.5% decrease) to electrolytes containing only lupine saw extract.

Nie et al. [112] used an Al alloy with the following composition (wt.%): Al-0.024Mg-0.011Ga-0.01Sn-0.009Fe-0.001Cu-0.001Si to test a hybrid organic/inorganic corrosion inhibitor in 4 M NaOH electrolytes. Casein is an organic compound that is a protein with numerous polar amino acid functional groups [132]. The inorganic inhibitor was sodium stannate. Stannate addition alone decreased hydrogen evolution by up to 68% using gasometry at a concentration of 0.09 M $NaSO_3$. Beginning with 0.05 M

stannate like a baseline, casein was added in steps ranging from 0.2g l^{-1} to 1.0 g l^{-1}. At 0.6 g L^{-1}casein addition, the best performance (83% decrease in evolved hydrogen) was observed. The scientists hypothesized that casein concentrations over this threshold inhibited the hybrid inhibitor's geometric coverage effect. MnO_3 was used as a catalyst in the cathode oxygen reduction process during AAB cell discharge experiments. When compared to the blank electrolyte, cell tests with the optimum hybrid inhibitor level demonstrated nearly twice the discharge capacity (940 vs. 550 mAh cm^{-2}) at 100 mA cm^{-2} current density. The hypothesized mechanism revealed substantial casein adsorption via a coordination link formed between aluminum ions and casein molecules. This boosted hydrogen evolution reaction (HER) overpotential by promoting homogenous tin surface covering. Casein, in other words, brought stability to the deposited tin that was not present in the absence of the organic addition. As stated, the presence of the organic molecule prevents oxidation of the formed metallic layer. Wu et al. [113] extended the hybrid idea by investigating the synergistic effects of mixing alkyl polyglycolide (APG) with potassium stannate. The Al alloy anode composition was similar [112] to that utilized by Nie and colleagues. The performance of a blank electrolyte (4 M KOH) was compared to electrolytes with different additive levels. Gasometry research revealed that 0.05 M K_2SnO_3 decreased developed hydrogen by 87% when compared to a blank electrolyte, while 0.002 M APG reduced it by 81%. The use of both inhibitors at these concentrations resulted in a 94% reduction in hydrogen evolution. Discharge studies in complete cells at 100 mA cm^{-2} demonstrated a roughly 2.5x improvement in mass-specific discharge capacity (840 mAh g^{-1}, 2180 mAh g^{-1} with additive). Following electrochemical impedance spectroscopy studies and surface characterization using scanning electron microscopy and FTIR spectrophotometry, a method for inhibition by the hybrid additive was proposed. Tin deposition from solution facilitated hydrogen evolution reaction (HER) over potential, although stannate alone resulted in tin loosely attached in a porous layer. APG is made up of lengthy carbon chains and several hydroxyl groups. When OH is adsorbed, a hydrophobic layer forms on the surface, effectively isolating it. This allows for more uniform, stable tin deposition and better hydrogen evolution reaction (HER) hindrance. Overall, corrosion inhibitors face challenges such as electrolyte stability and concurrent inhibition of anodic Al dissolution, although progress in the sector is encouraging. If acceptable AAB cell performance with such electrolyte additives is demonstrated, the relative ease of electrolyte additions for activation of ordinary Al alloys is obviously appealing when compared to the formulation and manufacturing of AAB-specific alloys for anodes. If current supplies of aluminum and common alloys can be exploited, the path to AAB scale-up and commercialization may be shortened.

5.2.2 Non-aqueous electrolyte chemistry for aluminum-air batteries

Non-aqueous AAB electrolytes are appealing for two reasons: (i) the ability to employ pure aluminum or affordable, commercially accessible alloys, as the corrosion processes seen in aqueous electrolyte

systems are avoided; and (ii) the prospect of permitting a secondary (rechargeable) AAB cell. Because hydrogen evolution occurs before aluminum deposition, rechargeability cannot be considered in aqueous systems, as demonstrated by the Pourbaix diagram. Although mechanical recharging is an option, using it at scale would need a large availability (Fig. 13(a)). of replacement Al anode components with some degree of standardization between anode manufacturers and end-user designs for EV and other applications. In a market where electronically charged batteries are widely used, high-performance "plug-in" AAB solutions may be more readily accepted by consumers.

5.2.3 Ionic liquid electrolytes

A number of non-aqueous electrolytes, including solvent-free molten salts with tightly packed cations and anions, sometimes known as ionic liquids, have been studied for both primary and secondary AAB applications [114]. Electrolytes based on chloroaluminate chemistry were among the first to be investigated for use with aluminum anodes, as electrodeposition of aluminum from chloroaluminates has been recognized to be viable since the mid-20th century. Solid aluminum chloride ($AlCl_3$) occurs as an ionic crystal, with the aluminum atom surrounded by chlorine atoms octahedrally [77]. To fulfill the aluminum valence electron standard hydrogen electrode shell, two $AlCl_3$ molecules will dimerize. After melting to create a molecular liquid, a chlorine atom from each of the two molecules makes a dative covalent link (both electrons provided by chlorine) with one of its lone electron pairs to the aluminum center, forming the molecule Al_2Cl_6 .This liquid has a low ionic conductivity yet acts as a powerful Lewis acid. As a result, it interacts with other halogen compounds to generate ionic liquids known as chloroaluminates, with the general formula [115] MCl-$AlCl_3$ for binary aluminates and M_1Cl-M_2Cl-$AlCl_3$ for ternary aluminates. The MCl/$AlCl_3$ ratio determines whether the melt is acidic (ratio<1), basic (ratio > 1), or neutral (ratio = 1). The main acid-base equilibrium reaction is:

$$2AlCl_4^- \leftrightarrow Al_2Cl_7^- + Cl^- \quad (27)$$

The aluminum electrodeposition step required for secondary AAB can occur in any MCl/$AlCl_3$ ratio environment, albeit the process will change. According to [77] irreversible deposition occurs in neutral and basic melts:

$$AlCl_4^- + 3e^- \rightarrow Al + 4Cl^- \quad (28)$$

Because the aluminum electrodeposition process in acid melts is reversible, as demonstrated [77], acid melts are suitable for secondary AAB applications.

$$4Al_2Cl_7^- + 3e^- \leftrightarrow Al + 7AlCl_4^- \quad (29)$$

Kishimoto et al. examined aluminum deposition and dissolution in an acidic chloroaluminate ionic liquid containing aluminum chloride and 1-ethyl-3-methylimidazolium chloride (EMImCl). Using a 2:1 M ratio of $AlCl_3$-EMImCl electrolyte, cyclic voltammetry revealed anodic and cathodic peaks at 0 V vs.

Al/Al^{3+}, showing that aluminum deposition and dissolution proceeded in the ionic liquid. The maximum value of coulombic efficiency (70%) was observed at 25 ºC, and it declined as the temperature increased. The scientists hypothesized that this was due to an interaction between the deposited aluminum and contaminants in the ionic liquid. Aluminum deposited from an acidic $AlCl_3$-EMImCl combination was also studied by Ingale et al. Galvanostatic charging and discharging experiments were carried out, and deposited aluminum could be cycled for 70 cycles at 100% depth of discharge. After repeated cycling at the working electrode, a black deposit formed on the copper current collector, resulting in electrode failure. The deposit was discovered to be chlorine and aluminum using scanning electron microscopy and energy dispersive X-ray spectroscopy (EDS). Ingale and colleagues employed nuclear magnetic resonance (NMR) spectra to demonstrate that fresh electrolyte had solely $AlCl_4^-$ as an electroactive species, but after 50 cycles, both $AlCl_4^-$ and $Al_2Cl_7^-$ were present in roughly equal proportions. This shows that obtaining the reversibility in Equation (29) through repeated cycles will be difficult. The physicochemical properties of these first-generation ionic liquids make them unsuitable for AAB applications. For example, the 2:1 M ratio $AlCl_3$-EMImCl electrolyte has an electrical conductivity of 1.7 S m^{-1} at 30 ºC [116], but 4 M NaOH has an electrical conductivity of about 40 S m^{-1} at the same temperature [117]. Because chloroaluminates are exceedingly hygroscopic, they must be used with dry oxygen or dry air at the cathode. As a result, ionic liquids that are stable in the presence of air and water are preferred for AAB application. Since the material has shown promise in silicon-air battery applications, investigated 1-ethyl-3-methylimidazolium oligo-fluoro-hydrogenate (EMIm $(HF)_{2.3}$) as a main AAB electrolyte. Previously, explored the properties of EMIm $(HF)_nF$ for n = 1.0-2.6. The electrochemical window, defined as the difference between the cathodic and anodic limits, which are the potentials at which reduction and oxidation of the electrolyte components occur correspondingly, was shown to trend slightly downward as n increased. Finally, n = 2.3 was chosen since the material proved to be hygroscopic for n 2.3. Aside from air and water stability, this ionic liquid electrolyte also has electrical conductivity approaching 10 S m^{-1} and low viscosity [77]. Unlike organic solvent electrolytes used in lithium batteries, the EMIm $(HF)_{2.3}$F electrolyte may disturb the passive oxide layer through a $H_2F_3^-$ species to activate the aluminum. Gelman's work used aluminum (99.997%) foil as the anode and porous carbon as the cathode. For ionic liquid electrochemistry, the ferrocene/ferrocenium (Fc/Fc^+) reference electrode [73] was created. In half-cell potential dynamic tests, open circuit potential values relative to Fc/Fc^+ were obtained for both electrodes. The results (-1.1V for the Al anode and +1 V vs. Fc/Fc^+ for the carbon cathode) suggested that this AAB system had a cell rest potential of 2.1V. Linear polarization tests were used to assess the corrosion current density in EMIm $(HF)_{2.3}$F, and the observed value of 25 μA cm^{-2} was minimal when compared to that seen with aqueous alkaline electrolytes. Discharge measurements with current densities ranging from 0.1 to 1.5 mA cm^{-2} found a maximum charge capacity

of 160 mAh, compared to the aluminum foil anode's estimated capacity of 227 mAh. The study of anode surface morphology revealed that holes caused by aluminum dissolution grew in diameter with increasing discharge current density (20-50 nm diameter at 0.1 mA cm^{-2} vs. 200-400 nm diameter at 1.5 mA cm^{-2}). The accomplishment of 70% theoretical discharge capacity with exceptionally low corrosion current density indicates the viability of ionic liquid AAB electrolytes to some extent.

Gelman et al. [118] advanced the development of the EMIm $(HF)_{2.3}$F electrolyte. The authors established a steady anode potential of 1.15V vs. Fc/Fc+ following an initial reduction in voltage ascribed to surface activation of the aluminum by oxide layer dissolving and formation of a stable layer of corrosion products using the same electrode materials as in the previous study [119]. In a half-cell arrangement, impedance spectroscopy indicated the presence of an Al-O-F layer formed by the interaction of the oligofluorohydrogenate electrolyte with the aluminum surface. The creation of this Al-O-F layer allowed aluminum breakdown and significantly reduced corrosion. However, FTIR spectroscopy on the electrolyte throughout a series of discharge cycles revealed the presence of water, with moisture content rising as discharge duration increased. Gelman and colleagues proposed two probable explanations for the existence of water. To begin, water might be absorbed into the electrolyte as a function of time during ambient exposure. The second theory is an aluminum corrosion process, in which water is a probable byproduct of anode deterioration in EMIm $(HF)_{2.3}$F. The reduction in electrolyte conductivity seen with discharge cycling was attributed to parasitic interactions between aluminum ions and the electrolyte. Despite these obstacles, cathode performance limits (poor wetting, Al_20_3 precipitation) had the greatest influence on obtaining full cell capacity, and the aluminum anode paired with EMIm $(HF)_{2.3}$F electrolyte was deemed worthy of further investigation. Levy et al. [120] developed a hybrid ionic liquid-propylene carbonate electrolyte for primary AAB application more recently. The ionic liquid tetra-butyl ammonium dihydrogen trifluoride (TBAH_2F_3) was combined with propylene carbonate in different proportions (PC). The activating species ($H_2F_3^-$) of TBAH_2F_3 was predicted to be the same as that of EMIm $(HF)_{2.3}$F. The idea was to employ a dry ionic liquid containing an active oligo-fluorinated species, which would result in an activation and discharge process with PC delivering lower viscosity and higher electrical conductivity. The goal was to make cell activity independent of the concentration of activating species in the electrolyte. Except for the use of aluminum as the reference electrode, the experimental apparatus and materials were comparable to those employed by Gelman and colleagues [118&119]. At 22.5 ºC, electrolyte conductivity was measured as a function of propylene carbonate concentration.

Because of the impact of decreased viscosity, conductivity improves with increasing propylene carbonate concentration up to 25% (by volume). From this point on, conductivity decreases as the effect turns to the dilution of conducting species. In TBAH_2F_3 electrolyte, open circuit potential tests revealed an instantaneous

reduction in anode potential upon exposure, indicating activation via rupture of the aluminum surface oxide layer. As a $Al_xO_yF_z$ contact formed on the metal surface, the potential rose slightly and stabilized. A cell rest potential of 2.1V was measured, which is comparable to the value obtained when using the EMIm $(HF)_{2.3}$F electrolyte [118&119]. However, discharge studies at low current density revealed a significant increase in capacity for TBAH_2F_3-PC (50 vol% PC) electrolyte over EMIm $(HF)_{2.3}$F. At 0.1 mA cm^{-2}, 65% of the theoretical capacity was attained, compared to 14.5% for EMIm $(HF)_{2.3}$F at the same current density. The reduced influence of parasitic aluminum corrosion processes at the aluminum anode for TBAH_2F_3-PC was attributed to this. Even with propylene carbonate added, the electrical conductivity of TBAH_2F_3 is much lower than that of EMIm $(HF)_{2.3}$F, as evidenced by a lower (1.55 V) discharge voltage recorded at 0.1 mA $cm^{-2}$for TBAH_2F_3-PC (50 vol% PC) than that detected (1.7 V) for EMIm $(HF)_{2.3}$F. Levy and colleagues identified water in increasing proportions in the TBAH_2F_3-PC electrolyte by using FTIR-ATR as discharge cycles progressed. They suspected, like Gelman et al. [118], that water was absorbed via ambient air exposure or formed as a corrosion reaction product. The rise in electrical conductivity seen with the addition of propylene to TBAH_2F_3, as well as the higher discharge capacity compared to EMIm $(HF)_{2.3}$F, were shown as potential paths for future AAB ionic liquid electrolyte development.

As several charge/discharge performances were seen, over potentials at the cathode were greater than the electrolyte's potential stability. To fully exploit the battery's capabilities, improved air cathode performance was deemed required. Bogolowski and Drillet [121] established the viability of a rechargeable AAB cell using an AlCl_3-EMImCl electrolyte, an Al foil anode, and a Pt/C gas diffusion electrode. At a current density of 100 A cm^{-2}, charge/discharge cycles were performed. After attaining consistent cell voltage plateaus of 2.1 and 1.3V, respectively, the best cell performance in terms of overvoltage was obtained during the first 6 cycles, with energy efficiency approaching 62%. After ten cycles, there was an increase in over potential during discharge stages. The scientists hypothesized that this was due to electrolyte degradation and the presence of residual moisture in the cathode's air input, which may have interacted with chloroaluminate species to create Al$(OH)_3$ and chloric acid, thus passivating the Al foil surface. An average capacity of 0.76 mAh was observed during riding. The electrolyte capacity was determined to be 56 mAh, resulting in a gain of just 1.4% of theoretical capacity. Later, Bogolowski and Drillet evaluated [122] a variety of different AlCl_3-based ionic liquids for secondary AAB applications. Mi:$AlCl_3$combinations in a 1:1.5 M ratio were used to create two deep eutectic solvent electrolytes, where M1 = acetamide (C_2H_5NO) and M2 = urea (CH_4N_2O). The third electrolyte was a 1.5:1 M $AlCl_3$-EMImCl combination. A secondary complete cell was built with a Pt/C cathode. In a first charging process, aluminum from the electrolytes was deposited onto pyrolytic graphite substrates to generate the aluminum anodes. Each electrolyte was subjected to 35 cycles of operation, with reversible capacity decreasing in all cases after 10 to 15 cycles. Only a small percentage of the available Al in the electrolytes is deposited. The cell voltages were in the 1 V-1.5 V range. At 0.1 mA cm^{-2} current density,

the acetamide and urea variations obtained discharge capacities of 0.6 mAh, while the $AlCl_3$-EMImCl variant was roughly one-third less at 0.4 mAh. The scientists assumed that the acetamide and urea versions were less vulnerable to residual moisture, despite using dried, synthetic air in the cathodes throughout all trials. In one study, Mori [123] investigated byproduct formation/accumulation on electrodes in rechargeable AABs with a 2:1 M ratio of $AlCl_3$-EMImCl ionic liquid electrolyte. The use of a non-oxide ceramic (TiC) cathode material was demonstrated to decrease the development of $Al(OH)_3$and Al_2O_3 when compared to an activated carbon (AC) cathode. Cycling stability was generally steady after 50 cycles, with capacities of 444 mAh g^{-1} (1st cycle) and 424 mAh^{-1} (50th cycle) when charged to 1 V and discharged to 0.2 V at 0.5 mA cm^{-2} current density. X-ray diffraction measurements revealed that Al and Cl buildup was lower on TiC cathodes compared to AC cathodes, albeit the cause of the lower byproduct generation was not revealed. Mori [124] created a rechargeable AAB by combining a 2:1 M ratio $AlCl_3$-EMImCl electrolyte with an Al 1050 alloy anode and a metal-organic framework (MOF) cathode with aluminum terephthalate (AT) as the active material. Separately, the performance of an activated carbon (AC) cathode was compared to that of a MOF cathode. Cell voltages were close to 0.6 V in both cathode designs. The cell capacity of the AC cathode cell reached over 150 mAh g^{-1}after the first cycle but decreased to approximately 30 mAh g^{-1}after 25 cycles. The MOF cathode cell, on the other hand, achieved around 30 mAh g^{-1} in the first cycle and maintained constant performance through 25 cycles. In aqueous AAB cells, typical byproducts ($Al(OH)_3$, Al_2O) were not found. Despite the low activity of the AT active material, stability was connected to access to open metal sites in the consistent channels and large surface area of the MOF structure. Mori proposed that a more active cathode material in a MOF build would benefit AAB cells.

5.2.4 Semi-solid and solid electrolytes

Leakage from the battery assembly is a possible issue with liquid electrolytes, having obvious consequences for performance and operational life. The use of solid electrolytes in main AAB designs is a continuing area of study [125]. Armand et al. explored the notion of a solid polymer as a secondary battery electrolyte in 1979 [126], but its applicability to AAB designs has just recently surfaced. Hibino et al. [127] studied a solid anhydrous hydroxide ion conductor, $Sn_{0.92}Sb_{0.98}P_2O_7$, for secondary AAB application in 2013. This chemical, which was previously used in alkaline fuel cells [128], provides hydroxide ion exchange capacity through charge adjustment via partial replacement of antimony (Sb^{5+}) for tin (Sn^{4+}). This electrolyte, an aluminum plate anode, and an air cathode with a Pt/C catalyst were used to build an AAB cell. Discharge capacity varied from 800 to 1000 mAh g^{-1} at current densities ranging from 0.2 to 1.9 mA cm^{-2}. (Al). The open circuit potentials of the cells ranged from 1.53 V to 1.67 V. Although aluminate deposition on the anode after charging suggested a lack of total reversibility, a part of the aluminate species formed during discharge was converted to aluminum metal during recharge at 3.5 V. Mori [129] employed a solid electrolyte based on a deep eutectic solvent (3:2:1:1 M

ratio of $AlCl_3$, urea, carboxymethyl cellulose, and glycerin) in a secondary AAB cell with an aluminum anode and a cathode composed of titanium nitride and polyvinylidene difluoride in a 1:0.3 M ratio. The cell was subjected to 50 charge-discharge cycles at 0.1 mA cm^{-2} current density and cutoff voltages of 0.2V and 1.5V. Capacity was low in the first cycle (35.8 mAh g^{-1}) but stayed at 35.0 mAh g^{-1}g 1 or above during a 50-cycle test, indicating consistent functioning. The Al anode's X-ray diffraction patterns indicated no existence of Al$(OH)_3$ or Al_2O_3, as would be expected in aqueous systems, while the air cathode did grow a layer, most likely of NaCl and NH_4Cl, which did not appear to influence cathode performance. The process for aluminum deposition and stripping in the cell was detailed in Equations (29) in a manner similar to that for chloroaluminate melts. Despite the fact that these studies show that solid electrolytes are feasible for rechargeable AAB design, limited capacity from bulk and interfacial impedance between the electrode and solid electrolytes [130] remain key challenges.

5.3 Aluminum-air battery design considerations

In recent years, researchers have included non-flow AAB designs into coin cells for testing, like those that have long been used in commercial ZAB cells. Alva and colleagues [131] created a coin cell AAB using Al anodes made from soft drink cans, commercially available porous carbon cathodes, a 4 M NaOH electrolyte, and polymer separators made from Arabic gum. The best results were obtained with 20% (wt.) Arabic gum in NaOH. Cell voltage began at 1.3 V and remained above 1.0 V for 1.75 hours at 1.3 mA cm^{-2} current density. Corrosion was not quantified, but visual inspection revealed anode deterioration in the absence of Arabic gum that was not evident with the electrolyte containing 20% Arabic gum.

The scientists hypothesized that this was because the Arabic gum membrane had an OH functional gro up capable of delaying ion transport via hydrogen interactions. Liu et al. [48] investigated an aqueous alk aline (2 M KOH) primary coin cell with a 99.997 pure Al anode, an air cathode, and chitosan hydrogel m embrane separators between the electrodes. To prevent corrosion, aqueous alkaline electrolyte additives (SiO_2,SnO_2 and ZnO) were applied directly to the membrane throughout separator manufacture. Cell volta ges achieved were constantly near 1.2 V and could be sustained for up to 2.25 hours before falling to 0 V. At a current density of 1.0 mA cm^{-2}, a cell with a separator containing 10% (wt.) SiO_2 had the greatest specific cell capacity of 288.5 mAh g^{-1}. This was roughly double the capacity of a cell with no addition, and was attributable to the existence of SiO23, which worked as a corrosion inhibitor when produced by the reaction of SiO_3^{2-} and KOH. Mokhtar et al. [133] investigated the use of ZnO as a polymer membrane separator addition (to polyvinyl alcohol membranes), using KOH as the electrolyte in concentrations ranging from 0 M to 8 M. The best results were obtained with PVA/4 wt.% ZnO/2 M KOH, with cell voltage maintained between 1.49 and 1.53 V for nearly 20 hours and a capacity of up to 38 mAh at 0.8 mA cm^{-2}. The benefit of ZnO addition was reflected in greater discharge voltages due to Zn oxidation

happening concurrently with Al oxidation. Zn^{2+} formed a protective coating on the metal surface, minimizing corrosion. This lengthened both the Al oxidation process and the HER overpotential. These non-flow coin cell AABs do not yet match the performance of commercial ZAB coin cells (1.4 V, 200-600 mAh) [134], but they do exhibit practicality in this consumer-friendly format.

Flow AAB designs with alkaline electrolytes have traditionally been used in practice [135] to help in the prevention of aluminate accumulation on anode surfaces during operation. Draining electrolytes during idle periods can also help to decrease self-discharge. Figure 15 depicts the essential components of such a system. The AAB cell stack circulates electrolyte, eliminating aluminate by-products from surfaces while they form. The AAB system can be run in batch or steady-state mode. The battery functions in batch mode until the dissolved aluminate in the electrolyte achieves saturation.

This is an end-of-charge state that needs electrolyte replacement. In steady-state mode, aluminum hydroxide crystallizes out of the electrolyte. When the Al anode is refreshed to mechanically recharge the battery, the particles are normally removed. Aluminum may be recovered from hydroxide crystals using the Hall-Heroult technique [77] when NaOH electrolyte is used. The commercial use of AAB devices like this began in the 1980s. Alu-power, Inc. (and Alu-power-Chloride Ltd) created solutions for emergency lighting and telecommunications backup power. One such battery can deliver 1.2 kW of electricity for up to 50 hours. It was designed to be a permanent installation, with a rectangular capacity of 165 L and a mass of 160 kilograms (355 Wh l^{-1}/365 Wh kg^{-1}). It used a 20-AAB cell stack and had a constant operating voltage of 26-30 V. Within a few seconds, the battery was self-sustaining, and it achieved full power within 30 minutes. Recently, Vegh and Alonso [77] investigated an alkaline AAB propulsion system for short-range aircraft. Using design specifications from Yang and Knickle [77] (which were greatly influenced by a 1980 work by Salisbury et al. [77], the authors estimated that each cell operated at 1.2 V with a current density of 400 mA cm^{-2}. These factors, together with aluminum's comparatively low specific power (~0.2 kWkg^{-1}), imposed limits that resulted in rather unbalanced outcomes. For example, for flying ranges less than 1150 nautical miles, the aircraft could not even carry enough electrolyte to fully drain the battery, limiting its use. The addition of a LIB auxiliary power source allowed for the adoption of a more sophisticated AAB design, although problems remained. These included an estimate that a completely LIB-powered aircraft would be more cost-effective for trips between 500 and 800 kilometers.

The usage of AAB systems for EV primary propulsion has advanced. Most notably, in 2014, Phinergy and Alcoa announced an electric vehicle with a 100-kg aluminum anode with a driving range of 1100 miles [136,137]. EV-related patent materials shed light on practical AAB design concerns. Draining the electrolyte and cleaning the anode until the wash solution achieves a predetermined pH value is part of a method for limiting self-discharge in standby mode [138]. Another method of reducing self-discharge [139] is to apply a strong polymer coating to anode surfaces to keep them separate from the electrolyte when the system is not in use. Membrane electrolysis (on-board or at a service station) and solid-liquid

separation and subsequent chemical reactions are two methods [140,141] for electrolyte regeneration. The drainage of used electrolyte from the cell and injection of an aluminum-containing slurry is reported as a method for rejuvenating the anode without disassembly [142]. The anode is reconstituted by sedimentation and compaction performed by a liquid or gas-inflated balloon. Control logic profiles include [143] current load and corrosion rate management via managing battery and electrolyte temperatures, as well as possible integration of rechargeable power sources to provide adequate power when loads exceed the AAB design maximum. AAB energy efficiency can be increased [144] by structural design that controls electrolyte flow in such a way that corrosion and parasitic losses are minimized. A hybrid power system [145] has been developed to employ corrosion-generated hydrogen in conjunction with an internal combustion engine or fuel cell. A controller might govern the corrosion rate to maximize power production from the integrated power sources. Electrolyte heat can be used in passenger temperature control systems [146]. Thus, engineering measures to alleviate AAB design difficu lties may typically be incorporated, albeit at a cost and weight penalty. Aqueous alkaline AAB primary cells have significantly better capacity and energy density than LIB cells while having cell potentials that are one-quarter to one-third of that of the LIB cell.

In alkaline electrolytes, pure aluminum has the lowest cell potential,
indicating corrosion and polarization effects. This kind of battery has mostly been employed in lowpower applications, although its usagein EVs isbeing aggressively researched. Wen et al. [147] reported a power density of 0.55 W cm^{-2} in anoxygen environment at a current density of 600 mA cm^{-2} in their cel. In laboratory settings, primary non-aqueous AAB designs have shown competitive capacity and energy density, with higher cell voltages than aqueous AAB cells, although practical current density is almost two orders of magnitude lower. Corrosion rates are significantly lower as compared to aqueous AABs, albeit at the expense of limited electrolyte conductivity. This is still a significant barrier to developing a workable non-aqueous primary AAB. Emerging rechargeable AAB cells (both liquid and solid-state) frequently employ electrolytes with chemistries similar to those found in primary cells, and thus face the same electrical and ionic transport problems. When the cells are operated at current densities of around 10^{-1}mA cm^{-2}, stable charge and discharge may be accomplished in a few tens of cycles.

LIB cells may normally be cycled around 1000 times. Rechargeable AAB designs are still in the early phases of feasibility, and more work needs to be done before practical usage is even contemplated.

CHAPTER 6

Rechargeable metal-air batteries

6.1 Zinc-air battery

Zinc-air battery has received the most positive reviews. Smee reported the ZAB idea for the first time in 1840 [148], and Maiche received a French patent for a ZAB model in 1878 [149], in which he altered the Leclanche cell [150] by swapping out the manganese dioxide cathode for a porous tank holding platinized carbon. The porous vessel was immersed in an electrolyte solution of sodium bisulfite, ammonium chloride, and sulfuric acid. With the help of a zinc amalgam anode and carbon material that absorbed oxygen from the air, a potential of 1.25 V was attained. Oxygen and hydrogen are mixed in the carbon pores by the electrolyte and zinc interaction to produce continual depolarization. The 1930s saw the first instances of this idea being used commercially. G.W A patent for an air-depolarized main battery by Heise, who worked for the National Carbon Company, was granted in 1933 [151] and was made for "continuous, heavy use. The essential elements of the Maiche cell were included, but with improved carbon and catalyst compositions and a solid electrolyte characterized as "salted paste" containing ammonium chloride in place of the liquid electrolyte. The "Eveready Air Cell" battery [152] was created by the business in 1939 for use in telephone transmission service. The Type-600 model included two series-connected cells that each provided 1.25 V and was rated at 600 Ah. They needed to be added to regular tap water at the place of usage and were designed to be transported dry. To avoid flooding, wax was added to the carbon cathode. This fundamental layout has stood the test of time. A comparable product known as the Carbonaire battery was released in 1950 by Thomas A. Edison Industries for applications needing continuous low power, such as railroad signal systems and navigation buoys. The Eveready Air Cell series remained in use until the 1960s.

The theoretical energy density of Znair battery is 1218 Wh kg^{-1} (gravimetric) and 6136 Wh L^{-1} (volumetric) [153]. However, the energy density of Znair is commonly between 350 and 500 Wh kg^{-1} in practice [154]. Their commercial devices have insufficient rate capability due to air catalyst inefficiency and are designed primarily for low-power applications such as small hearing aids. Furthermore, due to significant abilities of the air cathode, rechargeable Zn-air batteries have a low energy efficiency of 60% and 150 cycle [155]. Due to the general lack of stable bifunctional electrocatalysts and cyclable metal anodes, the cycle life of rechargeable batteries is also inadequate. When batteries are fully cycled at high currents, this weakness is increased. The rational design and engineering of both cathode and anode elements are the solutions to these difficulties [156]. However, long-standing barriers have stymied their

growth and commercialization. Zn-air batteries have only recently regained popularity, owing mostly to breakthroughs in material science and nanotechnology [157].

6.1.1 Current status and obstacles

The degradation of the Zn anode produced by water-induced parasitic reactions in the electrolyte is one of the most severe hurdles affecting battery performance. A typical Zn-air battery consists of a Zn anode, an alkaline electrolyte such as KOH, an electrically insulating separator to control ion transport, and an air cathode. Despite the alkaline electrolyte's excellent conductivity, low cost, and quick electrochemical kinetics, it produces a harsh chemical environment for the zinc electrode. This section will focus on the current challenges confronting the standard alkaline-based system, which is the foundation of many Zn-air battery articles recorded so far.

The primary design and operation of a typical alkaline-based rechargeable Zn-air battery are shown in Fig. 15. During the discharge of a Zn-air battery, the alkaline electrolyte produces zincate ions (Zn $((OH)_4^{2-})$, whereas the oxygen reduction process (ORR), $O_2 + 2H_2O + 4e^- \leftrightarrow 4OH^-$ (cathode) $Zn + 4OH^- \leftrightarrow Zn(OH)_4^{2-} + 2e^-$ (anode) produces hydroxyl ions (OH). According to $Zn(OH)_4^{2-} \leftrightarrow ZnO + 2OH^- + H_2O$, when $Zn(OH)_4^{2-}$ deposition exceeds the saturation limit, it will further degrade into insoluble ZnO and deposit on the anode surface. However, after several cycles, the ZnO passivation layer would grow more compact, progressively increasing the internal resistance and decreasing the anode's electrical conductivity. Surface passivation eventually entirely blocks ionic access, which has a negative impact on Zn consumption and reversibility [158].

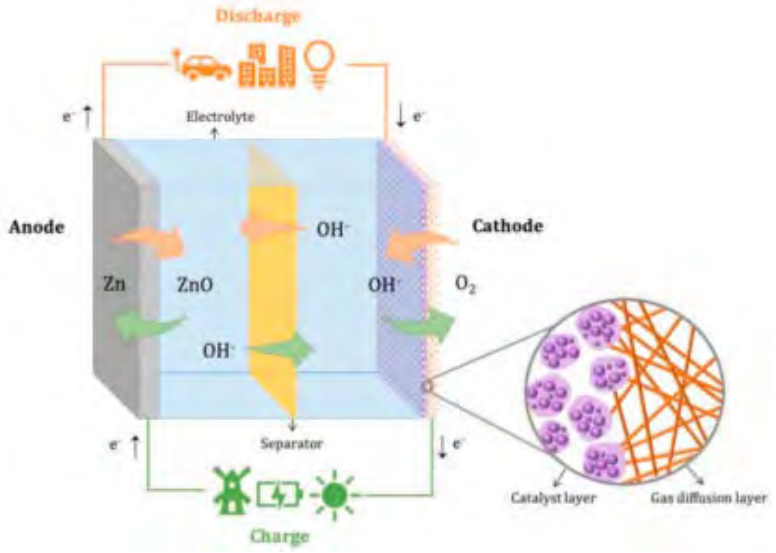

Figure 15 A rechargeable Zn-air battery structure is shown schematically from [158].

After electrochemical recharging, ZnO will be reduced back to Zn, and the cathode will experience the oxygen evolution reaction (OER). However, the Zn deposition is frequently uneven due to the unequal distribution of current densities, which would thicken certain areas of the anode and produce a

considerable change in shape. Then, Zn buildup on elevated surface heterogeneities would result in dendrites, which are pointed, needle-like protrusions. Zn dendrites can penetrate the separator, reduce battery capacity, and potentially fracture off the anode [153]. Numerous studies have been conducted on the negative impact of anode deformation and dendritic growth on battery rechargeability. (Table 3 Cathode, anode, and overall reactions of metal-air batteries)

Another phenomenon that impacts performance is the hydrogen evolution process during battery recharging. As shown in equation (30), HER would compete with the anode for electrons, decreasing the charging process's energy efficiency [159]. In addition, the HER controls how quickly the thermodynamically unstable Zn anode corrodes in the alkaline electrolyte. The Zn-air battery will self-discharge while at rest, reducing its shelf life. Additionally, dendrite-containing areas with high current densities are where HER mostly occurs. Anode deterioration would be hastened further because hydrogen creation frequently results in convective electrolyte flow [158]. One of the most important problems impacting the cycle lifespan of the Zn-air battery at the moment is Zn anode failure brought on by passivation, shape change, dendritic development, and hydrogen evolution in the aqueous alkaline electrolyte.

$$2H_2O + 2e^- \leftrightarrow 2OH^- + H_2 \quad (30)$$

It is also important to consider any potential difficulties caused by the air cathode's interaction with the electrolyte. Because water is used in the cathode, the aqueous electrolyte evaporates over time, increasing the concentration of $Zn(OH)_4^{2-}$ ions and hastening anode deterioration. Or, even worse, the battery might stop working when the electrolyte dries out. Additionally, it is frequently noticed that water vapor will build up and diffuse out of the air cathode, creating cathode flooding. This is because the catalyst layer of the cathode must be wetted to enable the ORR. This causes issues with mass transportation, accelerates electrolyte evaporation, and increases the cell over potential. Although the air cathode is currently covered in a hydrophobic gas diffusion layer to prevent cathode flooding (Fig. 15), a more integrated electrode design is preferred. Additionally, electrolyte reactions with carbon dioxide in the surrounding air would result in the production of insoluble carbonates such as potassium carbonate (K_2CO_3), which might obstruct oxygen transport when deposited onto the air cathode and reduce the Zn-air battery's energy efficiency [160].

More significantly, the sluggish redox pathways at the air cathode are a problem for battery efficiency. Strong oxygen bonds make the four-electron oxygen chemistry depicted in Equation ($O_2 + 2H_2O + 4e^- \leftrightarrow 4OH^-$) notoriously slow, resulting in significant overpotentials in the ORR/OER. To speed up the kinetics of the oxygen reaction, researchers are now investing a lot of time and energy into the creation of bifunctional oxygen catalysts. The most recent Zn-air battery discharge voltages, nevertheless, are still less than the 1.66 V theoretical value under ideal circumstances. In the meantime, to stop the reactions, a recharge voltage of 2 V or more is frequently needed [153]. The large discharge-charge voltage gap and the low stated round-trip energy efficiency of many Zn-air batteries are indications of this. The ratio of usable

energy collected by the battery may also be determined by dividing the discharge voltage by the charge voltage for a specific current density. This is known as the round-trip energy efficiency. To encourage the practical use of rechargeable Zn-air batteries, it is also necessary to increase the inadequate energy efficiency during battery cycling in addition to reducing the discharge-charge voltage gap.

6.1.2 Recent advancements

In order to improve battery performance, the air catalyst and cathode design must be improved. Because ORR is a slow reaction, the air cathode in metal air batteries is the performance limiting electrode. This reaction mostly occurs at the triple-phase boundary at the air cathode, where the solid electrode is continuously connected with liquid electrolyte and gaseous O_2. As a result, using active air catalysts that boost ORR kinetics and designing suitable electrode architecture to widen the triple-phase boundary will significantly improve battery discharge performance. Fortunately, current information from alkaline fuel cells can be easily transferred to help with Zn-air battery development. Air catalysts that have worked well in the past are also viable prospects for the future. Over the last years, a wide range of materials have been explored as air catalysts, including precious metals (e.g., Pt and Ag), nonprecious metal oxides (e.g., MnOx and CoOx), and even metal-free carbonaceous materials (e.g., nitrogen-doped carbon nanotubes or graphene).It's important to note that in the concentrated alkaline electrolyte (e.g., 30 wt. percent KOH) commonly used for Zn-air batteries, the ORR activity of Pt, which is often used as a benchmark material, is suppressed due to its high surface coverage of OH ad species and surpassed by many nonprecious metal based materials [159].

6.1.2.1 Zinc anode additives and surface modification

To extend the cycle life of the Zn-air battery, many research investigations have concentrated on improving the reversibility of the Zn anode. Researchers have effectively addressed dendrite formation, passivation, hydrogen evolution, and corrosion by thoroughly examining anode design through anode additives and structural adjustments.

With alloying and chemical coating, the use of anode additives may be divided into inorganic and organic additives. Metals including bismuth, lead, nickel, and cadmium are able to block the HER because they have greater chemical stability [161]. Additionally, by initially reducing the metal ions during battery charging, a higher positive electrode potential allows for more uniform current distributions to promote the following deposition of Zn, which inhibits dendrite formation [158]. The incorporation of these metals and their oxides into the Zn anode has therefore been studied. Bismuth and its oxides have become popular additive options because of their high electrical conductivity and thermal stability as well as their capacity to create a solid electrolyte interface (SEI) on the Zn anode surface that lowers corrosion and passivation while boosting electrolyte access [162,163]. Jo et al. recently created a

Zn-Bi alloy in a primary Zn-air battery that had a high corrosion prevention effectiveness of 91.5% and a discharge capacity retention of 99.5% [161]. In another study, Aremu et al. employed a Zn anode covered with bismuth oxide, potassium sulfide, and lead oxide additions in a secondary battery, achieving dendrite-free cycling with higher capacity and no passivation [164].

Other metallic additions, including aluminum oxide, copper oxide, and titanium oxide, have also been investigated, and have all exhibited performance-enhancing benefits on the Zn-air battery by generating a protective anodic layer to prevent spontaneous side reactions [165]. Zhang et al. recently produced ZnO@TiN_xO_y core, shell nanorods as the anode, with the TiN_xO_y coating efficiently mitigating Zn dissolution, lowering internal resistance, and expediting charge transfer, as shown in Fig. 15a-e. The thin TiN_xO_y layer effectively inhibited larger $Zn(OH)_4^{2-}$ molecules while allowing water and OH^- access to the anode, resulting in a battery with a consistent discharge capacity of 508 mAhg^{-1}over 7500 cycles [166].

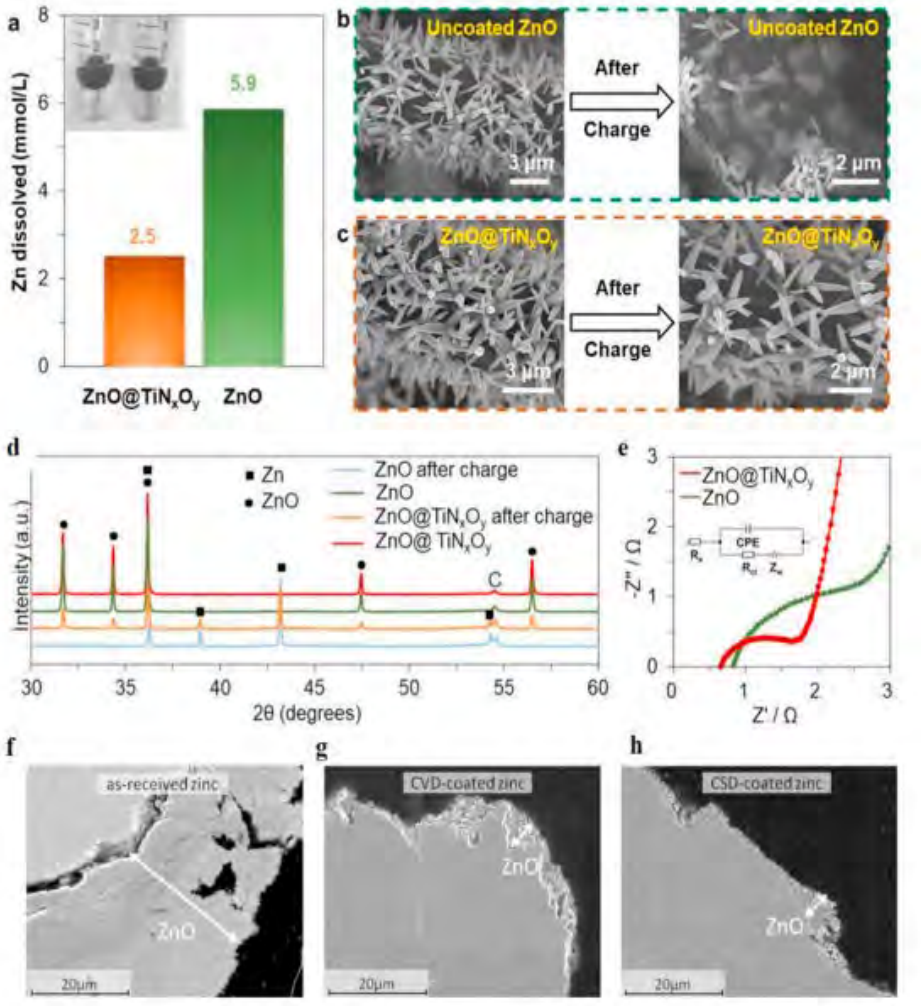

Figure 16 A review of the research on the effects of anode additives e (a) Zn dissolution in 4 M KOH solution, (b)–(c) SEM images taken before and after charging, (d) Pre- and post-charge XRD characterization, and (e) EIS data using ZnO@TiNxOy nanorod as anodes and uncoated ZnO. Reproduced with Elsevier's permission [166]. The thickness of the passivation layer is depicted in (f)-(h) SEM images, and (f) uncoated Zn, (g) CVD-coated Zn, and (h) CSD-coated Zn after discharge. Reproduced with Elsevier's permission [167].

Silica coatings were examined as a safer and more ecologically friendly alternative to metal-based additives. Silica coatings, such as an SEI, enable the formation of a $Si(OH)_4$ gel over the anode, limiting $Zn(OH)_4^{2-}$ ions and inhibiting ZnO precipitation. As illustrated in Fig. 16 f-h, Schmid et al. presented a silica-coated Zn anode made by chemical vapor deposition (CVD) and chemical solution deposition (CSD) techniques that lowered HER by 40% and prevented passivation. In the Zn-air battery, however, only two cycles were sustained [167]. The brief effects of silica-based coatings on Zn-air battery extended cycle stability are unknown.

Organic additives, on the other hand, such as polyvinyl alcohol (PVA), sodium polyacrylate (PANa), and polyaniline (PANI) hydrogel, have been shown to reduce corrosion and self-discharge [168]. Organic coatings are more controllable, simpler to fabricate, less expensive, and more ecologically benign than inorganic anode coatings. Cellulose has also been shown to be more effective than lead oxides in dendritic removal. Zhang et al. recently proposed a unique ZnO/PVA/β-CD/PEG composite electrode with polymer binders, resulting in a robust 3D structure that encapsulates the Zn metal and reduces anode deformation while delivering over 80 dendrite-free cycles [169]. Nonetheless, organic additions may raise battery impedance by serving as insulators and impurities [170]. In general, the use of additives may reduce the specific energy of the battery while increasing weight and costs; consequently, cautious additive application and anode composition optimization are critical.

The application of inorganic and organic anode additives has demonstrated significant benefits in suppressing parasitic anodic reactions by forming an SEI-like protective barrier to restrict direct electrolyte access and immobilize zincate ions. However, most papers do not include enough information on the underlying processes linked with the specific additive material, making it impossible to determine the distinct mechanism and efficacy of each type of additive in comparison to others. Because the majority of current research emphasis has been concentrated on cathode materials, the number of studies on anode additives is equally limited. More thorough research into the specific impacts of each coating material on anode deterioration and battery cycle stability is urgently encouraged.

6.1.2.2 Structural modification

Changing the anode morphology is an efficient way to increase activity and further manage anode deformation. A structure with overly wide holes may reduce electrode resistance and corrosion rate, but with careful adjustment, the increased surface area may improve mass transfer and electrochemical activity. Lin et al. discovered that a porous Zn anode electroplated at 500 Hz could deliver 60% more power density with a doubled specific surface area [171]. Tan et al. also mentioned an electroplated Zn on carbon paper with a battery discharge capacity of 814 mAh$g^{-1}cm^{-2}$ at 10 mAcm^{-2}. However, due to the breakdown of the electroplated Zn, the battery could only persist for one cycle [172].

Some researchers have recently thermally treated the Zn anode to generate 3D porous and sponge-like topologies for improved reversibility. The new 3D shape facilitates more uniform current distribution and more effective ionic and electron channels than standard powder-based zinc electrodes. The compression tolerance of sponge-like electrodes has further expanded the possibilities for battery applications in flexible and elastic wearable devices. Pan et al. produced a sponge-like Zn-air battery with a low discharge-charge voltage gap of 0.657 V at 5 mA cm^{-2} and a remarkable power density of 260 mW cm^{-2} with high mechanical endurance features using electrodeposited Zn nanosheets on nitrogen-doped carbon foams [173].

Although anode additives and 3D porous structures have been shown to be effective solutions for mitigating anode deterioration, many studies have focused on corrosion suppression and HER inhibition without reporting overall battery performance metrics such as cycle stability, peak power density, and energy efficiency. The cycle lifetimes of Zn-air batteries were frequently inadequate when galvanostatic discharge-charge operations were evaluated. As a result, more extensive research investigations are needed in the future to promote long-term anode reversibility for actual operations.

6.1.2.3 Electrolyte

Another critical focus of current research efforts in rechargeable Zn-air batteries is the creation of electrolytes. Researchers have improved the standard alkaline electrolyte using additions, polymer gel materials, and circulation designs to boost anode reversibility and water retention rate. To explore with more efficient oxygen redox chemistries, more creative ways include generating alternate electrolytes such as quasi-neutral electrolytes and non-aqueous solutions.

6.1.2.3.1 Non-aqueous electrolytes

Non-aqueous electrolytes have recently been proposed to improve battery performance by reducing water evaporation and parasitic reactions. Liu et al. achieved a high coulombic efficiency of 96.9% and an ultralow discharge-charge voltage gap of 0.39 V over 110 cycles using a molten carbonate electrolyte in a Zn-air battery. However, the cyclic operation was carried out at 550ºC to keep the electrolyte molten, which is not feasible for room temperature applications [174].

Ionic liquid, on the other hand—a molten salt that persists in liquid form at a normal temperature—has become an appealing choice due to its great stability, low vapor pressure, and non-volatility. Ingale et al. recently established the water retention and dendrite removal capabilities of the DEMATfO ionic liquid in their research. Without the use of water as a solvent, the ionic liquid enabled a high-performance Zn-air battery with a 0.6 V discharge-charge voltage gap over 700 hours of steady cycling. Although the power density was unacceptably low due to the electrolyte's limited ionic conductivity [175]. Despite their promising performance, the primary limitations of ionic liquids are their poor conductivity, high

viscosity, and excessive cost, which limit their ability to replace traditional alkaline electrolytes in Zn-air batteries [176].

However, significant progress in reducing anode deformation, water evaporation, and carbonation, the average cycle life of Zn-air batteries remains far from satisfactory. A few recent experiments achieved round-trip energy efficiency of more than 70%, but the majority remained modest. The power density of neutral and non-aqueous Zn-air batteries is much lower than that of ordinary alkaline Zn-air batteries due to their weak conductivity. Although, cyclic stability may be greatly improved by avoiding side reactions like carbonation and corrosion. This is evident in research by Sumboja et al., who compared a ph-7 chloride-based Zn-air battery to a standard alkaline cell. The cyclic stability was increased from 245 cycles to 540 cycles, but the voltage gap quadrupled and the PPD fell eightfold [177]. Although these alternate electrolytes have immense promise, their poor conductivity necessitates more extensive experimental and model-based research.

6.1.2.3.2 Quasi-neutral electrolytes

The investigation of chloride- and sulfate-based electrolytes has recently resulted in the development of a new class of quasi-neutral Zn-air batteries as an alternative to the traditional alkaline electrolyte. The Leclanche electrolyte, a ZnCl_2-NH_4Cl-based solution with strong ionic conductivity, is the most typical example. The electrolyte's neutral pH inhibits dendritic growth and carbonate production by reducing Zn solubility and slowing carbon dioxide absorption [178]. In the gentler chemical environment, the electrodes are also more resilient. However, Zn is less active, and the oxygen redox kinetics are slower in neutral electrolytes. In response, Zhang et al. most recently created a Leclanche electrolyte that contains Mn^{2+} and increases oxygen redox efficiency. This electrolyte provides dendrite-free cyclic performance for 1350 hours with a 63% round-trip energy efficiency in a Zn-air battery [179]. The Zn^{2+} ions are predicted to produce zinc complexes that promote Zn deposition and mass transfer, inhibiting dendritic development [178].

As a kind of quasi-neutral electrolyte that exists between the aqueous and non-aqueous worlds, water-in-salt electrolytes have recently attracted a lot of attention. Even though water serves as the solvent in this case, the high concentration of metal salts and the lack of free water molecules may preclude the water-induced negative reactions that are frequently observed in aqueous electrolytes [180]. Due to the distinctive solvation structure of Zn^{2+}ions, Wang et al. produced a highly concentrated Zn-ion electrolyte in 2018. This electrolyte, when combined with an air cathode, provided a battery energy density of 300 Wh kg^{-1} and cycling stability over 200 cycles at 50 mA g^{-1}. Characterization findings supported cycling without dendrites, and modeling analyses further demonstrated HER suppression [181]. This ground-breaking work has shown the compatibility and electrochemical success of water-in-salt systems in a metal-air battery, despite the fact that they are more frequently studied in the context of metal-ion

batteries. This suggests the versatility of water-in-salt systems and opens new possibilities for the development of neutral Zn-air batteries.

Sun et al. [182] recently described a $Zn(OTf)_2$ electrolyte that produced zinc peroxide (ZnO_2) via a two-electron ORR rather than the slow, traditional four-electron process by employing a different Zn salt with a smaller fluorinated anion. On the air cathode, the hydrophobic OTf^- ions produced a Helmholtz layer that was both water-poor and ion-rich, promoting highly reversible redox reactions while inhibiting parasitic processes brought on by water. With hydrophilic anions like sulfate ions, the reversible O_2/ZnO_2 reaction chemistry at the air cathode is not achievable. When compared to a Zn-air battery using a KOH electrolyte, using the $Zn(OTf)_2$ electrolyte resulted in a significant suppression of self-discharge behavior and carbonate production. Additionally, it was surprising to find that only 1 mol kg^{-1} of salt was required in this experiment to deliver a discharge capacity of 684 mA h g^{-1} for 320 cycles at 1 mAcm^{-2}, indicating that super concentrated salt is not always required [182], opening up new opportunities for less expensive quasi-neutral electrolytes. It is crucial to keep in mind that the two-electron reaction produces peroxide intermediates, which have the potential to damage carbon-based catalysts [183]. Thus, careful consideration must be given to the catalyst material for the air electrode, and a deeper understanding of the chemistry of two-electron oxygen is essential.

The neutral Zn-air batteries show great potential in cycle stability since they avoid the parasitic reactions brought on by the extremely corrosive alkaline electrolyte. Even still, publications are still in short supply and research and development are still in their early stages. In order to surpass the conventional alkaline-based Zn-air battery, neutral electrolytes frequently experience pH instability, low ionic conductivity, and high cost. More crucially, the mechanism governing anode reversibility in quasi-neutral and water-in-salt electrolytes is similarly poorly known, necessitating more thorough characterizations to support methodical testing. Finally, in order to enhance the oxygen redox kinetics, it is crucial to create appropriate bifunctional oxygen catalysts in neutral media. Neutral Zn-air batteries have a lot of potential, but there are still significant problems that need to be fixed before they can reach their full potential.

6.1.2.3.3 Polymer gel electrolytes

Polymer gel materials have been added to alkaline gel hybrid electrolytes to minimize Zn anode failure and electrolyte water loss, creating quasi-solid-state, flexible Zn-air batteries with increased cycle stability. While PVA-based electrolytes have received a great deal of attention, more recent studies have found that alternative polymer gels, such as PANa, polyacrylic acid (PAA), and polyacrylamide (PAM), perform better electrochemically and retain more water [184].

A PVA, PAA, and GO co-crosslinked, KI-containing, alkaline electrolyte (KI-PVAA-GO) was recently demonstrated by Song et al., allowing flexible Zn-air batteries with low charging potentials of

1.69 V and 1.24 V at 2 mAcm^{-2}, a reliable cycling profile over 200 h, and an energy efficiency of 73%. Polymer gel electrolytes are frequently combined with extremely hydrophilic and alkaline tolerant additives, such as KI, quaternary ammonium, and cellulose, to increase their ionic conductivity and stability since gelling frequently hinders ionic mobility in the electrolyte [185]. Huang et al. reported the formation of a solid electrolyte interface in a new PANa-based electrolyte with cellulose additions, which promoted ionic transport and resulted in stable, dendrite-free battery operation through 800 cycles in 160 h [186]. In solid-state Zn-air batteries for a smart watch, Fig. 17 shows how the solid electrolyte interface forms and how polymer gel electrolytes are used in practice.

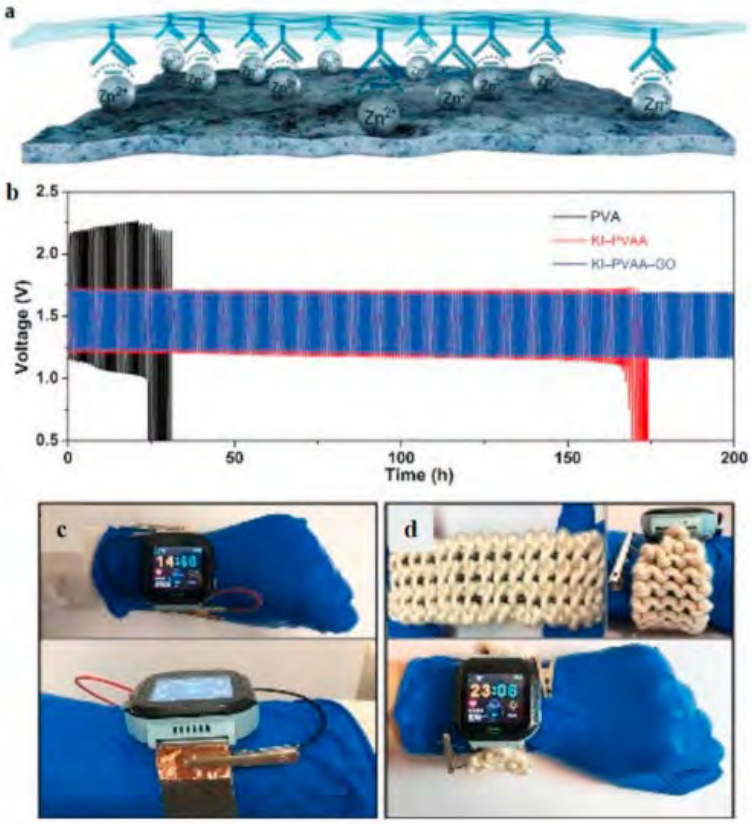

Figure 17(a) Schematic representation of the solid electrolyte contact that is created between the PANa electrolyte and the Zn anode Reproduced with John Wiley and Sons' permission [186], b) Discharge-charge curves for sandwich-type Zn-air batteries using PVA, PVA, (c–d) .It is shown a flexible Zn-air battery used to power a smart watch in a (c) sandwich-type and (d) cable-type configuration. Reproduced with permission from John Wiley and Sons [185].

However, in order to expand the operational lifetimes of commercial wearable electronics, significant improvements in ionic conductivity and mechanical resilience are required. Because of the volatility of organic solvents and the poor solubility of Zn salts, polymer gel electrolytes are still not totally practicable for use in practical Zn-air batteries, despite solid-state batteries being considered to be far safer than flammable liquid batteries [178].

6.1.2.4 Bifunctional oxygen catalyst

Recent Zn-air battery research has largely concentrated on improving the structural and material design of bifunctional oxygen catalysts, which can speed up the kinetics of electrochemical reactions at the air cathode while enduring alternating cycle operations. Historically, catalysts have been made of expensive and non-renewable noble metals like Pt, Ir, and Ru. Commercial Pt (Pt/C) supported by carbon demonstrates higher ORR activity, but its OER performance is subpar due to the formation of an insulating oxide layer [187]. As a result, transition metal-based catalysts have emerged as a plentiful and affordable substitute in recent years.

Due to their incompletely filled d-orbitals, transition metals (Co, Mn, Fe, and Ni) and their compounds offer a variety of possible oxidation states, which supports the electrochemical activity of the catalyst [188]. Transition metal alloys can improve the catalytic activity of electrodes by combining several transition metal species in a synergistic manner [189,190]. On the other hand, transition metal oxides, such as oxides of monoxide, dioxide, perovskite, and spinel, can have various lattice or crystal structures. Because of their abundance of oxygen vacancies, ABO_3 (A: 12-fold oxygen-coordinated metal; B: 6-fold oxygen-coordinated transition metal) and spinel oxides (AB_2O_4) provide enhanced active sites and flexibility for electronic manipulation [191,192]. As an illustration, consider the well-studied cobalt oxide (Co_3O_4), in which the presence of Co^{2+} species in tetrahedral sites encourages OER activity while the presence of Co^{3+} in octahedral sites aids in the adsorption of oxygen intermediates during ORR [193]. In recent years, research has increasingly focused on other derivatives of transition metals. Transition metal nitrides have more electron conductivity than transition metal oxides [194], but transition metal phosphides have more potent OER catalytic activity [195]. Additionally, transition metal sulfides provide quick charge transfer and effective intermediate oxygen adsorption [196].

However, transition metal complexes on their own are susceptible to particle aggregation in severe redox conditions and strong electrolytes. The creation of metal-carbon composites as dual-purpose oxygen catalysts for zinc-air batteries was motivated by this. Metal-based nanoparticles are often anchored or grown directly on the functional groups of carbon substrates like carbon black and porous carbon to create metal-carbon composites. Carbon supports have the potential to improve stability, electron conductivity, active site dispersion and utilization, as well as provide modulation flexibility [190,197].

Metal-free carbon-based catalysts are being researched as a way to further reduce costs and environmental implications by avoiding the use of any metals, notwithstanding their rarity [198]. Furthermore, research has started on using biomass as a sustainable carbon source for carbon-based catalysts due to worries about the environment and the cost of their traditional production from fossil fuels [199]. Table sugar and bamboo leaves have recently been used as eco-friendly biomass supplies for the carbon-based catalyst in rechargeable Zn-air batteries [200,201]. However, pure metal-free carbon has

few active sites and is susceptible to corrosion. To improve catalytic activity and stability, their electrical and morphological structures must be altered [202].

To achieve this, structural control and defect engineering have been applied to enrich active sites, speed up electron transport, and modify electronic structures in order to maximize the activity of bifunctional oxygen catalysts. Recent years have seen a rise in interest in promising approaches such as metal organic frameworks and single-atom catalysts, which has led to lengthened cycle operations and decreased charging potentials in Zn-air batteries.

Charge transfer, molecule reconstruction, bond breaking, and creation are just a few of the surface reactions that take place on the catalyst surface or interface in the ORR and OER catalytic processes. In this regard, the catalytic performance is greatly influenced by variables like the density of exposed active sites, electrical conductivity, and reaction energy barrier of the electrocatalyst surface/interface. In a recent experiment [203], graphitized carbon and transition metal sulfides were coupled to create a bifunctional catalyst for ORR and OER by encapsulating Co_9S_8 in N, S codoped carbon matrix (Co_9S_8@N, S-C), which was then employed for ZnABs. The Co_9S_8@N, S-C material, in its as-prepared state, has a significant degree of macroporous structure; this property can lead to the material having a high mass transfer capacity of gas and ionic liquid, while the large specific area can also lead to more active sites. The Co_9S_8@N, S-C materials demonstrated exceptional ORR and OER activity in the experiment; their overall oxygen redox potential difference in 0.1 M KOH is 0.647 V, significantly better than Pt/(0.78 V C+IrO_2). Tests on primary and rechargeable Zn-air batteries show that they have a specific capacity of 862 mAh $g_{Zn}{}^{-1}$ and a peak power density of 259 mW cm^{-2}. Additionally, the Co_9S_8@N, S-C-assembled ZnABs have extremely high stability; a comparison reveals that this stability outlasts that of Pt/C+IrO2-based Zn-air batteries. After 110 hours of nonstop operation, the round-trip efficiency only dropped by 4.83%, and the charge-discharge voltage gap only marginally widened by around 90 mV. However, the roundtrip efficiency of the Pt/C+IrO2-based Zn-air batteries decreased by 14.48% after 110 continuous hours of operation. According to theory, the ideal catalyst should have a medium binding strength, not too strong to desorb the products that would obstruct the catalytic surface or too weak to activate the reactant.

This study demonstrates that the adsorption energy of Co_9S_8@N, S-C on O intermediates is more advantageous when Co_9S_8 and N, S-C are combined than when they are used separately. Additionally, the density of states (DOS) further investigated the material's high activity because N, S codoped carbon layers and Co_9S_8 adjusted each other's Fermi levels, considerably enhancing the material's conductivity and facilitating the speedy flow of electrons to the active site. Moreover, theoretical simulations demonstrate that for ORR and OER, the Co_9S_8 (4 4 0) crystal plane is more active than (3 1 1). Designing highly bifunctional catalysts involves using a critical technique called exposing the (4 4 0) crystal plane of Co_9S_8.

Another research for developing a bifunctional catalyst with high catalytic activity toward both OER and HER in alkaline electrolytes in order to reduce the production cost of the resultant hydrogen is important to mention. Yu and colleagues [63] discovered that CoNi-OOH-30. After 40 hours of oxidation, the hydrogen evolution reaction (HER) and oxygen evolution reaction (OER) in alkaline solution need minor over potentials of 210 and 279 mV, Tafel slopes of 67 and 62 mV /dec, and demonstrate good stabilities. An oxygen vacancy and core-shell heterojunction integration engineering technique to build an anemone-like CoP@CoOOH core-shell heterojunction with high oxygen-vacancies supported on carbon paper (CoP@CoOOH/CP) advantages from the synergy of CoP core and oxygen-vacancy-rich CoOOH shell [75]. In neutral and alkaline environments, the derived CoP@CoOOH/CP catalyst has low over potentials at 10 mA $cm^{-2}$for HER (89.6 mV/81.7 mV) and OER (318 mV/200 mV). Furthermore, a two-electrode electrolyzer that uses CoP@CoOOH/CP as a bifunctional catalyst to reach 10 mA cm^{-2} requires only low-cell voltages in neutral (1.65 V) and alkaline (1.52 V) electrolytes.

It is important to mention that the overall-potential difference (ΔE) between the OER potential at 10 mA cm^{-2} and the ORR half-wave potential (ΔE = $Ej_{=10}$ -$E_{1/2}$) may be used to analyze the bifunctionality of an oxygen redox activity. The excellent catalytic bifunctionality is indicated by the lower ΔE value. The ΔE value of Co_9S_8 @N, S-C is 0.647 V, which is lower than that of Pt/C+IrO_2 (0.76 V), as shown in Figure 18**.** Additionally, several comparisons reveal that the Co_9S_8@N, S-C catalyst as synthesized outperforms the majority of the amazingly effective bifunctional catalysts that have been previously described [203].

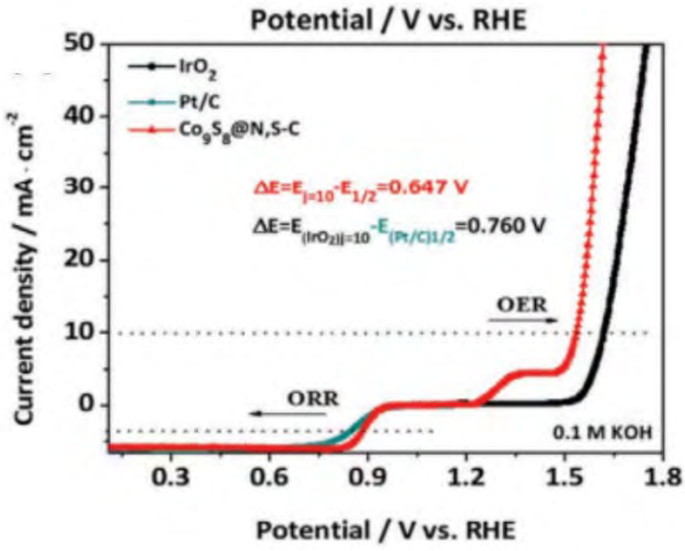

Figure 18 Comparison of the oxygen activity of the catalysts 〖Co〗_9 S_8@N, S-C, and Pt/C-IrO_2 (ΔE = 〖Ej〗_(=10) - E_(1/2)), from [203].

6.1.3 Future perspectives

Rechargeable Zn-air batteries are now more readily available thanks to recent developments, but most of them can only cycle for a few hundred hours and have a 60–70% round-trip energy efficiency. In some

instances, the discharging and charging over potentials are still considerable even when the power densities are insufficient. Additionally, the majority of reported batteries are only cycled at modest depths of discharge, which minimizes material deterioration and delays cell capacity fading [158]. Such circumstances unreasonably overstate the claimed cycle life and energy density, which do not accurately represent the battery's actual working performance. Zn-air batteries need to achieve superior long-term cycling performances under real-world operating settings in order to replace Li-ion batteries as the energy source for electric cars and consumer devices. This requires more investigation and improvement. Alternative electrolytes, sophisticated catalysts, and hybrid Zn batteries, which have already made it possible to cycle for extended periods of time, up to a few thousand hours, are some of the most promising research prospects. However, each tactic has its own drawbacks, such as those that reduce conductivity, increase complexity, and raise prices. More crucially, a common issue with many of these recent developments is the insufficient understanding of the underlying processes, which serves as the primary roadblock to future research discoveries.

Firstly, rather than continue with trial-and-error iterations in the future, a more logical design framework for bifunctional oxygen catalysts is greatly sought. For this purpose, interesting research areas that may open the door for the methodical tuning of catalysts include MOFs and single atom engineering. Future research should therefore broaden our current understanding of the specific mechanics behind MOF formation in order to provide a more systematic tailoring of catalyst materials. Future research should concentrate on stabilizing high-loading single atom catalysts, as this is currently the greatest challenge to their practical production. It is also important to investigate other innovative design concepts, such as solar-powered photoactive catalysts, which might improve battery performance and reaction kinetics, particularly for outdoor applications [204].

The majority of the recent research on Zn-air batteries have focused on the material improvement of bifunctional oxygen catalysts. As a result, this viewpoint strongly stimulates additional research efforts on the creation of electrolytes, which may have an even greater influence on the basic workings of a Zn-air battery. For instance, neutral electrolytes might fully avoid the parasitic reactions that traditionally restrict the cycle life of Zn-air batteries and are based on alkaline chemistry. The creation of improved electrolytes is crucial to creating a high-energy Zn-air battery since parasitic processes, electrolyte oxidation, and internal resistance all have a significant impact on the battery's energy efficiency. Although research on quasi-neutral electrolytes, such as water-in-salt systems, is expanding, there is still a paucity of literature on the subject, and there are few particular uses of these materials in Zn-air batteries. Having a thorough grasp of the oxygen redox chemistries and anode reversibility mechanisms in the many kinds of electrolytes, such as salts and ionic liquids containing various anion species, is essential further their development. Studies on additive materials likewise experience the same lack of characterization data in the same way. To determine the specific impacts of each

type of addition on the performance of alkaline-based Zn-air batteries, careful characterizations and analyses are required rather than blind experiments [158].

Future initiatives in mathematical modeling and dynamic simulations may also help hasten the development of both electrode and electrolyte research. Modeling contributions might efficiently exclude undesirable possibilities without time-consuming trial-and-error testing by focusing on the effective screening of novel materials and design methodologies. Experimental studies should then offer a wealth of readily available data to back up and validate these models.

The development of quasi-solid-state batteries, inspired by recent advancements like sponge-like electrodes and polymer gel electrolytes, is another potential future prospect for rechargeable Zn-air batteries that is worth mentioning. Solid-state batteries are regarded as the next-generation power source after conventional liquid batteries because of their high energy density, inherent safety, and extended lifespan [158]. Solid-state batteries provide strong potential in applications for electric car technology, in addition to powering flexible wearable electronics. Toyota intends to introduce a solid-state battery-powered electric vehicle prototype with a 500 km driving range and ultra-quick charging time in 2021. Other automakers and startups have also set manufacturing targets for solid-state batteries for 2025 [205]. Although quasi-solid-state Zn-air batteries are still in the early stages of research and their performance is currently more suited for low-power wearable devices, they might show significant potential for applications in the expanding EV sector in the future.

Finally, the future commercialization of Zn-air batteries depends critically on effective battery production. The invention of 3D-printed porous electrodes [206] and paper-based Zn-air batteries [207], as well as the emergence of modern manufacturing processes like 3D printing and laser processing in recent years, have opened up new opportunities for low-cost, scalable battery assembly. To enable personalized devices for on-demand manufacture, the notion of hand-drawn printable batteries has also been put forth [208]. However, the manufacturing process has to be effective and scalable while preserving cost-competitiveness, which is a significant hurdle at the moment. This will enhance the use of Zn-air batteries in EVs and grid-scale applications. As a result, ongoing research into electrodes, electrolytes, and bifunctional oxygen catalysts is required, with a focus on cost reduction and manufacturing effectiveness.

In the case of electrically rechargeable metal air batteries, the air cathode should be able to catalyze both ORR and its reverse process, oxygen evolution reaction (OER), with efficiency. As a result, several researchers stress the significance of creating bifunctional oxygen electrocatalysts. Despite the reduced material choices, a dozen high-performance bifunctional electrocatalysts have been produced successfully in the last decade. Alternatively, the air cathode's bifunctionality can be accomplished by properly combining various functional components. Because researchers may independently improve ORR and OER catalysts and then combine them, the second technique offers for more flexibility in air cathode design.

However, even with the best available ORR and OER catalysts, the polarization of the air cathode between charge and discharge is still so big that the round-trip energy efficiency of rechargeable Zn-air batteries at current densities relevant to practical applications would be unlikely to exceed 65 percent. In compared to standard lithium-ion technology (>90 percent), this is a significant disadvantage of metal air batteries.

Given the fact that zinc is more plentiful than lithium and it can be recycled [209], a lot of work has recently been made into the creation of a high-performing, rechargeable ZAB design. The most active metal that can be electrodeposited from aqueous solutions is zinc because of its low equilibrium potential and large over potential for the hydrogen evolution process (HER) [210]. Although there has been some effort put towards using acidic aqueous electrolytes, the activity of the air cathode catalyst might decline [211]. Low zinc solubility, which may aid to reduce dendrite formation, and extremely low CO_2 absorption, which minimizes carbonate effects, are two positive characteristics of neutral aqueous electrolytes [212]. Research is being done on the stability of pH at the electrode/electrolyte interface since locally acidic conditions at the cathode might also affect the stability and performance of the air catalyst [198]. Among aqueous electrolytes, alkaline solutions have attracted the greatest interest due to their appealing properties, which include a high ionic conductivity of the electrolyte, ideal cathode operating conditions, and a high solubility of zinc salts [77]. Carbonate formation within the electrolyte [213], zinc redistribution over charge/discharge cycling, which results in electrode morphology alters that can reduce active surface area, and uneven zinc deposition throughout charge cycles, which results in dendrite formation that can cause short-circuiting are some of the obstacles that need to be mitigated. Due to these problems, as well as hydrogen evolution and the consequences of aqueous electrolyte water evaporation, researchers are now looking at non-aqueous electrolytes for secondary ZAB systems. Non-aqueous electrolytes (such as aprotic solvents and ionic liquids) ought not to be volatile, have minimal toxicity, and have good ionic conductivity for safety and performance. Even while research on this subject is still in its early stages, several encouraging findings suggest that it might eventually be fruitful. A secondary ZAB cell with a polyaniline emeraldine cathode, zinc metal as an anode, and 0.3 M zinc-bis (trifluoromethyl-sulfonyl) imide Zn $(TFSI)_2$ dissolved in propylene carbonate as the electrolyte was examined by Guerfi et al. [77]. However, the battery demonstrated an output capacity of 148 mAh g^{-1}at 1 ºC rate (full discharge in 1 h), with a columbic performance of 99.5 percent across 2000 cycles between 0.4 V and 1.4 V. Dissolution of the zinc anode resulted in considerable self-discharge. Published works frequently reflect experimental conditions that are not necessarily typical of those anticipated in operational environments, as Masa et al. [214] stated generally for electrocatalysis. To effectively evaluate real cycling performance, Zhang et al. [215] recommend that charge/discharge cycles be performed at a current density of at least 10-20 mA cm^{-2}, with charge/discharge periods of greater than 1 h (referring to an areal capacity of at least 10 mA cm^{-2}) for a minimum of 10 cycles.

6.2 Iron-air battery

Iron is the most frequently utilized, non-toxic, and inexpensive metal, with the second most abundant metal and the fourth most abundant element in the Earth's crust, reserves 560 times that of zinc, and a price of 1/43 that of zinc [216]. Because of its adequate redox potential (0.44 V against SHE in an acidic solution and 0.88 V vs. SHE in an alkaline solution), iron metal may be utilized as an anode directly in aqueous electrolytes. Iron's greater redox potential gives it superior stability in aqueous electrolytes than zinc [217]. Iron metal has theoretical specific and volumetric capacities of up to 960 mAh g^{-1} and 7557 mAh cm^{-3} [218]. Because of the high specific capacity of iron metal, aqueous iron-metal-based batteries (AIMBBs) have a high theoretical specific capacity. Consider nickel-based batteries: the Ni-Fe battery has a greater theoretical specific capacity (224 mAh g^{-1}) than the Ni-Cd battery (181 mAh g^{-1}), the Ni-MH battery (178 mAh g^{-1} , and the Ni-Zn battery (215 mAh g^{-1}). Furthermore, iron is less prone to producing dendrites during aqueous electrolyte cycling, which is beneficial to battery safety and stability. These benefits make AIMBBs ideal for use in large-scale energy storage [219].

Fe-air batteries are electrically rechargeable, their practical energy density is substantially lower, ranging from 60 to 80 Wh kg^{-1}, which is barely equivalent to contemporary lithium-ion technology. Because of their extended cycle life (>1000 cycles), inexpensive ($100/kWh), and environmental friendliness, they are well suited for stationary energy storage, however they are clearly not ideal for pure EV applications [156].

6.2.1 Reaction mechanisms of iron anode

The composition of the electrolyte affects the electrochemical reactions of the iron anode throughout charge and discharge. The chemical conversion reaction in the alkaline electrolyte and the plating/stripping reaction in the acidic electrolyte have been postulated as the two primary reaction mechanisms of the iron anode in AIMBBs.

(i) Iron anode in alkaline electrolyte

Fig. 19 depicts a typical discharge/charge curve for the iron anode in the alkaline electrolyte. The oxidation of Fe^0 to Fe^{2+} and Fe^{2+} to Fe^{3+} are represented by the first and second plateaus throughout the discharge of the whole iron-metal battery, respectively. Two pair large peaks are visible on the cyclic voltammetry (CV) curve within a wide potential window (-1.3~ -0.3 V vs. Hg/HgO) at 0.79/-1.17 V (Ox_1/Red_1) and 0.62/-1.09V (Ox_2/Red_2), respectively.

According to equation: $Fe + 2OH^- \leftrightarrow Fe(OH)_2 + 2e^-$ ($E^O = -0.88V vs\ SHE$), the creation of $Fe(OH)_2$ is attributed to the first oxidation peak (Ox1). According to equations $Fe + 3OH^- \leftrightarrow HFeO_2^- + 2e^- + H_2O$, and $HFeO_2^- + H_2O \leftrightarrow Fe(OH)_2 + 2OH^-$, this reaction is specifically dependent on the issolution/deposition of soluble. The accompanying steep peak (Red1) and concomitant reduction peak (Red1) indicate the unavoidable parasitic hydrogen evolution process (HER). Complex transitions between

Fe^{2+} and Fe^{3+} can be seen in the second oxide/reduction processes (Ox_2/Red_2). In the reactions Eqs. $Fe(OH)_2 + OH^- \leftrightarrow FeOOH + e^- + H_2O$,

$3Fe(OH)_2 + 2OH^- \leftrightarrow Fe_3O_4 + 2e^- + 4H_2O$ $(E^O = -0.66Vvs\ SHE)$ and

$2Fe_3O_4 + 2OH^- \leftrightarrow 3Fe_2O_3 + 2e^- + H_2O$ $(E^O = -0.60Vvs\ SHE)$,

FeOOH, Fe_3O_4, Fe_2O_3 [219,220,221], or their mixes were considered as the synthesis of iron during the oxidation process. Yushin et al. identified four phases as the development, retention, fading, and failure of iron anode during cycling. The rise in specific capacity throughout the development stage is attributed to the fragmentation of iron particles, which is known as "formation" [222]. The capacity deterioration and eventual failure were caused by the production, accumulation, and final aggregation of irreversible monocrystalline, Fe_2O_3 *;* these processes are often regarded as the iron electrode's passivation characteristics. Researchers have asserted that, Fe_3O_4 is an irreversible phase. Alkaline AIMBBs function poorly at high rates and at low temperatures due to the iron anode's passivation since the irreversible product will block the iron anode's active surface. Additionally, the iron anode's practical capacity can only reach a third of its theoretical value [219], which is detrimental to the practical use of batteries. HER will take place during the charging process because to the lower over potential of HER at the iron anode and the greater negative reaction potential of the iron anode ($Fe + 2OH^- \leftrightarrow Fe(OH)_2 + 2e^-$ $(E^O = -0.88Vvs\ SHE)$ in alkaline electrolyte compared to that of HER ($2H_2O + 2e^- \leftrightarrow H_2 + 2OH^-$ $(E^O = -0.83Vvs\ SHE)$). The iron anode may spontaneously corrode while it is charged as a result of the HER, which will produce a negative self-discharge process. Nickel-iron alkaline batteries typically self-discharge at a rate of up to 20% per month. The parasitic HER while charging will also lose some energy, which limits the total Coulombic efficiency of the alkaline AIMBBs to an extremely low level (50–70%). Additionally, the HER results in constant electrolyte loss, rendering the cells unsuitable for seal packaging and free maintenance, severely restricting the applications of batteries. Therefore, to maximize the electrochemical performance and applicability of alkaline AIMBBs, HER must be suppressed on the iron anode [219].

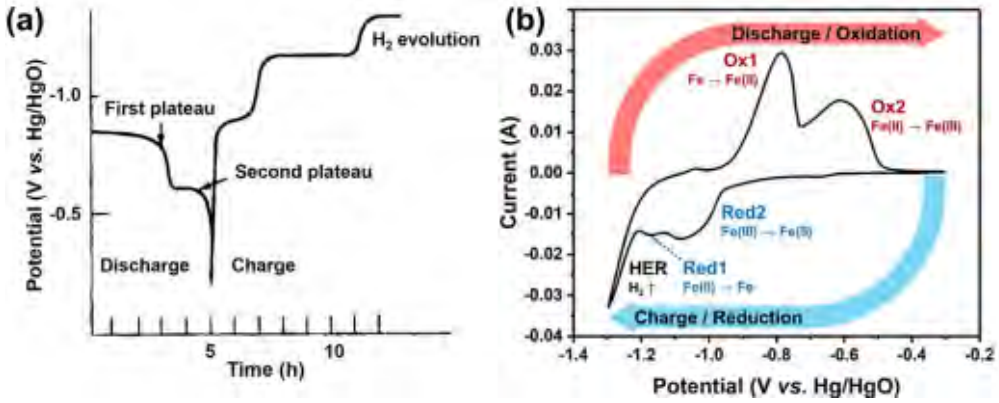

Figure 19 a) The usual iron anode discharge-charge curve in alkaline electrolyte, with discharge and charge matching to the total battery operation. b) The first oxidation peak, second oxidation peak, first reduction peak, and second reduction peak, respectively, are represented by Ox1, OX2, Red1, and Red2 on the iron anode's CV curve in an alkaline electrolyte [221].

(ii) Iron anode in acidic electrolyte

Reversible plating/stripping of Fe^{2+}ions is the reaction mechanism of the iron anode in the acidic electrolyte ($Fe^{2+} + 2e^- \leftrightarrow Fe^0$ ($E^O = -0.44Vvs\ SHE$)). In 0.5 M FeSO_4 solution (PH=5.5), iron anode electrochemical activity exhibits considerable polarization. Due to the high energy barrier of ferrous dehydration and iron nucleation, iron plating specifically displays an over-potential of 200 mV, whereas iron stripping only exhibits a 50-mV over-potential. In acidic electrolytes, the iron anode encounters parasitic HER more severely than in alkaline electrolytes. The HER potential in FeSO_4 solution (PH =5.5) is -0.32 V ($2H^+ + 2e^- \leftrightarrow H_2$ ($E^O = -0.32Vvs\ SHE$), which is 0.12 V greater than that of iron plating, indicating that the acid electrolytes have higher H^+ activity [223]. Second, the high iron plating over potential provides HER with a more powerful driving force, which results in the iron anode's poor plating/stripping efficiency in acidic electrolytes [231].

6.2.2 Battery systems based on iron metal anode.

(i) AIMBBs with alkaline electrolyte

Junger and Edison created the nickel-iron alkaline battery at the beginning of the 20th century, and it was used by the general public as early as 1910. The cells were widely used in traction applications, vans, mining vehicles, and emergency lamps [224] due to their tough physical structure (able to stable after mechanical shocks and vibrations), excellent electrical abuse tolerance (can maintain performance after overcharge/over discharge, storage in charge/discharge state for long-term), and superior life-cycling characteristics 3000 cycles corresponding to the 20 years calendar life [226]). The main active component of the positive electrode in nickel-iron alkaline batteries is nickel oxyhydroxide (NiOOH), and the electrolyte is typically a potassium hydroxide solution containing lithium hydroxide. The negative electrode in nickel-iron alkaline batteries contains iron metal, iron oxide, or a combination of both. Fig. 20a shows the schematic representation of a typical nickel-iron alkaline battery. The nickel-iron alkaline batteries' charge and discharge processes can be seen as:

$$Fe + 2NiOOH + 2H_2O \leftrightarrow 2Ni(OH)_2 + Fe(OH)_2 \quad (31)$$

$$3Fe(OH)_2 + 2NiOOH \leftrightarrow Fe_3O_4 + 2Ni(OH)_2 + 2H_2O \quad (32)$$

The overall reaction is:

$$2Fe + 8NiOOH + 4H_2O \leftrightarrow 8Ni(OH)_2 + Fe_3O_4 \quad (33)$$

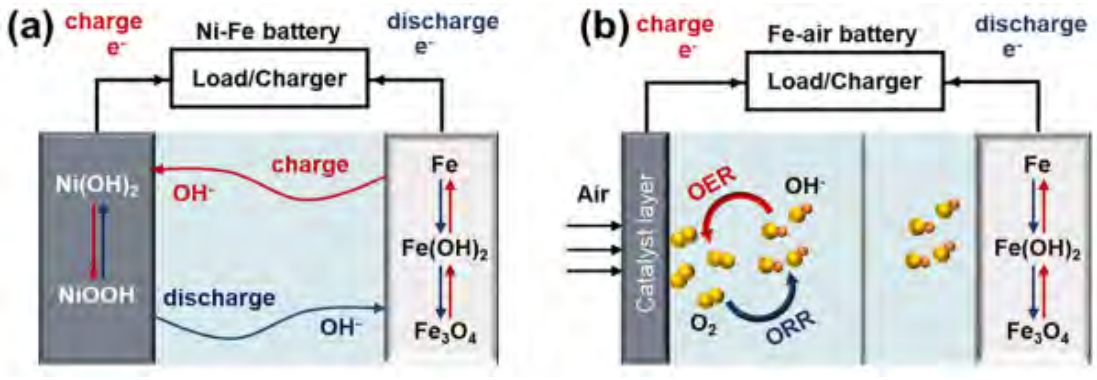

Figure 20 Schematic diagram of typical (a) nickel-iron alkaline battery and (b) iron-air battery [226].

Nickel-iron alkaline batteries have been replaced by newer battery types including Ni-MH, Ni-Cd, lead-acid, and Li-ion batteries despite their excellent qualities. The main causes of this are the iron anode's rapid self-discharge rate, low energy density, and low Coulombic efficiency [226]. Nickel-iron alkaline batteries have made a comeback in the public research arena due to the advancement of nanotechnology and characterization techniques in recent years. These batteries are valued for their low cost and environmental friendliness. The cells with increased capacity, rate performance, and cycle stability have considerable potential for application in large-scale energy storage since nickel-iron alkaline batteries are inherently affordable and secure. In addition, it has been shown that Pt/CeO_2, WN/nitrogen-doped carbon, and W_2C/porous graphene are efficient catalysts for the recombination of parasitic products (hydrogen and oxygen). As a result, sealed, maintenance-free Ni-Fe batteries are feasible, greatly increasing the practicality of the cells.

The Swedish National Development Corporation created the alkaline iron-air battery in 1970 for use in vehicles [225]. The typical alkaline iron-air battery, as depicted in Fig. 20b, is made up of an iron anode (typically metallic iron or iron oxides), an alkaline electrolyte (typically KOH solution), and an air electrode with dual functionality that can catalyze both oxygen reduction and evolution (for example, transition metals and their oxides). An alkaline iron-air battery can be thought of as a partial replacement for a nickel-iron alkaline battery, with the bifunctional air-breathing electrode acting in place of the nickel electrode. Iron-air batteries, as compared to nickel-iron batteries, are lighter and have a higher energy density thanks to the air electrode. Additionally, iron-air batteries have benefits comparable to those of nickel-iron alkaline batteries, including a durable mechanical design, a long cycle life of around 2000 cycles, a cheap cost of under US$100 per kW$h^{-1}$, and environmental friendliness due to the use of an iron anode [227].

Alkaline iron-air batteries' charge and discharge reactions at the iron anode are the same as those of nickel-iron alkaline batteries. The reaction can be expressed as follows at the electrode for air breathing:

$$O_2 + 2H_2O + 4e^- \leftrightarrow 4OH^- \ (E^O = -0.40V vs\ SHE) \quad (34)$$

The whole iron-air battery reactions may be summarized as

$$2O_2 + 3Fe \leftrightarrow Fe_3O_4 \quad (35)$$

Theoretically, the open-circuit cell potential of an alkaline iron-air battery is 1.28 V, its theoretical specific energy density is 764 Wh kg^{-1}, and its price is about US$59 kWh^{-1} [226]. Iron-air batteries have a low practical specific energy density, but due to their extremely low cost and good safety, the cells are suited for economically large-scale energy storage. The electrochemical efficiency of the iron-air battery may be considerably increased by optimizing the iron anode. An iron-air battery with nanocomposite electrodes was reported by Figueredo-Rodriguez et al. [228], and it produces 453 Wh kg_{Fe}^{-1} of energy density. Research into iron-air battery research is still in its infancy. Therefore, the creation of a high-performance iron-air battery will necessitate the use of an improved cell design, an optimized bifunctional cathode, and mathematical models.

(ii) AIMBBs with acidic electrolyte

Hruska and Savinell suggested the use of all-iron redox flow batteries (RFBs) in 1981. All-iron RFBs have a cheap cost and low toxicity because of the affordable and environmentally acceptable iron metal electrode and the aqueous electrolytes [229]. Two dissolved electroactive species are held in the catholyte and anolyte, respectively, of the RFBs. The catholyte and anolyte are separated from one another using an ionic conducting membrane. Due to the decoupling of the RFBs' energy storage capacity from their power rating, the specific operating model is especially well suited for grid applications. The negative crossing of redox species between the catholyte and anolyte (electrolyte contamination) might substantially endanger the performance of the RFBs, but the present ionic conducting membranes cannot meet the needed requirements. On the other hand, all-iron RFBs use a reactant couple that involves Fe^0/ Fe^{2+} / Fe^{3+} and three different valence states of iron (Fe^{2+} / Fe^{3+} oxidation reaction at the cathodic electrode and the iron plating/stripping at the anodic electrode). The same redox-active element can effectively reduce the risks of electrolyte contamination [226]. The electrochemical processes that occur while the all-iron RFBs are being charged (ahead) and discharged (reverse) are best described as follows:

With the negative electrode: $Fe^{2+} + 2e^- \leftrightarrow Fe^0\ E^O = -0.44Vvs\ SHE$ (36)

With the positive electrode: $2Fe^{2+} \leftrightarrow 2Fe^{3+} + 2e^-\ E^O = -0.77Vvs\ SHE$ (37)

Total: $3Fe^{2+} \leftrightarrow 2Fe^{3+} + Fe^0$ (38)

All-iron RFBs have a theoretical voltage of 1.21 V. Due to the fact that the cost of the active materials, iron salts, is less than US$20 k$Wh^{-1}$, which is less expensive than the majority of other battery chemistries, all-iron RFBs have exceptionally low costs [230]. For large-scale energy storage applications, Energy Storage Systems Company has successfully commercialized all-iron RFBs that can operate steadily more than 10,000 cycles, or a life of around 25 years [231]. The iron plating efficiency is crucial for enhancing the electrochemical performance of all-iron RFBs because the plating reaction used

in these devices prevents the decoupling of energy and power. Apart from the aforementioned iron anode optimization techniques, utilizing slurry electrodes is a successful method of boosting the effectiveness of all-iron RFBs. Petek et al. demonstrated how multiwalled carbon nanotube slurry electrodes can significantly improve voltaic efficiency by separating the energy density and power density of all-iron RFBs [226]. However, the associated electrolyte has yet to be investigated.

A few intriguing and cutting-edge all-iron RFBs have also been reported in recent years. For instance, Tucker et al. suggested an affordable, eco-friendly all-iron RFB [226]. The system can reach 40 mW cm^{-2} power density with 88% iron utilization and exceptionally low running costs (less than US$0.03 per mobile phone charge). Using immiscible aqueous anolyte (dissolved FeSO_4 as active species) and organic catholyte Bamgbopa et al. created a macroscale membrane-less all-iron RFB that, after 25 cycles, maintained over 60% initial discharge capacity and over 80% Coulombic efficiency [232].

Ji et al. [233] presented a novel form of aqueous battery that uses iron metal as an anode. The operating mechanism of an iron-ion battery with Fe include plating/stripping at the iron anode and ferrous ions intercalating/deintercalation. This battery, which operates in an aqueous FeSO_4 electrolyte, can reversibly produce a discharge capacity of 60 mAh g^{-1} (based on cathode material mass) at 1 C rate (1 C= 60 mAg^{-1}) and may run for over 1000 cycles at a 10 C rate. They further developed an Fe/LiFePO_4 hybrid battery to increase the energy density of the cell. By combining Li inserting/extracting in LiFePO_4 with iron plating/stripping at the anode, the cell provides a discharge capacity of 155 mAh g^{-1} at 1 C rate (1 C= 155 mA g^{-1}). They then proved that a sulfur cathode had excellent electrochemical performance in an aqueous iron-ion battery without the use of polysulfide shuttling [234]. The Fe/S battery uses S/C nanocomposite, iron metal, and aqueous FeSO_4 solution as the cathode, anode, and electrolyte, respectively. Due to the advantageous all-solid-state conversion process, the sulfur cathode has a high discharge capacity of 1050 mAh g^{-1} at 50 mA g^{-1} and good stability of 150 cycles. Bai et al. presented a Fe/I_2 battery with an iodine/nitrogen-doped hierarchically porous carbon composite (/I_2/N-HPC) cathode, an anode of ascorbic-acid-modified iron metal, and an electrolyte of aqueous FeSO_4 solution [235]. The current battery has an excellent power density of 1300 W kg^{-1} at 120 W kg^{-1} and an exceptional stability of 100% capacity retention after 550 cycles at 2 A g^{-1}.

The innovative iron-ion batteries, which use a mild/slightly acidic electrolyte, are more ecologically friendly and safe than alkaline iron batteries and have promising applications in clean energy storage systems. However, research on iron-ion battery systems is still in its early stages, and a number of challenges remain cathode materials with suitable potential and stable structure, iron anodes with reduced corrosion and HER rate, low-cost electrolyte capable of increasing iron plating efficiency while remaining compatible with cathode materials.

6.3 Lithium-air battery

6.3.1 Li-metal anode

6.3.1.1 The remaining challenges of Li metal anodes

When running LMBs through the charging and discharging process, the aggressive Li metal chemistry has encountered significant difficulties. Due to the Li atom's high diffusion barrier, which is an intrinsic feature, Li dendrite development is one of the most urgent problems, posing a serious safety concern [236]. To be more precise, the surface of the originally plated Li anode or the pits of the initially stripped Li metal foil are where Li dendrites most frequently develop [237]. According to earlier observations [237,238,239], there are a lot of Li dendrites on the anode surface and a low Coulombic efficiency (CE) as a result of the recurrent lithium plating/stripping (deposition/dissolution) processes. Li dendrites can develop continuously, pierce the separator, and create a short circuit in the battery, which can result in high current discharge, a lot of heat, and even explosions. A lithium dendrite will detach from the matrix as a result of the fast and uneven dissolution around the active site, producing "dead Li" [240]. The term "dead Li" in this context mostly refers to electrically isolated Li metal that is covered by a thick solid electrolyte interphase (SEI)layer made up of inorganic and organic Li-species following repeated volume changes. As a result, the fragmented Li needles and particles no longer transport electrons and ions. The development of "dead Li" results in the loss of active lithium in the electrode and lowers the battery's specific capacity. For instance, Archer and colleagues discovered that Li naturally exhibits fiber-like deposition and that Li's poor reversibility performance is mostly due to physical orphaning [241].

Additionally, the consumption of electrolytes, which is mostly due to the interaction between highly reactive Li metal and electrolyte, was a major factor in the cycle performance of LMBs. A solid electrolyte interphase (SEI) layer will develop on the Li metal anode's surface when it comes into contact with the electrolytes [242]. The following Li plating/stripping process will result in surface pulverization, consumption of the electrolyte, development of SEI, and "dead Li" due to defects in the SEI layer brought on by infinite volume expansion and shrinkage. While this is happening, the fractured SEI layer will reveal flaws, which will speed up the deposition of Li atoms, resulting in the formation of Li dendrites. As a result, "dead Li," electrolyte consumption, and thick SEI would significantly harm the electrochemical performance of LMBs, resulting in poor CE, short cycle life, and safety hazards.

Li-ion metal pouch cells have been considered a potential battery system for future uses beyond coin cells in the lab. Under higher current densities, higher areal capacities, and no-pressure environments, they would invariably experience even worse conditions. The remaining difficulties with Li metal anodes already mentioned would naturally be more difficult in pouch cells. For instance, polarization and powdering are more important in LMBs than in pouch cells [243]. According to the study by Zhang and

colleagues powdering of Li metal with an accumulation of "dead Li" in the polarization zone causes the degradation of Li metal anode at low current density, while the main challenge at high working current density is the short-circuit, posing a safety hazard. Both the production of "dead Li" and Li dendrites were possible in the transition zone [244].

In terms of the practical uses of LMBs, Li metal anodes now confront certain challenging issues. For instance, the strong reactivity between Li and air (which contains moisture and oxygen) makes it too harmful to employ in electric cars, comparable to the risk brought on by the production of Li dendrites. It is possible for LMBs to explode due to short circuits or traffic accidents, which makes it challenging to employ LMBs on a broad scale in EVs. Additionally, due to Li metal's incredibly low plasticity, bending and extrusion can result in microscopic flaws and irreversible deformation on the metal's surface, which are permanent alterations to the substance itself. During cycling, the deformation-induced imperfections would serve as active locations for the growth of Li dendrites. A Li metal foil with a similar thickness of 20–30μm attached to a copper current collector is required to meet the areal capacity of 4-6 mAh cm^{-2}in traditional cathodes. Due to the strong reactivity, high corrosivity, high air-sensitivity, and low plasticity of Li metal, the automated mass manufacturing of acceptable lithium metal negative electrodes is extremely difficult, in addition to the safety risk in applications.

6.3.1.2 The recent benefits of Li metal anodes

The fundamental goal is to produce homogeneous Li deposition during lithium plating and stripping, safeguarding lithium metal against dendrite development, in order to overcome the aforementioned difficulties. To date, a number of methods have been put forth to produce high-performance Li metal anodes. Fig. 21 provides a summary of the recipe and associated technique or justification for improving the long-term cycle stability of Li metal anodes. The most common method is to cover Li metal with a thin, thick, ionically conductive protective layer (either before or during cycling) (Fig. 21(a)). The ion conductor layer should ideally be thin and thick, successfully preventing electrolyte penetration and Li dendrite development in order to achieve uniform Li deposition. This type of ion conductor layer can be solid electrolyte interphase (SEI) layers, which are formed in-place by electrolyte changes from liquid to solid (Fig. 21(d)). On the Li metal anode, in addition to the ion conductor, a protective layer or matrix for the electron conductor was also used (Fig. 21(b)). We will mention that the nucleation sites for uniform Li deposition should be evenly distributed across the electron conductor layer or matrix. Otherwise, the Li dendrite may develop on the electron conductor's surface. These surface defenses would, however, be eroded by infinite volume change over the course of repeated cycles, leading to an increase in SEI thickness, Li loss, dendritic development, and electrolyte consumption. Significant work was put into creating lithiophilic hosts with complex topologies to contain active Li in order to further improve the stability of the reaction interface and avoid the production of Li dendrites (Fig. 21(c)). By using porous

carbons, carbon hollow spheres, carbon nanotubes (CNTs), graphene, 3D current collectors, and 3D electron (or ion) conductive frameworks, which may inhibit the volume change to drive more stable SEI, such a result was gradually attained. Additionally, it has been observed that different binder designs can increase the mechanical stability of the composite architecture and counteract volume change, resulting in a more stable response interface (Fig. 21(e)). The improved separators with good mechanical qualities are stiffer to stop Li dendrites from penetrating them and causing a short circuit (Fig. 21f.)

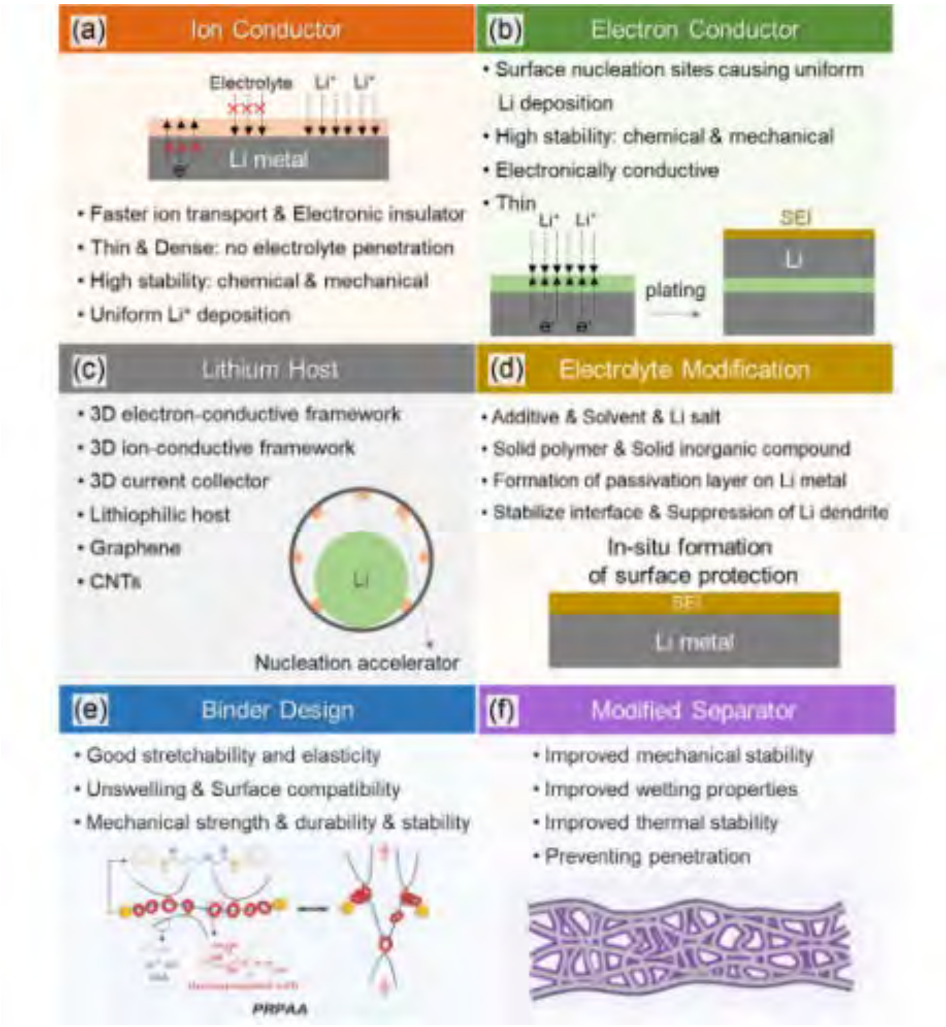

Figure 21 Principal methods for improving high-performance Li metal anodes and their justification: formation of (a) ion conductor layer and (b) electron conductor layer on Li metal anode, (c) design of Li hosts, (d) modification of electrolyte, (e) binder design, (f) modification of separator. Schematic figure in (e) reproduced from [245].

6.3.2 Electrolyte

Effective electrolytes for high-performance solids and non-aqueous liquid electrolytes are used in Li metal anodes, as shown in Fig. 21(d). The stable contact between the reactive Li metal and the electrolytes during electrochemical reactions should be the design guiding concept. The in-situ generated, thoroughly passivated surface layer on Li metal would be crucial in preventing the ongoing, undesirable side reactions between fresh Li and electrolytes. The upcoming high-voltage cathode-based LMBs need

to push both liquid and solid electrolytes to high oxidation potentials in particular. For solid electrolytes, Li ion conductivity, acceptable physical dynamics, and ease of manufacture for large-scale use are crucial for solid electrolytes. Solid electrolytes are also predicted to have low electrical conductivity and good interface affinity/contact on Li. Different strategies have been extensively investigated in liquid electrolytes to improve the overall cycling performance, including functional additives, fluorinated solvents, new salts, and significantly high salt concentrations. Additionally, operational temperature range, industrial cost, and flammability must be considered for large-scale utilization in future applications. In addition to the methodologies mentioned above, simulations in conjunction with experimental data have been widely used to give insightful explanations of the Li-metal battery chemistry under diverse situations [246–249].

6.3.2.1 Liquid electrolyte modifications

When Peled and his colleagues began researching batteries employing alkali and alkaline earth metals as anodes in 1979, they came up with the SEI concept [250]. They discovered that when the metal anode contacted the nonaqueous electrolytes, a very thin coating with a complicated composition was created in-situ. The idea of SEI was expanded to include electrodes made of various metal and nonmetal materials, and it has been thoroughly studied over the last 20 years [226,227,251,252]. The composition of electrolytes is essential for causing the production of a thin, stable, thick, and elastic SEI layer since electrolytes are the primary determinant of SEI formation. Therefore, it has been determined that the most successful method for stabilizing the Li metal anodes in LMBs is to modify the electrolytes with additives, salts, and solvents. As reported in [245], the main SEI species on the Li metal varied depending on the solvent. For instance, in propylene carbonate (PC), ethylene carbonate (EC), dimethyl carbonate (DMC), methyl formate (MF), tetrahydrofuran (THF), and 1,2-dimethoxyethane (DME), respectively, the surface compositions of CH_3CH-(OCO_2Li)CH_2OCO_2Li, $(CH_2OCO_2Li)_2$ (CH_3OLi, HCOOLi, ROLi($CH_3(CH_2)_3OLi$ and ROLi(CH_3OLi). Solvents for carbonate electrolytes are crucial for the future development of LMBs. A recent study was conducted to fully comprehend the impact of various substituents on cyclic carbonates, and the results have offered recommendations for the design and choice of cyclic carbonates [253]. Typically, the organic salts in electrolytes determine the inorganic salts in the SEI layer. Because Li salt anions, such as LiTFPFB, have different reduction properties with the Li metal anode, they also contribute to the formation of SEI [254]. Functional additives with greater reduction voltages are added to the electrolytes to improve the SEI layer's quality. A more stable and thicker SEI layer is often formed by the addition of the Li metal more quickly than by other electrolyte components.

Delnick discovered that the ionic conductivity of SEI depends on its flaw and that its resistance rises as its thickness increases [255]. From the inner surface with the Li metal anode to the outer surface with the solution, the composition and structure of SEI progressively shift. The majority of the constituents in

the SEI layer's inner surface are low oxidation materials, whereas those in the outer section are mostly greater oxidation compounds that are intimately associated with the solvent. Low viscosity, short ether-based electrolytes are less reactive with Li metal than esters and have demonstrated reduced dendrite formation. Yamada and colleagues have showed that, under some conditions, single solvent systems for high voltage (5.0 V) chemistries may be enabled by simply raising the salt content (> 3 M) in dimethyl carbonate (DMC) solvent [245]. Meanwhile, the higher oxidative/reductive stability of the highly concentrated electrolytes provided a remedy for the larger electrochemical stable potential window [256–257]. Excessive cost (which is inversely proportional to salt concentration), low ionic conductivity, and poor wetting capacity are the drawbacks of high concentration electrolytes (HCEs). Be aware that one crucial factor in the practical manufacture of lithium-based batteries is the wettability of the non-aqueous electrolyte, which not only affects production efficiency but also negatively affects the yield of conforming batteries. Lack of wetting ability would make it take longer to implement full electrode invasion in non-aqueous electrolyte, lowering the manufacturing line's efficiency and making the initial SEI creation worse. By diluting an HCE with an "inert" diluent, Zhang and colleagues created a localized high-concentration electrolyte (LHCEs), which may significantly reduce the overall Li salt concentration to a practicable level while keeping (or even increasing) the special properties of the HCE [258]. Cosolvent electrolyte use is another method for addressing HCE shortcomings. Dong et al. [259] created a co-solvent electrolyte with a high concentration of dichloromethane (DCM) diluent and bis(trifluoromethanesulfonyl)imide (LiTFSI)/ethylacetate (EA) electrolyte. Excellent ionic conductivity, low viscosity, and a wide variety of stable potential windows are all obtained at an extremely low temperature of about 70 °C, displaying high energy and power densities in a rechargeable metallic Li battery [259]. Despite the not always great Coulomb effectiveness, Li and Ji were able to obtain a dense and macroscopically smooth surface morphology of the plated Li surface by utilizing an oxidizing co-solvent of ethyl methyl sulfone (EMS) in the electrolyte [260]. Zhang et al. created the carbonate/ether co-solvent electrolytes utilizing fluoroethylene carbonate (FEC) and dimethoxyethane (DME) as solvents and the addition of $LiNO_3$ to address the problem of $LiNO_3$'s insoluble in carbonate solvents such as fluoroethylene carbonate (FEC). The combination of FEC and $LiNO_3$ improved the homogeneity of the SEI and produced a high CE (99.96%) even under extremely demanding conditions, as well as a much longer cycle life (over 1000 cycles) [261]. Similar to this, the Li_2S_5 and $LiNO_3$ used as co-additives in the LiTFSIDOL/DME electrolyte resulted in a uniform and sulfurized SEI on the Li metal anode and achieved a CE of 98% over 200 cycles at 1.0 $mAcm^{-2}$ [262]. It has been demonstrated that a number of additives, including polysulfides, FEC, and $LiNO_3$, as well as lithium bis(oxalate)borate (LiBOB), methyl viologen (MV), magnesium $(TFSI)_2$ and vinylene carbonate (VC), can drive in-situ SEI layer formation through spontaneous and preferential reaction with the contact of Li, can stabilize the Li metal anode

[263,264,265]. A number of inorganic salt additives containing metal ions, such as MClx (M=As, In, Zn or Bi), $AlCl_3$, AlI_3, and In $(TFSI)_3$, stabilize lithium metal with the new SEI formation (Li-rich composite alloy films), which can successfully inhibit the growth of Li dendritic fibers [266,267,268]. This is based on the mechanism of easily creating thin layers by alloying with Li. For instance, at a practical current density of 2 mA cm^{-2}, the combination of fast lithium-ion migration through Li-rich ion conductive alloys and an electronically insulating surface component can stabilize and sustain electrodeposition over 700 cycles (1400 h) of repeated plating and stripping [266]. Additionally, Nazar and associates developed an in-situ generated Li^+ single-ion-conducting Li_3PS_4 layer to homogenize the Li^+ flow and so prevent the unregulated growth of Li dendrites [269].

Many variables involving the salts and solvents affect the morphology of plated Li metal. According to Liu and colleagues [270], increasing the molar ratio of salt to solvent improved the stability of non-flammable phosphate electrolytes. The reactivity of these non-flammable electrolytes toward Li-metal electrodes is decreased. Wang and colleagues demonstrated that the Li metal anode in carbonate electrolytes has outstanding CE performance by increasing the LiFSI concentration to 10 M [271]. When two anions (TFSI and FSI) coexist, completely new interphases are created by preferential breakdown processes, according to research by Alvarado et al. on the basalt influence on the interphasial chemistry of both Li metal and high Ni cathode materials [272]. The outcome is a denser, more conformal morphology for the plated Li metal. Li and colleagues created a type of high-concentration full-fluoride (HFF) electrolyte with a large donatable fluorine concentration (DFC) for 5 V rechargeable LMBs by the fluorination of the electrolyte, resulting in outstanding performance in the high-voltage cathode-based LMBs [273]. Wang and colleagues created LMBs with F-rich CEI and F-rich SEI (dendrite-free) and high energy densities for the Li metal anode and high-voltage cathodes. Poor Li plating/stripping, the development of Li dendrites, poor safety; and aggressive. The simultaneous solution of all high-voltage cathodes has been achieved [271].

Ionic liquids are non-flammable and have a strong ionic conductivity. They can also withstand wetness in Labs. The influence of the operation temperature on the morphology of the discharge product generated was investigated using the non-aqueous LMB. Because the solid discharge product Li_2O_2 blocks the cathode pores, the discharge process is interrupted. Before it can be utilized in the charging process, the product must be oxidized.

6.3.2.2 Solid-state electrolyte modifications

The ionic conductivity of liquid electrolytes may be improved by modifying their composition, which can also cause the formation of an in-situ passivation coating on electrodes and significantly enhance the cycle stability of the Li metal anode [274,275,276]. However, the liquid electrolytes used in LMBs pose significant safety issues due to their extensive usage of volatile organic solvents. Li dendrites may

develop freely in the electrolytes since they are liquid, which allows them to penetrate the SEI layer and eventually produce a short-circuit. Li dendritic development may be inhibited by the solid-state electrolytes (SSEs) and prevented from reaching the separator. But according to recent research, SSEs also developed Li dendrites, which contributed to the degradation problems [277]. As a result, SSE adjustments are required to create high-performance solid-state LMBs. Solid polymer electrolytes (SPEs), gel polymer electrolytes (GPEs), and inorganic solid electrolytes are the three basic categories into which SSEs are often separated (SEs).

SPEs are often defined as electrolytes that contain or are composed of macromolecular structures. The systems of organic polymer electrolytes and organic-inorganic composite electrolytes can therefore be further represented by the SPEs. Polyethylene oxide (PEO), polyphenylene oxide (PPO), poly methoxyethoxyethoxy phosphazene (PEEEP), polyacrylonitrile (PAN), and others are examples of frequently used organic polymer electrolytes. When compared to liquid electrolytes, SPEs typically have low ionic conductivity. However, raising the temperature may increase this conductivity. Electrolytes made of composite polymers are one potential remedy [278,279,280]. Wan et al. recently created a solid polymer electrolyte with an ultrathin (8.6 μm) and light weight nano porous polyimide (PI) sheet packed with polyethylene oxide/lithium bis(trifluoromethanesulfonyl)imide (PEO/LiTFSI). The created solid polymer composite (PI/PEO/LiTFSI) electrolyte allowed for high safety operating at a high temperature as well as long-term cycling of the Li metal anode (over 1000 h) [281]. To address the contact issue and prevent the production of Li dendrites, Ma et al. created a composite polymer electrolyte CPL (Cellulose acetate/Polyethylene glycol/$Li_{1.4}Al_{0.4}Ti_{1.6}P_3O_{12}$) with a viscoelastic and nonflammable interface [282]. In comparison to 0D or 1D materials, 2D materials, like MXene, have higher specific surface areas, making them interesting options for composite electrolytes. To create the MXene-based nanocomposite polymer electrolytes (CPEs), Pan et al. evenly dispersed tiny quantities of $Ti_3C_2T_x$ into a poly (ethylene oxide)/LiTFSI complex (PEO_{20}-LiTFSI) [283]. These CPEs improved the electrochemical performance of LMBs. By using various electrolyte components/electrode interfaces, Duan et al. created a heterogeneous multilayered solid electrolyte (HMSE) displaying low voltage hysteresis and a Li metal anode devoid of dendrites following cycling [284]. Additionally, they created an in-situ plasticized SPE with a double conducting polymer network (DN-SPE) via simple polymerization of two different types of liquid polymer monomers with the right chain length [285]. This DN-SPE exhibits improved ion conductivity, excellent mechanical flexibility, a broad electrochemical window (4.7 V vs. Li^+/Li), high thermal stability (stable up to 200 °C), and an effective capacity to inhibit Li dendrites. Hybrid electrolytes have also been suggested to make up for the drawbacks of organic and inorganic electrolytes. A 3D discontinuous hybrid electrolyte with an ionic conductive polymer layer on one side and the ceramic solid electrolyte $Li_{1.4}Al_{0.4}Ge_{1.6}(PO_4)_3$ (LAGP) on the other side was created by Bruce and colleagues [286]. The electrolyte's mechanical characteristics have been enhanced thanks to this technique without appreciably

affecting its ionic conductivity. The prior study [287] also reported using a similar methodology. They suggested an asymmetric solid electrolyte (ASE) that had a hard layer of polymer electrolyte on one side and a soft layer of polymer electrolyte on the other. The LMBs using ASE produce exceptionally high CE, surpassing 99.8% per cycle [287] and strong capacity retention, reaching 94.5% for more than 200 cycles.

Combining SPEs with liquid electrolytes' strong ionic conductivity feature is another way to offset the limitations of SPEs. The polymer electrolytes will change into GPEs after absorbing the organic solvents. GPEs have a jelly-like appearance and they are made of polymers and liquid electrolytes. The ion conductivity of GPEs is high due to the presence of liquid electrolytes, which also ensures the cycling performance of batteries. PEO, PPO, PAN, polyethylene glycol (PEG), polymethyl methacrylate (PMMA), polyvinyl chloride (PVC), and polyvinylidene fluoride (PVDF) are the primary polymer materials. Research on GPEs has been conducted for many years. In 1995, Matsui and Takeyama looked into the effects of mixing PEO-PPO and LiClO_4 in EC/PC. In 1999, Tatsuma et al. enhanced the GPE of PAN and LiClO_4 in EC/PC. Choi et al. used ionic liquid to study GPE. However, because of the unique construction of GPEs, neither their mechanical strength nor the liquid electrolytes contained within them have sufficient thermal stability to prevent the formation of Li dendrites [245].

SEs are ideal materials to stop Li dendrites from reaching the separator because they are inorganic solid-state Li ion conductors. Several types of Li compounds have been widely studied up to this point [288,289,290,291]. In comparison to liquid electrolytes, the SEs have been discovered to have a slower rate of Li-ion diffusion, and their stiffness makes for worse interaction with the Li metal anode. Its use in large capacity batteries have been hampered by the critical current density of SEs, which is significantly lower than that of liquid electrolytes [292,293]. A thermodynamically stable interface, a thermodynamically unstable interface with a mixed ionic-electronic conducting interphase, and a thermodynamically unstable interface with a kinetically stabilized SEI film are three categories into which the interfaces between Li anode and SEs can be subdivided [245]. Between Li_3PS_4-SEs and the Li metal anode, Wang and colleagues produced an SEI layer that was rich in LiF, which inhibited the formation of Li dendrites [294]. ALD and MLD are better methods for fabricating uniform thin films because they can regulate the film thickness at the atomic level [295,296] and operate in environments with temperatures between 28 and 250 °C [245]. To lessen side reactions and stabilize the LATP/Li contact, Sun and colleagues proposed using the ALD coating on the $Li_{1.3}Al_{0.3}Ti_{1.7}(PO_4)_3$ (LATP) solid electrolytes surface [297]. On the Li_3BO_3-Li_2CO_3(LBCO) SE, Dasgupta and colleagues successfully created an ALD interlayer. The film growth is linear and self-limiting over a range of deposition temperatures [298]. The created ALD LBCO electrolyte has high ionic conductivity and great cycle stability, making it suitable for use in Li metal thin-film batteries. Sun et al. used MLD to create an inorganic-organic hybrid interlayer in order to address the issue of interfacial instability between Li metal and SEs [299]. At the interface between Li and SEs, the side effects and Li dendrites are effectively controlled.

The garnet type SSEs, such as $Li_7La_3Zr_2O_{12}$, have been recognized as particularly attractive ceramic electrolyte candidates among the inorganic SSEs, which include oxides, sulfides, and nitrides due to their relatively greater ionic conductivity of 10^{-3} to 10^{-4} S cm^{-1}. The garnet solid was coated with an Al layer to increase the contact (excellent wettability) with Li through the formation of a Li-Al alloy at the interface, which also stabilized the interfacial resistance upon continuous Li plating/stripping operation [300]. Due to the benefits of the combined characteristics of the ceramic and polymer, performing better mechanical properties and contact surface wetting, ceramic/polymer composite electrolytes have recently been recognized as a highly promising technology for high-performance LMBs [301].

CHAPTER 7

Working principle of lithium-ion battery

Lithium-ion batteries are made up of four primary components: cathode, anode, separator, and electrolyte [302]. The charge carriers that contribute to LIB energy storage and release are cathodes and anodes. The separator divides the electrodes physically to avoid internal short-circuits while allowing Li+ flow. Ions, including Li+, are carried by the electrolyte. The failure of these components, either collectively or separately, can have a significant impact on LIB safety. The electrodes generate heat while functioning, which might become unpredictable if the battery fails [303]. When a separator breaks, LIB operations switch from regulated to uncontrolled electrochemical reactions, resulting in considerable heat generation [304]. Because the electrolyte works as a fuel source for other heat generation in such instances, adequate safety standards, which can be formed by investigating the controllable and uncontrollable elements in battery failures, are critical for enhancing LIB safety performance. Figure 22 presents the working mechanism of a typical LIB, using a $LiCoO_2$/graphite cell as an example [302]. Li+ de-intercalates from the cathode materials (LiCoO2, in this example), diffuses into the electrolyte, and passes through the separator nano-pores to intercalate into the anode material during charging. To preserve electro-neutrality, electrons migrate in the opposite way across the external circuit. During discharging, Li+ ions move from the anode to the cathode. The following are the charge and discharge reactions:

Cathode: $LiCoO_2 \Leftrightarrow Li_{1-x}Co0_2 + xLI^+ + xe^-$ (39)

Anode: $6C + xLi_+ + xe^- \Leftrightarrow Li_xC_6$ (40)

Reactions: $LiCo\ O_2 + 6C \Leftrightarrow Li_{1-x}Co\ O_2 + Li_xC_6$ (41)

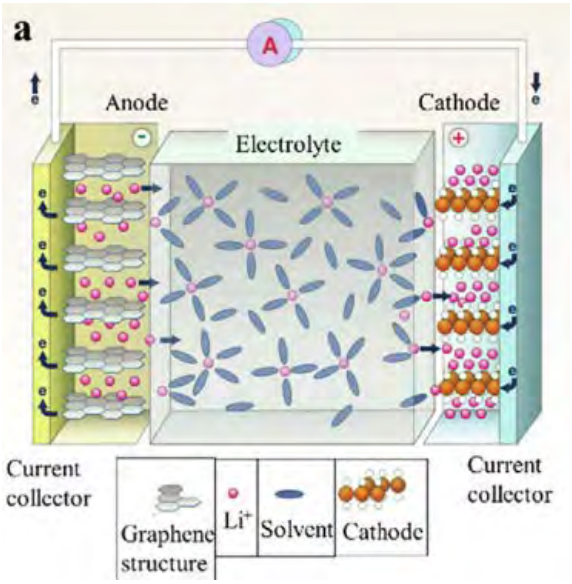

Figure 22 Schematic diagram of the fundamental structure of a LIB cell, which is the same for different cell types [302]. Copyright (2011) American Association for the Advancement of Science [302].

Due to their high cycle efficiency, lack of toxicity, and usage in portable electronics, lithium-ion batteries (LIBs) have drawn a lot of interest as high-performance electrochemical energy storage devices. However, because of the sluggish Li^+ ion diffusion rate in solid bulk materials, which results in relatively low power densities, they frequently experience severe kinetic issues. Numerous metal oxides, including molybdenum oxides, CO_3O_2 , nickel oxides, copper oxides, manganese oxides, and iron oxides, have been studied to address the aforementioned issue. Due to its high theoretical specific capacity (1007 mAh g1), plentiful supplies, low cost, and lack of toxicity, Fe_2O_3 is regarded as one of the most promising anode materials for lithium-ion batteries. Although Fe_2O_3 has low electric conductivity, a large volume change, strong agglomeration these factors lead to capacity attenuation and poor rate capability [305].

The two approaches described below have been used to deal with these problems: Creating nanostructures is step one. In this situation, a larger electrode/electrolyte contact area and a shorter transport distance for Li^+ions and electrons can considerably enhance the cycle life and charge/discharge rates of Fe_2O_3 in the electrochemical processes. Fe_2O_3 nanostructures of various types, such as nanosheets, nanoflakes, nanotubes, nanorods, and nanofibers, have been created using a variety of techniques. Creating carbon-based materials is the second step. In this situation, volume growth may be reduced while electron transport can be enhanced. Aside from that, graphene-based materials (GCs) are regarded as a good alternative for LIBs because of their superior mechanical characteristics and substantial specific surface area [305].

The use of GCs can eliminate the dangerous Fe_2O_3 aggregations and offer the following significant benefits: Better electrical conductivity, lower volume expansion, a greater specific surface area, superior capacity, and stronger cycle stability are only a few of the benefits listed above. Using the gel approach, hydrothermal procedure, solvothermal method, or microwave-assisted method, numerous GCs supported Fe_2O_3 nanostructures with outstanding electrochemical properties have been described. However, finding a simple and efficient method to obtain Fe_2O_3-based anode materials with superior electrochemical characteristics remains a difficulty [305].

CHAPTER 8

Lithium-ion batteries vs metal-air batteries

Sony launched commercially effective LIB devices with hard-carbon anodes and LiCoO2 cathode materials approximately 30 years ago [306]. Capacity evolution has enabled current anodes to obtain capacities close to the theoretical limit of graphite (372 mAh g^{-1}) [307,175,308], the most often used LIB anode material. In Fig. 23, lithium has the largest theoretical specific capacity, however it has significant disadvantages as a LIB anode material.

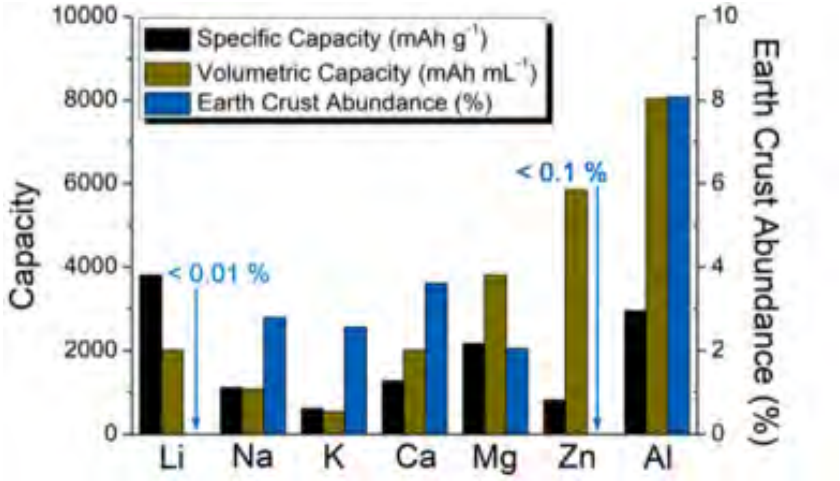

Figure 23 Theoretical metal-air energy densities and earth abundance for several metal-air battery materials adapted from [77].

Water and organic electrolytes are extremely reactive to lithium metal [309]. Internal short circuits caused by lithium dendrites can be dangerous [77]. LIB cathode capacities are often lower than graphite anode capacities, with LIB cathode capacities larger than 200 mAh g^{-1} considered high performing [302]. Faraday's laws of electrolysis [303] may be used to calculate the impact of individual electrode capacities on overall LIB cell capacity, as illustrated in Equation (42) [77]:

$$C_{LIB} = \frac{1}{\frac{1}{C_{anode}} + \frac{1}{C_{cathode}} + m_{inactive}} \quad (42)$$

where C is the capacity (typically expressed in mAh g^{-1}) and m-inactive is the particular mass (g m$(Ah)^{-1}$) of inactive material (separator, electrolyte, case, etc.) necessary to create the cell. Equation (42) clearly shows that the capacity of one electrode, the cell capacity is simply associated with that of the limiting electrode. As a result, it is clear that both the anode and the cathode must be upgraded in order to achieve a considerable gain in total efficiency. Capacity of LIB cells only gradual improvements in LIB electrode capacity have been obtained over decades. Liu et al. [310] gathered readily attainable data for existing LIB components and computed a specific energy of roughly 350 Wh kg^{-1} to represent what is

typically obtained in today's LIBs. A series of potential enhancements (Fig. 24(a) & (b)) were explored, and capacity gains were computed with each subsequent upgrade.

Each of these processes has its own set of difficulties. Although, it is clear that cathode performance characteristics are critical to boosting specific energy, significant development in LIB cathode capacity has been challenging. The development of novel designs with fundamentally different electrode layouts, such as MAB cells, is one method to accelerate improvement in battery performance. It is not a physical part of the cell, rather oxygen itself serves as the MAB cathode material. The MAB cell capacity is represented by Equation (43):

$$C_{MAB} = \frac{1}{\frac{1}{C_{anode}} + m_{inactive}} \tag{43}$$

According to estimates [77], the porous air cathode "skeleton" makes up less than 10% of the MAB system's overall inactive mass. These features, together with large anode metal capacities (Fig. 24(a)), significantly increase the window for MAB capacity improvement as opposed to LIB systems. A quantitative comparison of LIB capacity to that of a Li-air battery may be used to demonstrate this. Using Equation (42) and assuming (i) the imaginary best cathode capacity scenario from Liu et al. [310] (250 mAh g^{-1}); (ii) a 372 mAh g^{-1} graphite anode capacity; as well as (iii) a specified LIB inactive mass of 6.2 g $(Ah)^{-1}$; the LIB capacity is estimated to be close to 80 mAh g^{-1}. The lithium anode is used in the LAB cell (figure 24) has a 3861 mAh g^{-1} capacity. The LAB's inactive mass is approximately 1 g $(Ah)^{-1}$ [77]. Equation (43) predicts that the LAB capacity will be close to 1000 mAh g^{-1}, at least a 10x improvement over the best-case LIB. This has encouraged a significant amount of study to realise the potential of LAB designs.

Four types of LAB systems may typically be distinguished [311–313]. As mentioned by Galbraith in the initial description of a LAB system in 1976 [313], one category uses aqueous electrolytes. The implementation of a LAB cell in an aqueous electrolyte is difficult in reality due to the solubility of LiOH in aqueous electrolytes [77]. A non-volatile solid-state electrolyte shields lithium metal from moisture as well as from ambient oxygen and carbon dioxide in a second LAB cell type in an effort to get around this problem.

A lot of research is being done on this concept, which calls for strong ionic conductivity and straightforward, inexpensive production from solid electrolyte materials that prove chemical, thermal, and mechanical stability [311]. The third type, which uses aprotic (non-aqueous) electrolytes, is likely the one that has been investigated the most. By using a lithium foil anode, a thin carbon composite cathode, and a polymer electrolyte, Abraham and Jiang first suggested the viability of secondary operation in 1996 [77]. The envisioned cell response is:

$$4Li + O_2 \rightarrow 2Li_2O \qquad E^o_{cell} = 2.91\ V \tag{44}$$

Cell discharge was shown to stop when the oxygen-breathing carbon cathode became obstructed by lithium oxide production. The authors' analysis of this discharge product wrote down that, in reality, it was Li2O2 and cell response:

$$2Li + O_2 \rightarrow Li_2O_2 \qquad E^{O}_{cell} = 2.91V \tag{45}$$

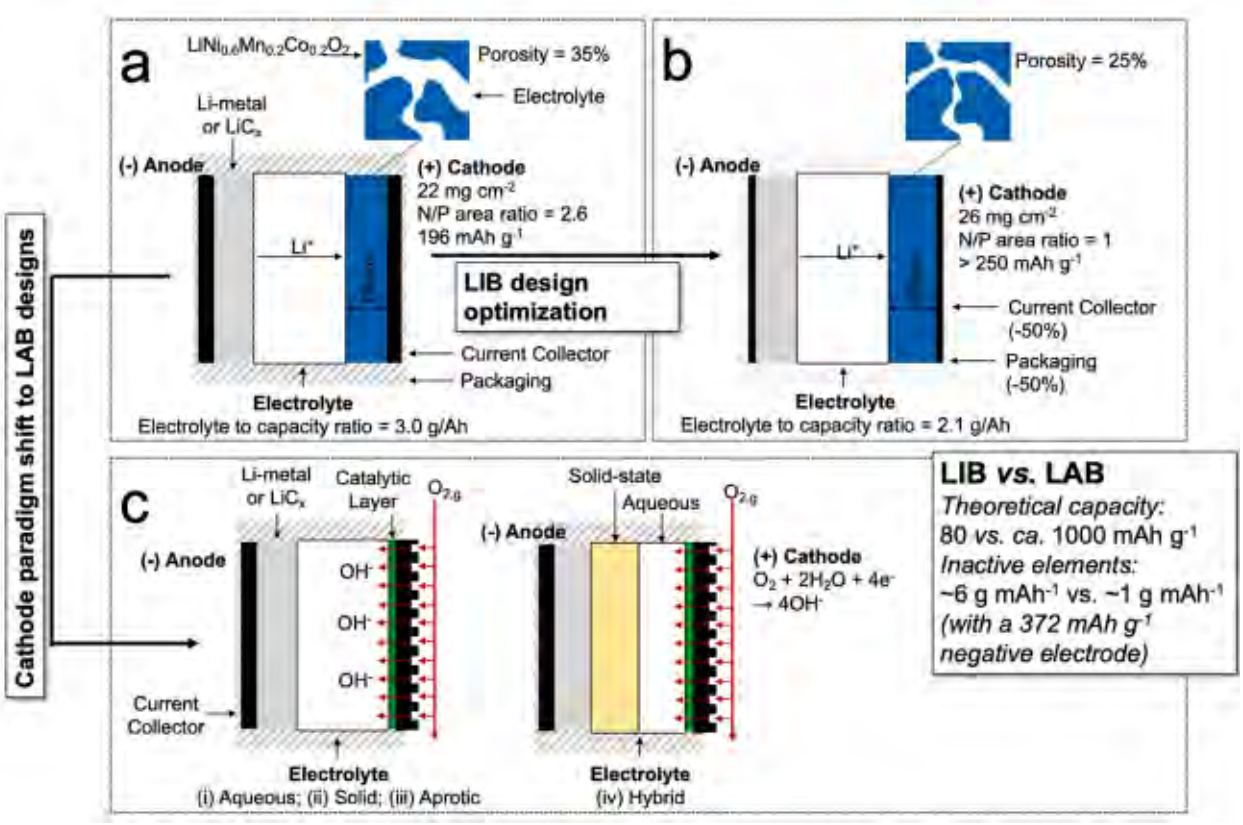

Figure 24 (a) Illustration of a standard lithium-ion battery (LIB) with its main characteristics; (b) characteristics modification undergone to achieve LIB advances through optimization of the current design; (c) illustration of a standard lithium air battery, with an emphasis on the different types of electrolytes to be considered for such designs [77].

Standard Gibbs free energy of formation data for Li_2O and Li_2O_2 were used to establish Equation (42) [314]. The design's cycling efficiency demonstrated its degree of rechargeability. The carbon electrode of this cell, which used a cobalt phthalocyanine catalyst, displayed an open-circuit voltage of 3.07 V. The cell was able to recharge to a cutoff voltage of 4.1V after being discharged three times to a capacity of 100 mAh $g^{-1}$and then discharged to that capacity three more times.

The advancement of aprotic LAB materials and performance has since seen several publications and initiatives, with this work serving as the first. Developments in electrolyte stability and conductivity are now being researched [315], as they are preserving performance when extracting oxygen from ambient air that contains moisture and CO_2 , as well as boosting capacity and longevity when recharging [77]. The fourth kind of LAB tries to resolve these problems by employing a hybrid design in which the air-breathing cathode side of the cell uses an aqueous electrolyte while the lithium anode is in contact with a solid-state electrolyte. Low oxygen diffusion rates within the cathode restrict the power output of LAB

cells [316], although alkaline catholytes enable the use of ORR catalysts created for fuel cells. The creation of a soluble discharge product (LiOH), in alkaline electrolytes) as opposed to insoluble lithium oxides is another benefit.

Additionally, safety can be improved by avoiding combustible organic catholytes. Wang and Zhou [210] first proposed the hybrid idea in 2010, and they subsequently developed an intriguing variation in which a capacitor electrode was used in parallel with the air-breathing cathode as an extra cathode in contact with the non-aqueous electrolyte solution. The goal was to show that the air-breathing cathode would perform well in situations with high energy demand, while the capacitor cathode could guarantee peak power generation when high power was required. They estimated that a battery with LAB + capacitor cells had a peak power capacity that was approximately 10 times more than a battery with LAB cells only [77].

CHAPTER 9

Conclusion and perspective of metal-air batteries

9.1 Progress done in the cathode of MABs

Noble metal-based electrocatalysts have amazing performance, however their electrocatalytic activity is restricted by their low durability and expensive cost [317,318,319]. Research created a graphene quantum dot/graphene hydrogel GH-GQD that has outstanding durability and strong electrocatalytic action in alkaline solution in primary ZABs to solve these difficulties. The GQD has a higher number of active sites than GH, resulting in higher ORR electrocatalytic activity. Then, different GQD concentrations (45 mg, 90 mg, and 180 mg GQD) were compared, and it was discovered that the GH-GQD-90 exhibited high ORR activity and excellent durability in alkaline primary MABs, high performance as an ORR catalyst in non-rechargeable ZAB, and its discharge property performance at higher current densities can be compared to platinum on carbon catalyst (Pt/C). The GH-GQD, when applied in MABs and fuel cells, shows great potential for ORR as a replacement for noble materials.

Figure 25 shows a one-dimensional manganese cobalt oxide (spinel-type), Mn Co_2O_4 (MCO), and CoMn_2O_4 (CMO) nanofiber that functioned as bi-functional cathode catalysts for rechargeable MABs developed during research into rechargeable MABs. They were therefore evaluated as catalysts in ZABs and found to greatly reduce the voltage gaps between discharge and charge. As a result, of comparison to a cathode without a catalyst, the round-trip performance was enhanced. The CMO-NF and MCO-NF catalysts retain their stability during repeated discharge–charge cycling; whereas carbon corrosion in the catalyst/carbon composite cathode cause the battery's cycling performance to decline dramatically. It's probable that the construction of MCO-NF and OMC-NF is what's causing the electrochemical characteristics to improve.

A study blended Ni, Co, and S to generate Pt-based alternative electrocatalysts with higher electrochemical performance. Due to the combination of transition metal elements with single sulfides or metal oxides, mixing sulfides and metal oxides including transition metals frequently exhibited useful electrochemical efficiency. In an alkaline media, NiCoCO_2S_4 microspheres show strong electrocatalytic activity for OER and ORR, as well as high stability, making them a useful catalyst for aqueous AABs and rechargeable ZABs.

As a possible air cathode catalyst, a PdCo/C bimetallic nano catalyst was developed in research. From 4 to 24 hours, the produced catalysts were heat treated at 200°C in an H_2/Ar environment. The heat treatment and overall catalyst performance were shown to be inextricably linked. The best heat treatment

time was 8 hours, which resulted in the most activity for ORR and OER. As a result, rechargeable Zn–air and Mg–air batteries were evaluated using the HT-8 h PdCo/C catalyst. The stability and activity of the Zn–air and Mg–air batteries are enhanced, and the activity is raised when the HT-8 h PdCo/C catalyst is applied, showing that it has the potential to be utilized on a large scale [320].

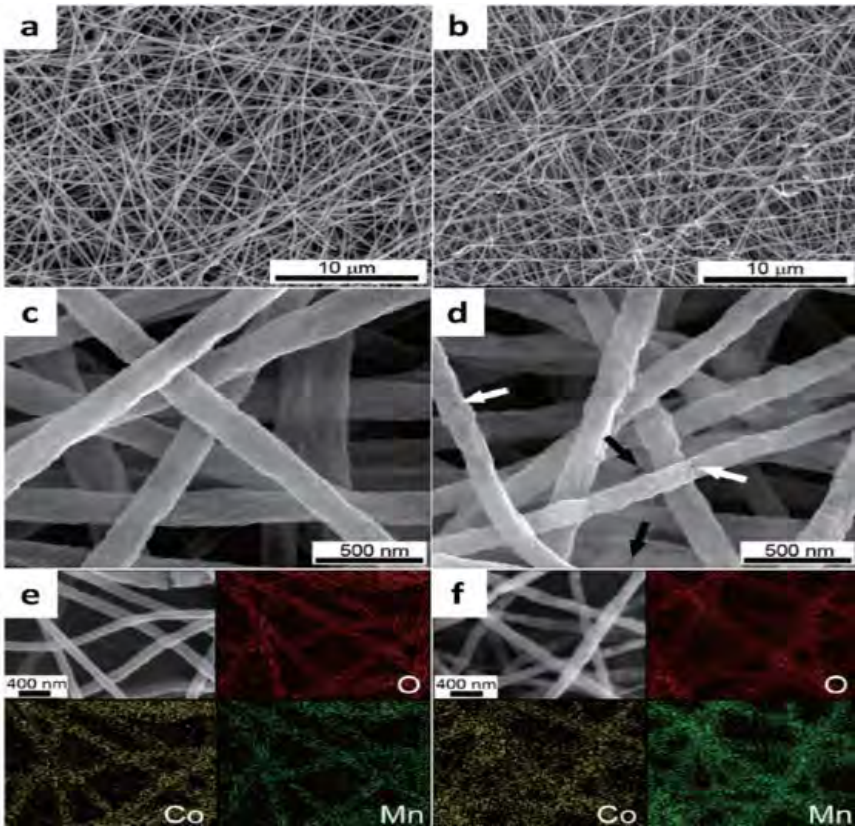

Figure 25 Scanning electron microscope of (a-c) MCO-NF and (b-d) CMO-NF. The arrows in (d) show fiber surface pores. EDS mapping data which present the element distributions of Co, Mn, and O for (e) MCO-NF and (f) CMO-NF, adapted from [52].

A new way of producing air cathodes uses cost-effective methods to minimize cathode structure while keeping excellent quality. To further examine the performance and properties of the newly constructed air cathode, the study team used a variety of characterization methods, which then compared to commercial air cathodes. The gas flow restriction and internal electrical resistance of the system are both reduced because the developed air cathode does not require the heat seal coating materials that are used in commercial air cathodes, allowing for more water to be transported to the reaction sites as well as in flow ability. The performance of a magnesium–air single cell with produced air cathodes is equivalent to a commercial air cathode [321]. The newly developed air cathode, on the other hand, is both cost-effective and acceptable as a cathode for an MAB in a neutral or alkaline electrolyte in terms of manufacturing and materials.

9.2 Progress in the design of the MABs

Primary and secondary MABs are the two types of MABs. The primary MABs are not rechargeable, however the secondary MABs are. The secondary MABs have two or three electrodes, each with an ORR

and OER catalyst, depending on the model. The non-rechargeable MABs have two electrodes, each with an ORR catalyst. The metal electrode is placed between the air cathode electrode and the charging electrode for the OER in the three-electrode setup, which is a useful position. During the charging process, the air cathode is electrically segregated, extending its longevity by keeping it from being exposed to the high oxygen evolution reaction potential during the charging phase. Rechargeable MABs, on the other hand, have a two-electrode design with a metal electrode and a bifunctional air electrode that contains catalysts for ORR and OER, as well as other functionalities. This design is straightforward and does not require the separation of the two electrolyte flows because the air cathode may function as both an anode for OER and a cathode for ORR [81]. It also has less mass (leading to a greater specific energy) and fewer interfaces, reducing the risk of kinetic rate losses [52].

9.3 Cell structure

The categorization of MABs into three variants is shown in Figure 26: the traditional static battery, the flow battery, and the flexible battery.

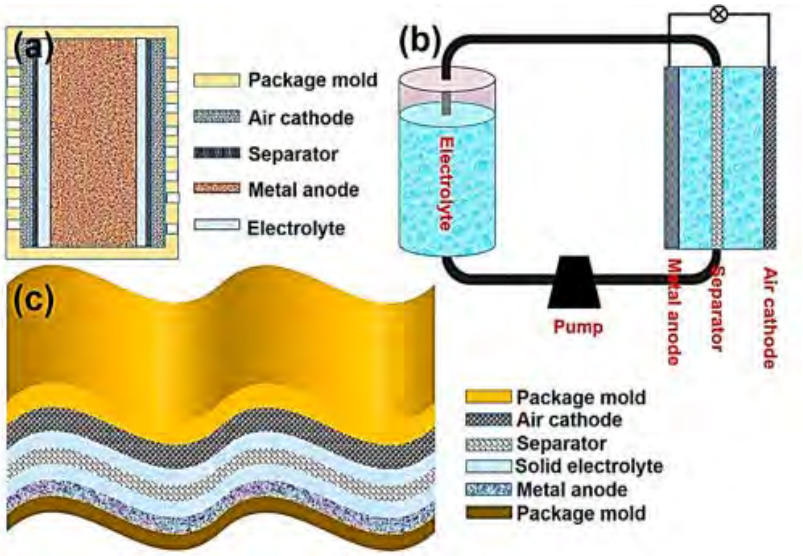

Figure 26 Configurations of MABs in a (a) multi-cell static battery, (b) flow battery and (c) flexible battery, adapted from [61].

The classic static air battery, which includes the three major components (anode, cathode, and electrolyte) as well as a separator, is the original arrangement. The kinetics of the anode reaction are fast in this configuration compared to the cathode reaction, requiring highly efficient catalysts to facilitate the reactions, in addition to the challenge of by-products that deposit insoluble on the surface of the electrodes during charge-discharge cycles, resulting in a decrease in battery performance due to the blocking of the electrode pores, limiting the air diffusion step. The flow battery is the second configuration, and it includes an anode, cathode, electrolyte, separator, and electrolyte bank, with a pump to drive the electrolyte flow. The electrolyte flow arrangement reduced volume density and power efficiency; also, extra tubes and pumps complicated the discharge process. The third design is the flexible

battery, which is gaining popularity as the need for flexible, portable electronics has increased in recent years, demanding the use of a flexible energy storage device. A thin metallic plate anode to minimize battery weight, a cathode such as carbon fiber, a highly conductive electrolyte, and a separator make up this type of battery. Due to their safe and efficient operation, high energy density, and low cost, ZABs and aluminum-air batteries are now the perfect flexible batteries [61].

9.3.1 Static battery

Metal–air batteries with a static structure have attracted considerable attention, although their performance is limited in terms of practical power, energy density and energy efficiency. On the other hand, combining a static cell structure with other energy technologies is complicated and difficult. These batteries may be utilized in a variety of applications, from small and portable electronic devices to large-scale electronics [322].

9.3.1.1 Coin type

Figure 27 depicts a coin cell type and its components, while Figure 28 shows the performance of this design with several electrolytes at a concentration of 6 M: potassium hydroxide (KOH), polyvinyl alcohol (PVA), poly acrylic acid (PAA), and polyacrylamide (PAM).

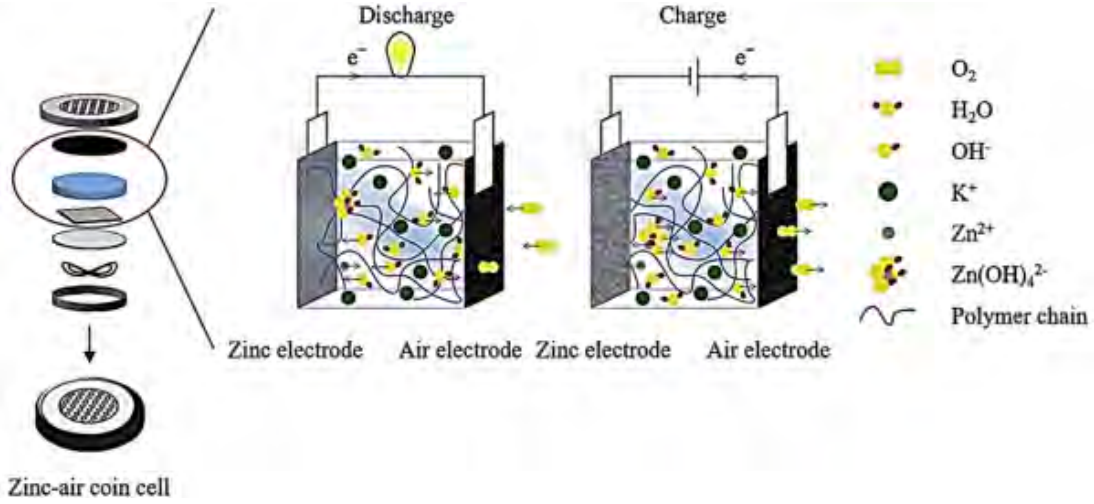

Figure 27 Schematic diagram of a coin cell, with permission to reproduce from [323].

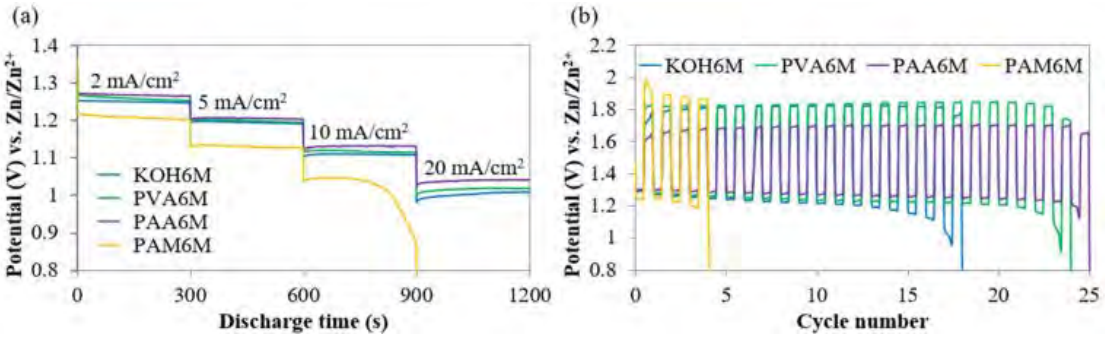

Figure 28 Zn–air coin cell: (a) discharge curves at different current densities and (b) discharge–charge cycling performance at 0.5 mA cm^{-2} using various electrolytes, with permission to reproduce from [323].

9.3.1.2 In situ cell

Figure 29 depicts the numbered components of a situ cell. The 1 and 2 numbers refer to the alloy clamp rings, and PEEK screws used to shut the cell after construction.

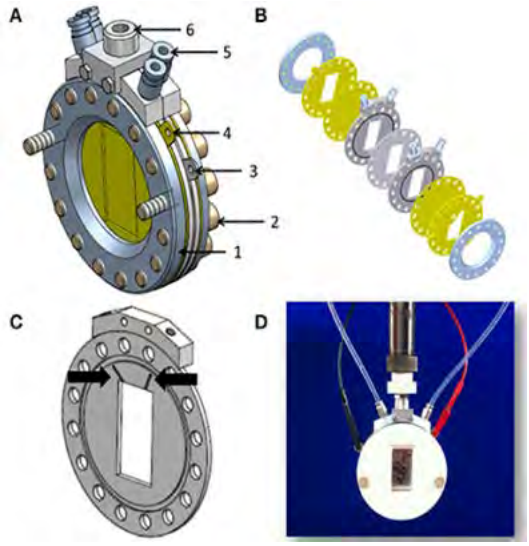

Figure 29 (A) Schematic diagram of in situ cell. (B) The cell components sketch. (C) Close-up view of the separator module (the black arrows represented the apertures which connect the battery inner compartment with the cell exterior). (D) Real assembled cell, from [324].

The negative and positive electrodes (thin sheets of Ni metal) are numbered 3 and 4, respectively. The tube connectors for pumping electrolyte or gas fuel are labelled with the number 5. The thyristor has the number 6 on it.

9.3.2 Flow battery

When it comes to cell construction, the flow system is adaptable and may easily be integrated with various energy technologies. Because of the anolyte/electrolyte flow, it is safe and has an extremely long life, limiting adverse effects. It has the capability of being employed for both large-scale energy storage and stationary power plants**.** Figure 30, on the other hand, displays the anolyte circulation [325].

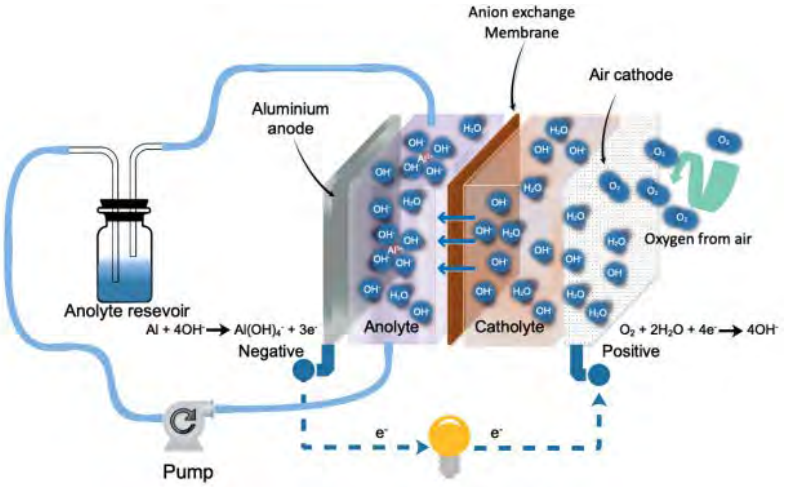

Figure 30 Schematic diagram of MAFBs' anolyte circulation from [325].

9.3.2.1 Circulation of Analytes

An anode electrode, an ion transport membrane, catalysts, a casting air electrode, and two current collectors compose the system. Figure 30 shows a cell with a redox couple flow at the negative electrode and air or oxygen at the positive electrode. To avoid concentration polarization, the flow rate of the anolyte must be restricted. By replacing the typical redox flow batteries REBs in the positive electrolyte tank with an oxygen GDE, the volume and overall weight are reduced, and the power and energy densities are improved. This technique to metal–air flow batteries is exemplified by vanadium–air and zinc–air flow batteries (VAFB, ZAFB) [325,322].

9.3.2.2 Electrolyte Cycling

Figure 31A displays a strategy, in which the flow through the electrochemical cell is continually supplied with fresh electrolyte. It boosts the metal anode charge and discharge efficiency while simultaneously removing by-products and side reactions. As a result, the cathode is even less blocked, making oxygen access easier. This method may be used to make sodium-air, zinc-air, and lithium-air flow batteries, and Figure 31B demonstrates the efficiency of zinc-air flow batteries made using a NiSxFeOy/sulfur-doped carbon fiber paper SCFP catalyst [322].

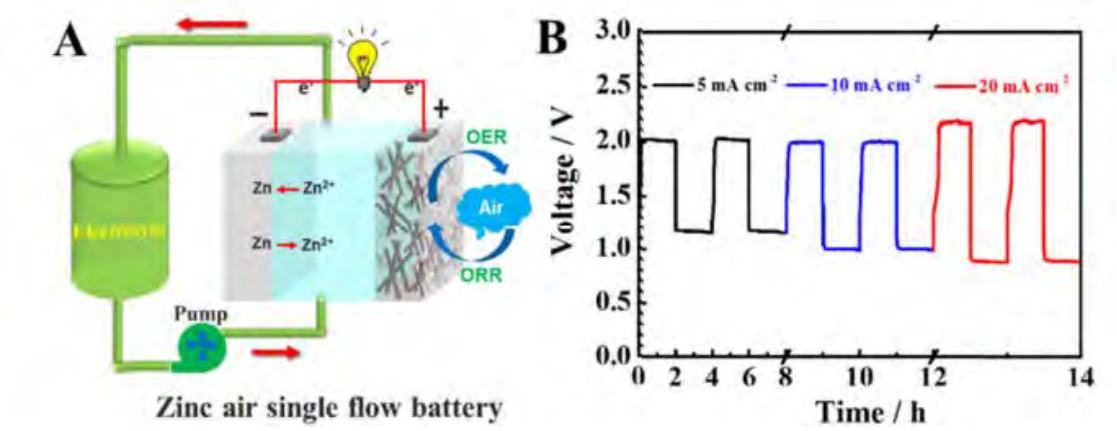

Figure 31 (A) The schematic diagram and (B) the charge-discharge curves of the assembled ZAFB, adapted from [326].

9.3.2.3 Hybrid Electrolyte Flow Battery

As several metals, such as Na and Li, are water-sensitive, their utility in watery conditions is challenged. In their flow arrangements, inorganic/organic hybrid electrolytes divided by a plate that is a superionic conductor are suggested. Additionally, in static sodium and lithium–air batteries, this idea has been greatly refined to protect the aprotic electrolyte and the highly reactive Na/Li metal anode from oxygen crossover or water and carbon dioxide pollutants in ambient air [322].

9.3.3 Flexible battery

When subjected to repeated mechanical strain over a lengthy period of time, the flexibility of the flexible MABs should be assured, and the security of the battery should be ensured when subjected to a

range of deformation situations. Flexible MAB electrodes must be capable of adapting to changing circumstances. Metal ribbons, metal rods, metal foil, or a flexible metal substrate coated in a metallic powder, as well as metal rods coated in a metallic powder, can all be used as anodes. A cathode current collector also has a lot of flexibility, a great of conductivity, and a lot of air permeability. Graphene and nanotubes, which have strong tensile strength and a high Young's modulus, are the carbon materials with the most promise as active materials. Putting metallic or metal oxide/nitride over a carbon substrate also improves the catalytic activity of the cathode **[**61**].** The tight contact between the cell components is credited with the flexible MABs' outstanding performance [327].

9.3.3.1 Fiber-Type

A polymer electrolyte (e.g., gelatin gel polymer electrolyte GGPE) is commonly used to surround the center metal anode and a flexible air cathode covered with the electrolyte in this form of MAB. It is capable of performing well under external strain. Other investigations have also shown that this arrangement type has outstanding mechanical stability and electrochemical performance [327].

9.3.3.2 Sandwich-Type

In a sandwich-type MAB, the components are made in plan form and then assembled as shown in Figure 32. Under bending circumstances, this structure has a high volumetric and gravimetric energy density, as well as outstanding electrochemical and cycling performance, even at a high current density. [327,328]

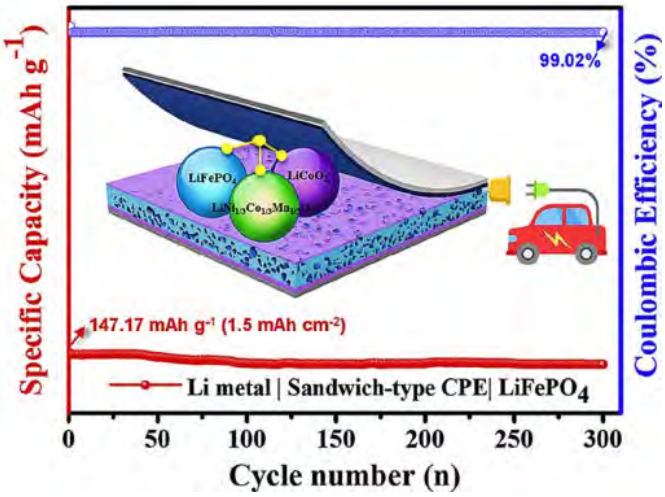

Figure 32. Stability of sandwich-type Li metal battery (inset shows schematic of the cell from [328].

9.3.3.3 Array

Figure 33 shows a planner multilayer MAB array setup. It has a thickness of about 3 mm, is flexible and stretchy, and has good stable and rechargeable battery performance. This array can be linked in series, parallel, or a hybrid of the two. It has the potential to be employed in wearable devices [329].

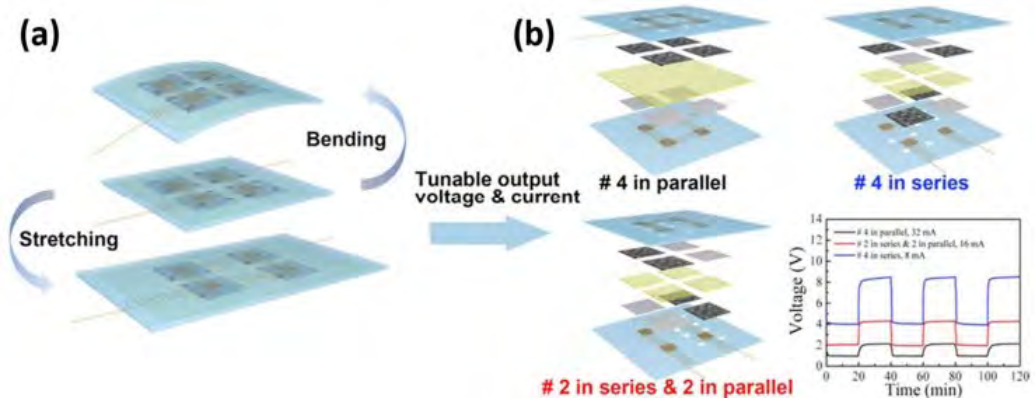

Figure 33 (a) Multilayered structure of a flexible/stretchable rechargeable ZAB array and (b) bending and stretching the battery and different array connections series and parallel, with permission to reproduce from [330].

9.4 Large-scale metal-air batteries

Global warming caused by fossil fuels is generating a lot of anxiety these days [331,332]. Several techniques have been used to reduce dependency on fossil fuels, including the use of efficient energy conversion devices such as fuel cells [333,334,335], enhancing the efficiency of present energy conversion devices, and employing renewable energy sources. Renewable energy sources are the most promising alternative among these many approaches since they are sustainable and have no or little environmental repercussions [336,337]. However, the huge rise in renewable energy necessitates the development of a proper energy storage system to meet these demands [338,339]. The electricity grid will require the assistance of a sizable electrical energy storage system as the popularity of renewable energy production sources such as wind [340,341] and solar energy [342,343] grows. Renewable energy is intermittent, non - periodic, and changing by nature, necessitating regular monitoring. As a result, storing energy during peak energy production periods is critical to maintaining the quality of the power produced and meeting rising demand. Electrochemical energy storage systems may satisfy the fundamental requirements for large-scale energy storage systems, such as a short life cycle, quick reaction time, scalability, and high efficiency, when compared to other systems [322,344]. Electrochemical energy storage systems may also be less expensive than other types of energy storage. Electrochemical energy storage often refers to electrochemical capacitors and rechargeable batteries, which can be employed in a hybrid design with other systems [345].

The airflow in the MABs supports the reaction of the air electrode, obviating the requirement for reactant storage tanks. Furthermore, in order to be successful for large-scale energy storage, the air electrode must be bifunctional for both ORR and OER during discharge and charge, respectively. MABs are a viable substitute to gasoline since they are cost-effective, ultralightweight, and have a high energy density that is theoretically equivalent to that of gasoline. Its energy efficiency, on the other hand, is low, and its charge/discharge life cycle is short. The low energy efficiency and power density of MABs, which are caused by a greater overpotential and delayed oxygen reactions at the air cathode, limit their usage on a broad scale.

Because of its low cost, environmental friendliness, simplicity of scaling up, long-term viability, and abundance of raw materials, iron–air batteries are a possible alternative for large-scale energy storage. Their cycle life and efficiency, however, must be increased before they can be considered a viable choice [344]. Furthermore, among MABs, aluminum–air batteries (AABs) have the lowest cost and the second highest specific capacity, making them a promising potential candidate for large-scale energy applications, notably in renewable energy. As a result, AABs are gaining popularity as a sustainable and efficient energy storage and conversion technology capable of powering autos and massive electronic equipment [346]. MABs and redox flow batteries (RFBs) have shown tremendous potential for large-scale electrical energy storage as efficient electrochemical systems due to their high energy density and unique structural architecture. Using a combination of MABs with the concept of flow batteries to overcome side reactions yields a promising way for the construction of a metal–air flow battery for large-scale electrical energy storage. Metal–air flow systems offer significant promise for large-scale energy storage and transformation in the future power grid because to their inherent advantages and the high degree of design freedom they allow. It's also worth noting that, before considering the commercial use of MAB technologies, efforts should be done to prove their security and reliability in the professional and academic sectors [322]. To be employed on a wide scale in commercial applications, vanadium–air flow batteries (VAFBs) must enhance their efficiency and energy density while simultaneously decreasing their stack cost [322].

9.5 Applications of metal-air batteries

Metal–air batteries are tiny power sources that may be used in electric automobiles and portable electronic gadgets. They may also be utilized as energy storage devices or as efficient energy transfer stations, especially for renewable energy producers, because they can manage the flow of energy from photovoltaic (PV) panels, wind turbines, and electric grids, among other sources.

9.5.1 Water desalination using metal-air batteries

Water desalination demands the development of high-performance as well as low-energy technologies since the process of creating fresh water consumes energy. Electrochemical technologies, in addition to their ability to store energy, have enormous potential for water desalination [347,348]. A metal-air desalination battery (MADB) is a device that can desalinate water and generate electricity at the same time. It is self-contained and has the potential to produce electricity. The MADB included an AAB that used seawater as both a desalination solution and an electrolyte, as shown in Figure 34. Desalination efficiency, stability, and power output have all been accomplished, demonstrating the MADB concept's success. The amount of dissolved oxygen in the cathode, however, limited the amount of energy generated and the rate of desalination. With a current density of 6.58 A m^{-2} and an output voltage of 0.43 V, the maximum power density attained was 2.83 W m^{-2}. It also decreases salinity by 37.8% while generating 10 mWh of energy over the course of

14 hours of operation. Further development of the MADB may allow this concept to be used in real-world applications on a big or small scale in the future [347].

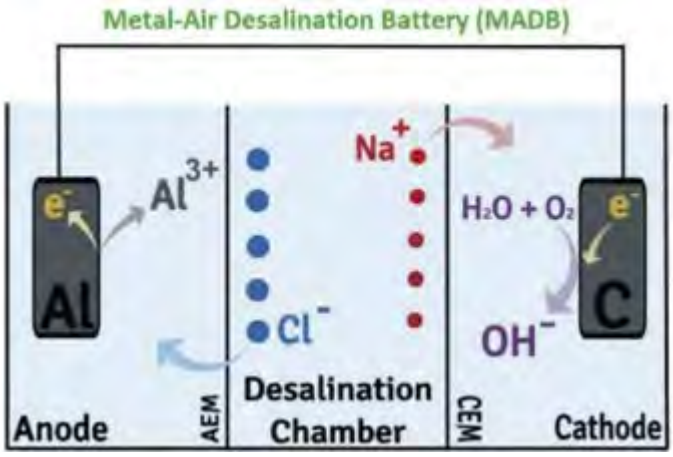

Figure 34 On the left is a schematic drawing of the MADB's three-chamber cell, and on the right is a picture that has been taken from [347].

Figure 35 shows how zinc-air desalination (ZAD) was used in the literature for electrochemical desalination using MAB technology. At a current density of 1 mA cm^{-2}, the ZAD cell utilizing MoS_2 bifunctional catalyst demonstrated a desalination capacity of 0.9 to 1.0 mg NaCl cm^{-2} and a charge efficiency of 70%. MAD (metal-air desalination) is a novel method that offers excellent electrochemical desalination performance using non-noble metal catalysts [348].

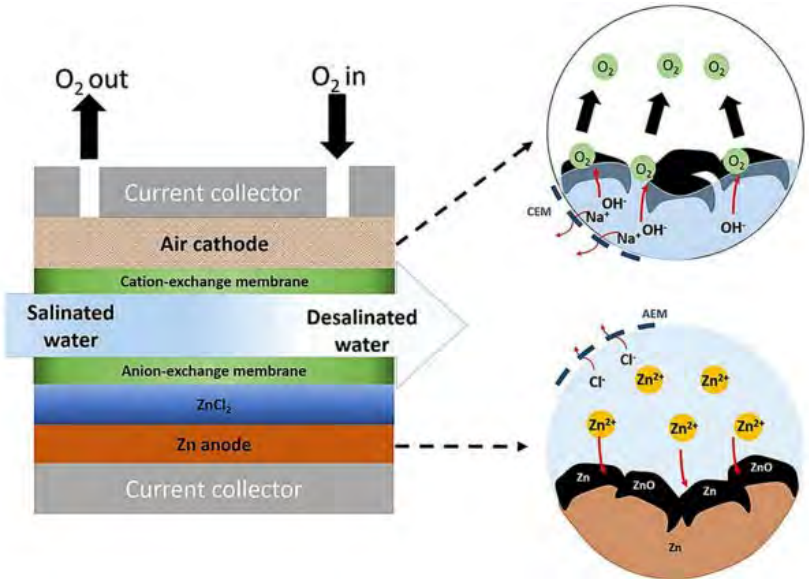

Figure 35 Configuration of Zn–air desalination ZAD cell, adapted from [348].

A considerable amount of interest has lately been devoted to the development of non-noble metal-based HER electrocatalysts, primarily due to their low-cost and earth-abundant properties. One novel family of non-Pt catalysts for the hydrogen evolution process is metal (Co, Mo, Ni)-encapsulated and heteroatom (N, S, P)-doped carbon (HER). Nitrogen doping may significantly boost carbon's electrocatalytic activity, and co-doping with phosphor can further activate the neighboring carbon atom and increase reactivity [275].

9.6 Challenges of metal-air batteries

Despite the fact that the MAB technology has been studied for the past decade, various technological challenges must be overcome before the idea can be commercialized.

9.6.1 Metallic anode challenges

Corrosion, passivation, and dendritic growth of the metallic anode are all serious issues for MABs. As seen in the following procedure, corrosion is one of the most important side reactions between a metal and an electrolyte.

$$M + (2 + x)\, H_2O \leftrightarrow 2M(OH) + H_2 \quad (46)$$

$$M + \ H_2O \leftrightarrow MO_x + H_2 \quad (47)$$

Because the typical voltage of M/MO is below the level of hydrogen development, hydrogen evolution is inherently favored in practically all MABs. The equations above can be used to determine the rate of corrosion produced by the hydrogen evolution reaction (HER). The hydrogen evolution reaction (HER) can reduce a metal anode's columbic efficiency, perhaps resulting in a battery explosion. Corrosion may occur in a variety of batteries, including FABs, AABs, ZABs, and LABs. The formation of an insulating layer on the electrode surface, which stops the discharge product from moving around, is known as passivation. The layer that forms prevent the discharge of electrons. This may be found in a variety of batteries, including AABs, ZABs, and LABs. The passivation layers in MABs include LiOH, ZnO, and Al_2O_3, depending on the system. When an air cathode was present, the produced soluble species formed a non-conductive layer on the metal's surface. They increase the internal electric resistance of the cell, which prevents metal from dissolving. A good way to avoid the formation of a passivation layer is to use porous electrodes [61].

Dendritic development and deformation cause the geometry of the metal electrode to alter over time, resulting in uneven surface roughness as dendrites form. This occurs as a result of metal ions accumulating in alkaline electrolytes during metal electrode cycling. This can cause a battery system to become unstable, or it might create a shortcut. In Li-air, Fe-air, and Zn-air batteries, dendritic structures emerge [61].

9.6.2 Electrolyte challenges

Some types of MABs, such as ZABs, find it difficult to dissolve CO_2 from the air in the aqueous KOH electrolyte because CO_2 interacts with OH^- and produces CO_3^{2-}, lowering the electrolyte conductivity and delaying the cell reaction. A CO_2 filter may fix the problem, but it would increase the system's complexity and cost [349].

Because the electrolyte becomes thermodynamically unstable when hydrogen gas evolves, electrolytes having a metal electrode with a lower potential than hydrogen evolution may face difficulties [349]. The deposition of insoluble byproducts on both electrodes' surfaces during charge-discharge cycles is a difficulty that must be considered when utilizing an active electrolyte. By obstructing the electrode pores and reducing air passage, these by-products degrade the battery's performance [61,350].

The absorption of moisture from the environment, as well as the evaporation of electrolytes, both contribute to the aqueous MABs' life being shortened. Air electrode flooding may occur as a result of water accumulation, obstructing oxygen supply to the catalyst's active regions. Water loss, on the other hand, boosts the body's electrolyte content, which has a negative influence on the discharge response. Furthermore, diluting the electrolyte reduces ionic conductivity, resulting in increased internal resistances in the system. The internal water balance of the battery may be optimized by taking into account the amount of metal utilized, the composition and volume of the electrolyte, and the degree of gas diffusion while building the battery. The electrolyte's polymerization may aid in reducing the quantity of moisture lost. In addition, using a siloxane barrier prevents flooding and drying out [351].

9.6.3 Cathode challenges

It is difficult to create a stable, active, and affordable bi-functional air catalyst that is suitable for both OER and ORR [349]. Solid products such as Li_2O_2 precipitate in the cathode, forming a thick coating that slows electron movement and may even result in the clogging of cathode pores, lowering the cell's total capacity. When running at high current densities, oxygen transfer is a concern for some types of MAB [349].

9.7 Conclusion

Metal–air batteries are promising electrochemical systems that are safe, ecologically acceptable, and lightweight, with a high energy density. Portable electric gadgets, wearable devices, and large-scale applications, such as electric automobiles, are just a few of the uses for MABs. The mechanism of MABs, kinds, electrode materials, electrolytes, innovative designs, and new applications are all comprehensively discussed in this paper. The problems and suggestions are presented.

- Anodes for MABs can be made of a variety of metals. Each metal has its own set of benefits and drawbacks. Due to its high energy density, low weight, strong recyclability, environmental friendliness, and low cost, Al is one of the most promising electrodes.
- Despite the aqueous electrolytes' high ionic conductivity, leakage, stability, and thermodynamic restrictions are obstacles to their use. Electrolyte additions or non-aqueous electrolytes can help to mitigate or eliminate these issues, increasing MAB durability and energy density.
- For commercial MABs, a thermally and mechanically porous cathode electrode capable of ORR and OER is required.
- Both Al-air batteries and iron–air batteries are viable options for MAB manufacture on a big scale.
- Because of the flow of anolyte/electrolyte, which reduces side reactions, flow MABs are safe and have a long operating life. Large-scale energy storage and stationary power plants can also benefit from flow MABs.
- MABs in water desalination and wastewater treatment have showed encouraging outcomes in a few trials. However, further research is still needed.

References

[1] Britannica, T. Editors of Encyclopedia (2022, October 18). '*Energy',* Encyclopedia Britannica.

[2] Robert Buckingham, Tristan Asset, Plamen Atanassov, (2021). *'Aluminum-air batteries: A review of alloys, electrolytes and design'*, University of California, Irvine, CA), 229762, 498.

[3] D.H. Evans, (2008).*'One-Electron and Two-Electron transfers in Electrochemistry and Homogeneous Solution Reactions'* Chem. Rev. 108(7), 2113–2144.

[4] Petrovic, S., & Petrovic, S. (2021).' *History of electrochemistry'.* Electrochemistry Crash Course for Engineers, 1-2.

[5] Funke, K., (2013*).' Solid State Ionics: from Michael Faraday to green energy-the European dimension.'* Sci Technol Adv Mater, 14 043502.

[6] Prentice, G. (2003). '*Electrochemical engineering'*. Encyclopedia of Physical Science and Technology, 143-159.

[7] Breitkopf, C., & Swider-Lyons, K. (2017). '*Electrochemical science—historical review'*. Springer Handbook of Electrochemical Energy, 1-9.

[8] Chen, Z., Hassan, F. M., & Yu, A. (2011). '*Electrochemical Engineering Fundamentals'*. Electrochemical Technologies for Energy Storage and Conversion, 1, 45-68.

[9] Ciribelli, B. N., Colmati, F., & De Souza, E. C. (2020). 'Nernst equation applied to electrochemical systems and centenary of his Nobel Prize in chemistry'. Int. J. Innov. Educ. Res, 8, 670-683.

[10] Ciobanu, M., Wilburn, J. P., Krim, M. L., & Cliffel, D. E. (2007). 'Fundamentals Handbook of Electrochemistry ed CG Zoski'.

[11] John B. Goodenough, (2015).*' Energy storage materials: A perspective',* Energy Storage Materials, 1, 158-161.

[12] Oxtoby, D. W., Gillis, H. P., & Butler, L. J. (2015). 'Principles of modern chemistry'. Cengage learning.

[13] Li, J., Du, Z., Ruther, R. E., An, S. J., David, L. A., Hays, K., & Wood, D. L. (2017). 'Toward low-cost, high-energy density, and high-power density lithium-ion batteries'. Jom, 69, 1484-1496.

[14] Wang, W., Wei, X., Choi, D., Lu, X., Yang, G., & Sun, C. (2015). 'Electrochemical cells for medium-and large-scale energy storage: fundamentals. In Advances in batteries for medium and large-scale energy storage', 3-28. Woodhead Publishing.

[15] Wang, S., Fan, Y., Stroe, D. I., Fernandez, C., Yu, C., Cao, W., & Chen, Z. (2021).'Lithium-Ion Battery Characteristics and Applications'. Battery System Modeling, 1-46.

[16] Team, M. E. V. (2008). 'A Guide to Understanding Battery Specifications'. *Guide to Understanding Battery Specifications'.*

[17] L. Yan, B. Zhang, J. Zhu, Y. Li, P. Tsiakaras, P.K. Shen, (2020).*' Electronic modulation of cobalt phosphide nanosheet arrays via copper doping for highly efficient neutral-pH overall water splitting'* Applied Catalysis B: Environmental, 265, 118555.

[18] G.-f. Long, K. Wan, M.-y. Liu, Z.-x. Liang, J.-h. Piao, P. Tsiakaras, (2017).*'Active sites and mechanism on nitrogen-doped carbon catalyst for hydrogen evolution reaction'* Journal of Catalysis, 348, 151-159.

[19] Giorgi, L., & Leccese, F. (2013).*' Fuel cells: Technologies and applications'*. The Open Fuel Cells Journal, 6(1).

[20] S Song, V Maragou, P Tsiakaras, (2007).*'How far are direct alcohol fuel cells from our energy future?'* J. Fuel Cell Sci. Technol. 4(2) 203-209.

[21] Ru-Shi Liu, Lei Zhang, Xueliang Sun, Hansan Liu, and Jiujun Zhang, (2011).*'Electrochemical Technologies for Energy Storage and Conversion',* 2, 1-38.

[22] C. Vayenas, S. Bebelis, I. Yentekakis, P. Tsiakaras, H. Karasali, (1990).*' Platinum Metals Review',* 4(3), 122.

[23] Shengyu Jing, Lishang Zhang, Lin Luo, Jiajia Lu, Shibin Yin, Pei Kang Shen, Panagiotis Tsiakaras, (2017).*' N-Doped Porous Molybdenum Carbide Nanobelts as Efficient Catalysts for Hydrogen Evolution Reaction,* Applied Catalysis B: Environmental 224, 533-540.

[24] C. Molochas, P. Tsiakaras (2021). '*Carbon monoxide tolerant Pt-based electrocatalysts for H2-PEMFC applications: current progress and challenges*'. Catalysts, 11(9), 1127.

[25] P. Tsiakaras, C. Athanasiou, G. Marnellos, M. Stoukides, J. E. ten Elshof, and H. J. Bouwmeester, (1998).*'Methane activation on a La0. 6Sr0. 4Co0. 8Fe0. 2O3 perovskite: Catalytic and electrocatalytic results,'* Applied Catalysis A: General, 169, 249-261.

[26] D. Medvedev, V. Maragou, E. Pikalova, A. Demin, and P. Tsiakaras, (2013) *'Novel composite solid state electrolytes on the base of BaCeO3 and CeO2 for intermediate temperature electrochemical devices,'* Journal of Power Sources, 221, 217-227.

[27] E. Gorbova, V. Maragou, D. Medvedev, A. Demin, and P. Tsiakaras, (2008) *'Influence of Cu on the properties of gadolinium-doped barium cerate,'* Journal of Power Sources, 181, 292-296.

[28] P.E. Lokhande, U.S. Chavan, A. Pandey, (2020).*'Materials and fabrication methods for electrochemical supercapacitors: overview',* Electrochemical Energy Reviews', 3, 155-186.

[29] B. Li, Z. Li, Q. Pang, Q. Zhuang, J. Zhu, P. Tsiakaras, P.K. Shen, (2019).*'Synthesis and characterization of activated 3D graphene via catalytic growth and chemical activation for electrochemical energy storage in supercapacitors* 'Electrochemical Acta, 324, 134878.

[30] A. Muzaffar, M.B. Ahamed, K. Deshmukh, J. Thirumalai, (2019).*'A review on recent advances in hybrid supercapacitors: Design, fabrication, and applications'* Renewable and Sustainable Energy Reviews, 101, 123-145.

[31] Goonan, T. G. (2012). *Lithium use in batteries*: *U.S. Geological Survey Circular 1371*, 14 p., available at https://pubs.usgs.gov/circ/1371/.

[32] Su, L., Badel, A. F., Cao, C., Hinricher, J. J., & Brushett, F. R. (2017). 'Toward an inexpensive aqueous polysulfide–polyiodide redox flow battery'. Industrial & Engineering Chemistry Research, 56(35), 9783-9792.

[33] Yabuuchi N, Kubota K, Dahbi M, Komaba, (2014). S: *'Research development on sodium-ion batteries.'* Chem Rev, 114(23), 11636-11682.

[34] Jialiang Tang, Arthur D Dysart and Vilas G Pol, (2015).*' Advancement in sodium-ion rechargeable batteries',* 9, 34-41.

[35] Wang, C.; Yu, Y.; Niu, J.; Liu, Y.; Bridges, D.; Liu, X.; Pooran, J.; Zhang, Y.; Hu, A., (2019*).'Recent progress of metal–air batteries—A mini review',* 9(14), 2787.

[36] Cachet, H., El Moustafid, T., Herbert-Guillou, D., Festy, D., Touzain, S., & Tribollet, B. (2001). '*Characterization of deposits by direct observation and by electrochemical methods on a conductive transparent electrode. Application to biofilm and scale deposit under cathodic protection'*. Electrochimica Acta, 46(24-25), 3851-3857.

[37] F. von Sturm, (1981).*' Comprehensive Treatise of Electrochemistry, Springer'*, 385, 3.

[38] Lewis, G. N., & Keyes, F. G. (1913). 'The potential of lithiumelectrode'. Journal of the American Chemical Society, 35(4), 340-344.

[39] J.-M. Tarascon and M. Armand, (2011). *'Materials For Sustainable Energy: A Collection of Peer-Reviewed Research and Review Articles from Nature Publishing Group'*, World Scientific, 171.

[40] Iwakura, C., Fukumoto, Y., Inoue, H., Ohashi, S., Kobayashi, S., Tada, H., & Abe, M. (1997). 'Electrochemical characterization of various metal foils as a current collector of positive electrode for rechargeable lithium batteries'. Journal of power sources, 68(2), 301-303.

[41] Baumann, W., & Muth, A. (2013). '*Batterien: Daten und Fakten zum Umweltschutz'*. Springer-Verlag.

[42] Κράββαρης, Α., & Τσακιρίδης, Δ. (2018). *'Ηλεκτροχημική ανίχνευση ασκορβικού και ουρικού οξέος με τη χρήση καταλυτών με βάση πλατίνα και παλλάδιο (Bachelor's thesis)'.*

[43] Arai, H., & Hayashi, M. (2009). *'Secondary batteries–metal-air systems| overview (Secondary and primary)'*.

[44] Liu, Y., Sun, Q., Li, W., Adair, K. R., Li, J., & Sun, X. (2017). *'A comprehensive review on recent progress in aluminum–air batteries'*. Green Energy & Environment, 2(3), 246-277.

[45] M. Root, (2011).*'The TAB™ Battery Book: An In-Depth Guide to Construction, Design and Use'*, New York: McGraw-Hill/TAB Electronics.

[46] Bruce, P. G., Freunberger, S. A., Hardwick, L. J., Peng, Z. Q., & Chen, Y. (2010, December). *'Lithium-air battery. In ACS National Meeting Book of Abstracts'.* American Chemical Society.

[47] Read, J. (2002). ‘Characterization of the lithium/oxygen organic electrolyte battery’. Journal of the Electrochemical Society, 149(9), A1190.

[48] Y. Liu, (2018). *'High-performance and recyclable Al-air coin cells based on eco-friendly chitosan hydrogel membranes'*, ACS Appl. Mater. Interfaces, 19730-19738, 10, 23.

[49] S.W. Kim, D.H. Seo, X. Ma, G. Ceder and K.J.A.E.M, (2012*).' Kang'*, 2 710.

[50] W. Liu, Q. Sun, Y. Yang, J.-Y. Xie and Z.-W.J.C.C. Fu, 49 (2013) 1951.

[51] Linden, D. and Reddy, T.B. (2002).*' Handbook of Batteries'*, 3rd, McGraw-Hill.

[52] Shem, Cai, (2021). *'Metal-Air Batteries—A Review', 7373, 14(21).*

[53] Mahajan, V., Mudgal, S., Yadav, A. K., & Prajapati, V. (2021). *‘Reliability modeling of renewable energy sources with energy storage devices’.* In Energy Storage in Energy Markets (pp. 317-368). Academic Press.

[54] Liu, Q. Pan, Z. Wang, E. An L. Sun, G, (2020). *'Aqueous metal-air batteries: Fundamentals and applications. Energy Storage Mater', 27,478-505.*

[55] L. Bockstie, D. Trevethan, S. Zaromb, (1963). *'Control of Al corrosion in caustic solutions*', J. Electrochem. Soc. 110 267.

[56] Zhang, X.-b, (2018*). 'Metal-Air Batteries: Fundamentals and Applications'*

[57] McKerracher, de Ponce Leon, Wills, Shah, & Walsh, (2015*). 'A review of the iron–air secondary battery for energy storage.’ 323-335, 80 2.*

[58] Bi, X.; Wang, R.; Yuan, Y.; Zhang, D.; Zhang, T.; Ma, L.; Lu, J., (2020). *'From sodium–oxygen to sodium–air battery: Enabled by sodium peroxide dehydrate.’ 4681-4686, 20, 6.*

[59] Li & Dai, (2014). *'Recent advances in zinc–air batteries.’ 5257-5275, 43.*

[60] Gür, (2018). *'Review of electrical energy storage technologies, materials and systems: Challenges and prospects for large-scale grid storage', 2696-2769, 11.*

[61] Wang, C.; Yu, Y.; Niu, J.; Liu, Y.; Bridges, D.; Liu, X.; Pooran, J.; Zhang, Y.; Hu, A., (2019*). 'Recent progress of metal–air batteries—A mini review', 2787, 9(14).*

[62] Mori, (2020). *'Recent developments for aluminum–air batteries', 344-369, 3.*

[63] C. Yu, F. Xu, L. Luo, H. S. Abbo, S. J. Titinchi, P. K. Shen, P. Tsiakaras, and S. Yin, (2019).*’Bimetallic Ni–Co phosphide nanosheets self-supported on nickel foam as high-performance electrocatalyst for hydrogen evolution reaction,’* Electrochemical Acta, 317, 191- 198.

[64] Wang & Xu, (2019). *'Materials design for rechargeable metal-air batteries’,* 1(3), 565-595.

[65] Kar, Simons, Forsyth, & MacFarlane, (2014*). 'Ionic liquid electrolytes as a platform for rechargeable metal–air batteries: A perspective.’ 16, 18658-18674.*

[66] Khan, Vagin, & Crispin, (2020). *'Can hybrid Na–air batteries outperform nonaqueous Na–O2 batteries?’ 7(5), 1902866.*

[67] Yu & Manthiram, (2017*). 'A voltage-enhanced, low-cost aqueous iron–air battery enabled with a mediator-ion solid electrolyte, 2(5), 1050-1055.*

[68] A.R. Despi´c, D.M. Draˇzi´c, J. Balakˇsina, Lj Gaji´c-Krstaji´c, R.M. Stevanovi´c, (1990). *'Investigation of oxidation potentials of substances accumulated during cathodic polarization of aluminium'*, Electrochim. Acta, 35, 1747-1755.

[69] S. Gudi´c, J. Radoˇsevi´c, I. Smoljko, M. Kliˇski´c, (2005*). 'Cathodic breakdown of anodic oxide film on Al and Al–Sn alloys in NaCl solution'*, 50(28), 5624-5632.

[70] Ingale P, Sakthivel M, Drillet J-F., (2017). *'Test of diethylmethylammonium trifluoromethanesulfonate ionic liquid as electrolyte in electrically rechargeable Zn/Air'.*

[71] Mori, (2020) *'Recent developments for aluminum–air batteries',* 3, 344-369.

[72] Li, Sun, Gebert, & Chou, (2017). *Current progress on rechargeable magnesium–air battery,* 7(24), 17000869.

[73] Zhang X.-b., (2018). *'Metal-Air Batteries: Fundamentals and Applications'*

[74] Durmus, Y.E.; Zhang, H.; Baakes, F.; Desmaizieres, G.; Hayun, H.; Yang, L.; Kolek, M.; Küpers, V.; Janek, J.; Mandler, D.; al., et, (2020). *'Side by Side Battery Technologies with Lithium-Ion Based Batteries.'* 10(24), 2000089.

[75] B. Zhang, J. Shan, W. Wang, P. Tsiakaras, and Y. Li, (2022).*'Oxygen Vacancy and Core–Shell Heterojunction Engineering of Anemone-Like CoP@CoOOH Bifunctional Electrocatalyst for Efficient Overall Water Splitting',* Small, 18(12), 2106012.

[76] X. Cai, L. Lai, J. Lin, & Z. Shen, (2017*). 'Recent advances in air electrodes for Zn–air batteries: Electrocatalysis and structural design',* 4, 945-976.

[77] Robert Buckingham, Tristan Asset, Plamen Atanassov, (2021*). 'Aluminum-air batteries: A review of alloys, electrolytes and design'*, Journal of Power Sources, 498, 229762.

[78] Pourbaix, (1974*). 'Atlas of electrochemical equilibria in aqueous solutions'*

[79] S.-M. Moon and S.-I. Pyun, (1997). *'The corrosion of pure aluminium during cathodic polarization in aqueous solutions'*, Corrosion Sci. 39, 399-408

[80] G.G. Perrault, (1979), *'The role of hydrides in the equilibrium of aluminum in aqueous solutions*', J. Electrochem. Soc., 126, 199.

[81] Doche, M. L., Rameau, J. J., Durand, R., & Novel-Cattin, F. (1999). *'Electrochemical behaviour of aluminium in concentrated NaOH solutions'*. Corrosion science, 41(4), 805-826.

[82] Y. Liu, (2017). *'A comprehensive review on recent progress in aluminum–air batteries',* Green Energy & Environment 2, 246-277

[83] Bratsch, S. G. (1989). *'Standard electrode potentials and temperature coefficients in water at 298.15 K.'* Journal of Physical and Chemical Reference Data, 18(1), 1-21.

[84] Keir, D. S., Pryor, M. J., & Sperry, P. R. (1967). *'Galvanic corrosion characteristics of aluminum alloyed with group IV metals'*. Journal of the Electrochemical Society, 114(8), 777.

[85] Pryor, M. J., Keir, D. S., & Sperry, P. R. (1968). '*U.S. Patent No. 3,368,952'*. Washington, DC: U.S. Patent and Trademark Office.

[86] Pryor, M. J., Keir, D. S., & Sperry, P. R. (1965).*' U.S. Patent No. 3,189,486'*. Washington, DC: U.S. Patent and Trademark Office.

[87] Pryor, M. J., Keir, D. S., & Sperry, P. R. (1966). '*U.S. Patent No. 3,240,688'*. Washington, DC: U.S. Patent and Trademark Office.

[88] Pryor, M. J., Keir, D. S., & Sperry, P. R. (1968).*' U.S. Patent No. 3,368,958'*. Washington, DC: U.S. Patent and Trademark Office.

[89] Pryor, M. J., Keir, D. S., & Sperry, P. R. (1965).*' U.S. Patent No. 3,189,486'*.. Washington, DC: U.S. Patent and Trademark Office.

[90] M.J. Pryor D. K., (1966). *'Heat Treating Process for Aluminum Base Alloys Containing Tin', US3250649A.*

[91] K. Yu, (2015). *'Effects of gallium on electrochemical discharge behavior of Al–Mg–Sn–In alloy anode for air cell or water-activated cell',* Nonferrous Metals Soc. China 25, 3747–3752.

[92] F. Ding, (2016). *'Aluminum–air batteries fundamentals and applications, in: V. Neburchilov, J. Zhang (Eds.), Metal–Air and Metal–Sulfur Batteries: Fundamentals and Applications',* CRC Press, 65-105.

[93] Wang, Q., Miao, H., Xue, Y., Sun, S., Li, S., & Liu, Z. (2017). *'Performances of an Al–0.15 Bi–0.15 Pb–0.035 Ga alloy as an anode for Al–air batteries in neutral and alkaline electrolytes'*. Rsc Advances, 7(42), 25838-25847.

[94] M.C. Reboul, P. Gimenez, J.J.A. Rameau, (1984). *'Proposed activation mechanism for Al anodes',* Corrosion 40, 366-371.

[95] P. Rüetschi, P. Delahay, (1955). *'Hydrogen overvoltage and electrode material. A theoretical analysis'*, J. Chem. Phys. 23, 195-199.

[96] Tuck, C. D. S., Hunter, J. A., & Scamans, G. M. (1987). '*The electrochemical behavior of Al-Ga alloys in alkaline and neutral electrolytes*'. Journal of the Electrochemical Society, 134(12), 2970.

[97] D.D. Macdonald, K.H. Lee, A. Moccari, D. Harrington, (1988*). 'Evaluation of alloy anodes for aluminum-air batteries: corrosion studies',* Corrosion 44, 652-657.

[98] Hunter, J. A. (1989). The anodic behavior of aluminium alloys in alkaline electrolytes (Doctoral dissertation, University of Oxford).

[99] Y.il Choi, R.S. Kalubarme, H.J. Jang, C.J. Park, (2011). *'Effect of alloying elements on the electrochemical characteristics of an Al alloy electrode for Al-air batteries in 4M NaOH solution TT -*

effect of alloying elements on the electrochemical characteristics of an Al alloy electrode for Al-air batteries in 4', Korean Journal of Metal Materials 4, 839-844.

[100] D.D. Macdonald, (1988*). 'Evaluation of alloy anodes for aluminum-air batteries: corrosion studies',* 44(9), 652-657.

[101] Hunter, (1989). *'The Anodic Behaviour of Aluminium Alloys in Alkaline Electrolytes'*, PhD thesis University of Oxford.

[102] Nie, Y., Gao, J., Wang, E., Jiang, L., An, L., & Wang, X. (2017). '*An effective hybrid organic/inorganic inhibitor for alkaline aluminum-air fuel cells'.* Electrochimica Acta, 248, 478-485.

[103] W. Wilhelmsen, T. Arnesen, Ø. Hasvold, N.J. Størkersen, (1991). *'The electrochemical behaviour of Al·In alloys in alkaline electrolytes',* Electrochim. Acta, 36, 79-85.

[104] S.Z. el Abedin, A.O. Saleh, (2004). *'Characterization of some aluminium alloys for application as anodes in alkaline batteries',* J. Appl. Electrochem., 34, 331-335.

[105] Zaromb, (1962*), 'The use and behavior of aluminum anodes in alkaline primary batteries'*, 109, 1125-1130.

[106] Z. Sun, H. Lu, (2015*). 'Performance of Al-0.5In as anode for Al–air battery in inhibited alkaline solutions',* J. Electrochem. Soc., 162, A1617–A1623.

[107] Han, X.; Qu, Y.; Dong, Y.; Zhao, J.; Jia, L.; Yu, Y.; Zhang, P.; Li, D.; Ren, N.; Feng, Y., (2018*). 'Microbial electrolysis cell powered by an aluminum-air battery for hydrogen generation, in-situ coagulant production and wastewater treatment,* 43(16), 7764-7772.

[108] D.D. Macdonald, C. English, (1990*). 'Development of anodes for aluminium/air batteries—solution phase inhibition of corrosion',* J. Appl. Electrochem., 20, 405-417.

[109] M.L. Doche, F. Novel-Cattin, R. Durand, J.J. Rameau, (1997). *'Characterization of different grades of aluminum anodes for aluminum/air batteries',* J. Power Sources 65, 197-205.

[110] S. Lapp, (1992). *'3 kW Net Power Aluminium/air Battery: System Verification and Performance'*

[111] A.M. Abdel-Gaber, E. Khamis, H. Abo-Eldahab, Sh Adeel, (2010). *'Novel package for inhibition of aluminium corrosion in alkaline solutions',* Mater. Chem. Phys. 124, 773-779.

[112] Y. Nie, (2017). *'An effective hybrid organic/inorganic inhibitor for alkaline aluminum-air fuel cells'*, Electrochim. Acta 248, 478-485.

[113] S. Wu, (2020*). 'Understanding the synergistic effect of alkyl polyglucoside and potassium stannate as advanced hybrid corrosion inhibitor for alkaline aluminum-air battery'*, Chem. Eng. J., 383, 123-162.

[114] Zhu, G., Angell, M., Pan, C. J., Lin, M. C., Chen, H., Huang, C. J., & Dai, H. (2019). *'Rechargeable aluminum batteries: effects of cations in ionic liquid electrolytes'*. RSC advances, 9(20), 11322-11330.

[115] Elia, G. A., Marquardt, K., Hoeppner, K., Fantini, S., Lin, R., Knipping, E., & Hahn, R. (2016). '*An overview and future perspectives of aluminum batteries'*. Advanced Materials, 28(35), 7564-7579.

[116] T. Jiang, M.J. Chollier Brym, G. Dub´e, A. Lasia, G.M. Brisard, (2006). *'Electrodeposition of aluminium from ionic liquids: Part I—electrodeposition and surface morphology of aluminium from aluminium chloride (AlCl3)–1-ethyl-3-methylimidazolium chloride ([EMIm] Cl) ionic liquids'*, Surf. Coating. Technol. 201, 1-9.

[117] Fang, G., Ho, W. K., Tu, W., & Zhang, M. (2018). *'Workability and mechanical properties of alkali-activated fly ash-slag concrete cured at ambient temperature'*. Construction and Building Materials, 172, 476-487.

[118] D. Gelman, (2017*). 'An aluminum ionic liquid interface sustaining a durable Al-air battery'*, J. Power Sources 364, 110-120.

[119] D. Gelman, B. Shvartsev, Y. Ein-Eli, (2014). *'Aluminum–air battery based on an ionic liquid electrolyte'*, J. Mater. Chem. 2, 47.

[120] N.R. Levy, S. Lifshits, E. Yohanan, Y. Ein-Eli, (2020). *'Hybrid ionic liquid propylene carbonate-based electrolytes for aluminum–air batteries'*, ACS Appl. Energy Mater. 3, 2528-2592.

[121] N. Bogolowski, J.-F. Drillet, (2017*). 'An electrically rechargeable Al-air battery with aprotic ionic liquid electrolyte',* ECS Transactions 75, 85-92.

[122] N. Bogolowski, (2018). *'Activity of different AlCl3-based electrolytes for the electrically rechargeable aluminium-air battery'*, Electrochim. Acta 274, 353-358.

[123] R. Mori, (2017*). 'Rechargeable aluminum–air battery using various air-cathode materials and suppression of byproducts formation on both anode and air cathode'*, ECS Transactions 80, 377-393.

[124] Mori, R. (2017). '*Electrochemical properties of a rechargeable aluminum–air battery with a metal–organic framework as air cathode material'*. RSC advances, 7(11), 6389-6395.

[125] Y. Wang, W. Pan, H. Kwok, X. Lu, D.Y.C. Leung, (2019*). 'Low-cost Al-air batteries with paper-based solid electrolyte'*, Energy Procedia 158, 522-527.

[126] Armand, M. B., Chabagno, J. M., & Duclot, M. J. (1979). '*Fast ion transport in solids. Electrodes and Electrolytes'*, 131.

[127] Hibino, T., Kobayashi, K., & Nagao, M. (2013). '*An all-solid-state rechargeable aluminum–air battery with a hydroxide ion-conducting Sb (v)-doped SnP 2 O 7 electrolyte'*. Journal of Materials Chemistry A, 1(47), 14844-14848.

[128] T. Hibino, K. Kobayashi, (2013*). 'An intermediate-temperature alkaline fuel cell using a Sn0.92Sb0.08P2O7-based hydroxide-ion-conducting electrolyte and electrodes*', J. Mater. Chem. 1, 1134-1140.

[129] R. Mori, (2019*). 'All solid-state rechargeable aluminum–air battery with deep eutectic solvent-based electrolyte and suppression of byproducts formation',* 9, 22220-22226.

[130] R. Mori, (2020*). 'Recent developments for aluminum–air batteries',* 3, 344-369.

[131] Alva, S., Sundari, R., Wijaya, H. F., Majlan, E. H., Arwati, I. G. A., & Sebayang, D. (2017, September). *'Preliminary study on aluminum-air battery applying disposable soft drink cans and Arabic gum polymer'*. In IOP Conference Series: Materials Science and Engineering 237(1), 012039 IOP Publishing.

[132] D.S. Horne, (2002). *'Casein structure, self-assembly and gelation'*, Current Opinion Colloid Interface Sci. 7, 456-461.

[133] M. Mokhtar, E.H. Majlan, A. Ahmad, S.M. Tasirin, W.R.W. Daud, (2018). *'Effect of ZnO filler on PVA-alkaline solid polymer electrolyte for aluminum-air battery applications',* 165(11), A2483.

[134] Yadav, G. G., Wei, X., & Meeus, M. (2021). Primary zinc-air batteries. In Electrochemical Power Sources: Fundamentals, Systems, and Applications, 23-45, Elsevier.

[135] A.v Ilyukhina, B.v Kleymenov, A.Z. Zhuk, (2017*). 'Development and study of aluminum air electrochemical generator and its main components'*, J. Power Sources 342, 741-749

[136] Y. Xue, S. Sun, Q. Wang, Z. Dong, Z. Liu, (2018). *'Transition metal oxide-based oxygen reduction reaction electrocatalysts for energy conversion systems with aqueous electrolytes'*, J. Mater. Chem. 6, 10595-10626.

[137] B. Chen, D.Y.C.A. Leung, (2016). *'Low-cost mechanically rechargeable aluminum–air cell for energy conversion using low-grade Aluminum foil'*, Journal of Electrochemical Energy Conversion and Storage 13(1), 011001.

[138] Tzidon, D., & Yakupov, I. (2017). *'*U.S. Patent No. 9,627,726'. Washington, DC: U.S. Patent and Trademark Office.

[139] A. Yadgar, Y. Miller, D. Tzidon, (2018). *'Protected Anode Structure Suitable for Use in Metal/Air Batteries',* US Patent 10,096,873, Google Patents.

[140] A. Melman, J. Lang, I. Yakupov, (2017).*'Electrolyte Regeneration',* 9,711,804 Google Patents.

[141] A. Tzidon, (2020). *'Systems and Methods for Regeneration of Aqueous Alkaline Solution'*

[142] Tzidon, A., Peretz, V., Yadgar, A., & Tzidon, D. (2020). U.S. Patent No. 10,581,061. Washington, DC: U.S. Patent and Trademark Office.

[143] Yadgar, A. (2019). '*U.S. Patent No. 10,193,201'*. Washington, DC: U.S. Patent and Trademark Office.

[144] Y. Miller, A. Yadgar, D. Tzidon, (2018*). 'System and Method for Increasing Electrical Efficiency of* Metal-Air Cell', 10,096,875, Google Patents.

[145] D. Tzidon, A. Yadgar, (2017). *'Hybrid Metal Air System and Method',* 9,768,479. Google Patents.

[146] A. Tzidon, A. Yadgar, K. Ono, (2018*). 'Thermal Battery for Heating Vehicles', 10,090,569.*

[147] H. Wen, (2020). *'High energy efficiency and high-power density aluminum-air flow battery',* Int. J. Energy Res. 44(9), 7568-7579.

[148] A.L. Smee III, (1840). *'On the galvanic properties of the metallic elementary bodies, with a description of a new chemico-mechanical battery'*, The London, Edinburgh, and Dublin Philosophical Magazine and Journal of Science 16, 315-321

[149] Bichat, M. (1878). '*Expériences relatives au tourniquet électrique.'* J. Phys. Theor. Appl., 7(1), 262-264.

[150] Barak, M. (1966). *'An electrical centenary Georges Leclanché (1839-82)'*. Electronics and Power, 12(6), 184-185.

[151] Heise, (1933). *'Air Depolarized Primary Battery'*

[152] Schallek, W. B. (1939). '*Big Abandoned Railroads'*. The Railway and Locomotive Historical Society Bulletin, (49), 62-68.

[153] Fu, J., Cano, Z. P., Park, M. G., Yu, A., Fowler, M., & Chen, Z. (2017). Electrically rechargeable zinc–air batteries: progress, challenges, and perspectives. Advanced materials, 29(7), 1604685.

[154] Zhang, J., Zhou, Q., Tang, Y., Zhang, L., & Li, Y. (2019).*' Zinc–air batteries: are they ready for prime time?'* Chemical Science, 10(39), 8924-8929.

[155] Fu J, (2019*). 'Recent progress in electrically rechargeable zinc–air batteries'* Advanced Materials, 31(31), Special Issue: Materials Electrochemistry for Chemical Transformation, 1805230

[156] Li, Y., & Lu, J. (2017). *'Metal–air batteries: will they be the future electrochemical energy storage device of choice?'* ACS Energy Letters, 2(6), 1370-1377.

[157] Gu, P., Zheng, M., Zhao, Q., Xiao, X., Xue, H., & Pang, H. (2017).*'Rechargeable zinc–air batteries: a promising way to green energy'.* Journal of Materials Chemistry A, 5(17), 7651-7666.

[158] Leong, K. W., Wang, Y., Ni, M., Pan, W., Luo, S., & Leung, D. Y. (2022). *'Rechargeable Zn-air batteries: Recent trends and future perspectives'.* Renewable and Sustainable Energy Reviews, 154, 111771.

[159] Zhao, Z., Fan, X., Ding, J., Hu, W., Zhong, C., & Lu, J. (2019). *'Challenges in zinc electrodes for alkaline zinc–air batteries: obstacles to commercialization'*. ACS Energy Letters, 4(9), 2259-2270.

[160] Chen, P., Zhang, K., Tang, D., Liu, W., Meng, F., Huang, Q., & Liu, J. (2020). *'Recent progress in electrolytes for Zn–air batteries'*. Frontiers in Chemistry, 8, 372.

[161] Jo, Y. N., Prasanna, K., Kang, S. H., Ilango, P. R., Kim, H. S., Eom, S. W., & Lee, C. W. (2017). *'The effects of mechanical alloying on the self-discharge and corrosion behavior in Zn-air batteries.'* Journal of industrial and engineering chemistry, 53, 247-252.

[162] Chotipanich, J., Arpornwichanop, A., Yonezawa, T., & Kheawhom, S. (2018). *'Electronic and ionic conductivities enhancement of zinc anode for flexible printed zinc-air battery'.* Engineering Journal, 22(2), 47-57.

[163] Park, D. J., Aremu, E. O., & Ryu, K. S. (2018). '*Bismuth oxide as an excellent anode additive for inhibiting dendrite formation in zinc-air secondary batteries'.* Applied Surface Science, 456, 507-514.

[164] Aremu, E. O., Park, D. J., & Ryu, K. S. (2019).*' The effects of anode additives towards suppressing dendrite growth and hydrogen gas evolution reaction in Zn-air secondary batteries'*. Ionics, 25, 4197-4207.

[165] Pyo, S., Eom, W., Kim, Y. J., Lee, S. H., Han, T. H., & Ryu, W. H. (2020). *'Super-expansion of assembled reduced graphene oxide interlayers by segregation of Al nanoparticle pillars for high-capacity Na-ion battery anodes.'* ACS applied materials & interfaces, 12(21), 23781-23788.

[166] Zhang, Y., Wu, Y., Ding, H., Yan, Y., Zhou, Z., Ding, Y., & Liu, N. (2018). *'Sealing ZnO nanorods for deeply rechargeable high-energy aqueous battery anodes.'* Nano Energy, 53, 666-674.

[167] Schmid, M., & Willert-Porada, M. (2017). *'Electrochemical behavior of zinc particles with silica based coatings as anode material for zinc air batteries with improved discharge capacity.'* Journal of Power Sources, 351, 115-122.

[168] Jo, Y. N., Santhoshkumar, P., Prasanna, K., Vediappan, K., & Lee, C. W. (2019). *'Improving self-discharge and anti-corrosion performance of Zn-air batteries using conductive polymer-coated Zn active materials'.* Journal of Industrial and Engineering Chemistry, 76, 396-402.

[169] Jo, Y. N., Santhoshkumar, P., Prasanna, K., Vediappan, K., & Lee, C. W. (2019). *'Improving self-discharge and anti-corrosion performance of Zn-air batteries using conductive polymer-coated Zn active materials.'* Journal of Industrial and Engineering Chemistry, 76, 396-402.

[170] Zhao, Z., Fan, X., Ding, J., Hu, W., Zhong, C., & Lu, J. (2019). '*Challenges in zinc electrodes for alkaline zinc–air batteries: obstacles to commercialization.'* ACS Energy Letters, 4(9), 2259-2270.

[171] Lin, H. E., Ho, C. H., & Lee, C. Y. (2017). *'Discharge performance of zinc coating prepared by pulse electroplating with different frequencies for application in zinc-air battery.'* Surface and Coatings Technology, 319, 378-385.

[172] Tan, W. K., Wada, Y., Hayashi, K., Kawamura, G., Muto, H., & Matsuda, A. (2019). *'Fabrication of an all-solid-state Zn-air battery using electroplated Zn on carbon paper and KOH-ZrO2 solid electrolyte.'* Applied Surface Science, 487, 343-348.

[173] Pan, Z., Yang, J., Zang, W., Kou, Z., Wang, C., Ding, X., & Wang, J. (2019). '*All-solid-state sponge-like squeezable zinc-air battery.*' Energy Storage Materials, 23, 375-382.

[174] Liu, S., Han, W., Cui, B., Liu, X., Zhao, F., Stuart, J., & Licht, S. (2017). '*A novel rechargeable zinc-air battery with molten salt electrolyte.'* Journal of Power Sources, 342, 435-441.

[175] Wu, Y., Jiang, C., Wan, C., & Tsuchida, E. (2000). '*Effects of catalytic oxidation on the electrochemical performance of common natural graphite as an anode material for lithium ion batteries.'* Electrochemistry Communications, 2(4), 272-275.

[176] Alwast, D., Schnaidt, J., Jusys, Z., & Behm, R. J. (2019). '*Ionic liquid electrolytes for metal-air batteries: interactions between O2, Zn2+ and H2O impurities.'* Journal of the Electrochemical Society, 167(7), 070505.

[177] Sumboja, A., Ge, X., Zheng, G., Goh, F. T., Hor, T. A., Zong, Y., & Liu, Z. (2016). *'Durable rechargeable zinc-air batteries with neutral electrolyte and manganese oxide catalyst.'* Journal of Power Sources, 332, 330-336.

[178] Mainar, A. R., Iruin, E., Colmenares, L. C., Kvasha, A., De Meatza, I., Bengoechea, M., & Blazquez, J. A. (2018). '*An overview of progress in electrolytes for secondary zinc-air batteries and other storage systems based on zinc'.* Journal of Energy Storage, 15, 304-328.

[179] Yu, N. F., Wu, C., Huang, W., Chen, Y. H., Ruan, D. Q., Bao, K. L., ... & Wang, J. (2020). '*Highly efficient Co3O4/Co@ NCs bifunctional oxygen electrocatalysts for long life rechargeable Zn-air batteries.'* Nano Energy, 77, 105200.

[180] Kar, M., & Pozo-Gonzalo, C. (2021). '*Emergence of nonaqueous electrolytes for rechargeable zinc batteries'.* Current Opinion in Green and Sustainable Chemistry, 28, 100426.

[181] Wang, F., Borodin, O., Gao, T., Fan, X., Sun, W., Han, F., & Wang, C. (2018). *'Highly reversible zinc metal anode for aqueous batteries.'* Nature materials, 17(6), 543-549.

[182] Sun, W., Wang, F., Zhang, B., Zhang, M., Küpers, V., Ji, X. & Winter, M. (2021). *'A rechargeable zinc-air battery based on zinc peroxide chemistry.'* Science, 371(6524), 46-51.

[183] Singh, H., Zhuang, S., Ingis, B., Nunna, B. B., & Lee, E. S. (2019). *'Carbon-based catalysts for oxygen reduction reaction: A review on degradation mechanisms.'* Carbon, 151, 160-174.

[184] Ma, L., Chen, S., Wang, D., Yang, Q., Mo, F., Liang, G., & Zhi, C. (2019). *'Super-stretchable zinc–air batteries based on an alkaline-tolerant dual-network hydrogel electrolyte.'* Advanced Energy Materials, 9(12), 1803046.

[185] Song, Z., Ding, J., Liu, B., Liu, X., Han, X., Deng, Y., & Zhong, C. (2020*). 'A rechargeable Zn–air battery with high energy efficiency and long life enabled by a highly water-retentive gel electrolyte with reaction modifier.'* Advanced Materials, 32(22), 1908127.

[186] Huang, Y., Li, Z., Pei, Z., Liu, Z., Li, H., Zhu, M., & Zhi, C. (2018). *'Solid-state rechargeable Zn//NiCo and Zn–air batteries with ultralong lifetime and high capacity: the role of a sodium polyacrylate hydrogel electrolyte.'* Advanced Energy Materials, 8(31), 1802288.

[187] Fu, G., Tang, Y., & Lee, J. M. (2018). *'Recent advances in carbon-based bifunctional oxygen electrocatalysts for Zn− air batteries.'* ChemElectroChem, 5(11), 1424-1434.

[188] Tomboc, G. M., Yu, P., Kwon, T., Lee, K., & Li, J. (2020).*' Ideal design of air electrode—A step closer toward robust rechargeable Zn–air battery.'* APL Materials, 8(5), 050905.

[189] Fang, G., Gao, J., Lv, J., Jia, H., Li, H., Liu, W., & Qiu, H. J. (2020). '*Multi-component nanoporous alloy/(oxy) hydroxide for bifunctional oxygen electrocatalysis and rechargeable Zn-air batteries.'* Applied Catalysis B: Environmental, 268, 118431

[190] Tian, Y., Xu, L., Qiu, J., Liu, X., & Zhang, S. (2020). *'Rational design of sustainable transition metal-based bifunctional electrocatalysts for oxygen reduction and evolution reactions.*' Sustainable Materials and Technologies, 25, e00204.

[191] Wu, M., Zhang, G., Wu, M., Prakash, J., & Sun, S. (2019). *'Rational design of multifunctional air electrodes for rechargeable Zn–Air batteries: Recent progress and future perspectives.'* Energy Storage Materials, 21, 253-286.

[192] Lang, X., Hu, Z., & Wang, C. (2021*). 'Bifunctional air electrodes for flexible rechargeable Zn-air batteries.'* Chinese Chemical Letters, 32(3), 999-1009.

[193] Dai, Y., Yu, J., Ni, M., & Shao, Z. (2020). *'Rational design of spinel oxides as bifunctional oxygen electrocatalysts for rechargeable Zn-air batteries.'* Chemical Physics Reviews, 1(1), 011303.

[194] Yu, X., Zhou, T., Ge, J., & Wu, C. (2020). *'Recent advances on the modulation of electrocatalysts based on transition metal nitrides for the rechargeable Zn-Air battery.'* ACS Materials Letters, 2(11), 1423-1434.

[195] Dutta, A., & Pradhan, N. (2017). *'Developments of metal phosphides as efficient OER precatalysts.'* The journal of physical chemistry letters, 8(1), 144-152.

[196] Sun, H., Yan, Z., Liu, F., Xu, W., Cheng, F., & Chen, J. (2020). *'Self-supported transition-metal-based electrocatalysts for hydrogen and oxygen evolution.'* Advanced materials, 32(3), 1806326.

[197] Zhu, Y. P., Guo, C., Zheng, Y., & Qiao, S. Z. (2017).*'Surface and interface engineering of noble-metal-free electrocatalysts for efficient energy conversion processes.'* Accounts of chemical research, 50(4), 915-923.

[198] Clark, S., Latz, A., & Horstmann, B. (2017). '*Rational development of neutral aqueous electrolytes for zinc–air batteries.'* ChemSusChem, 10(23), 4735-4747.

[199] Wang, Z., Shen, D., Wu, C., & Gu, S. (2018). *'State-of-the-art on the production and application of carbon nanomaterials from biomass.'* Green Chemistry, 20(22), 5031-5057.

[200] Marsudi, Maradhana Agung, et al. *"Manganese oxide nanorods decorated table sugar derived carbon as efficient bifunctional catalyst in rechargeable Zn-air batteries."* Catalysts 10.1 (2020): 64.

[201] Wu, Y. J., Wu, X. H., Tu, T. X., Zhang, P. F., Li, J. T., Zhou, Y., & Sun, S. G. (2020*).' Controlled synthesis of FeNx-CoNx dual active sites interfaced with metallic Co nanoparticles as bifunctional oxygen electrocatalysts for rechargeable Zn-air batteries.'* Applied Catalysis B: Environmental, 278, 119259.

[202] Wang, X., Vasileff, A., Jiao, Y., Zheng, Y., & Qiao, S. Z. (2019*). 'Electronic and structural engineering of carbon-based metal-free electrocatalysts for water splitting.*' Advanced Materials, 31(13), 1803625.

[203] Lyu, D., Yao, S., Ali, A., Tian, Z. Q., Tsiakaras, P., & Shen, P. K. (2021). *'N, S Codoped Carbon Matrix-Encapsulated Co9S8 Nanoparticles as a Highly Efficient and Durable Bifunctional Oxygen Redox Electrocatalyst for Rechargeable Zn–Air Batteries.'* Advanced Energy Materials, 11(28), 2101249.

[204] Liu, X., Yuan, Y., Liu, J., Liu, B., Chen, X., Ding, J., & Hu, W. (2019). *'Utilizing solar energy to improve the oxygen evolution reaction kinetics in zinc–air battery.'* Nature communications, 10(1), 4767.

[205] Asia, N. (2020).' *Toyota" s game-changing solid-state battery en route for 2021 debut.'* Nikkei, Dec, 10.

[206] Zhang, J., Li, X. L., Fan, S., Huang, S., Yan, D., Liu, L., & Yang, H. Y. (2020). '*3D-printed functional electrodes towards Zn-Air batteries'*. Materials Today Energy, 16, 100407.

[207] Ma, T., & MacKenzie, J. D. (2019). '*Fully printed, high energy density flexible zinc-air batteries based on solid polymer electrolytes and a hierarchical catalyst current collector.'* Flexible and Printed Electronics, 4(1), 015010.

[208] Choi, K. H., Kim, H. W., Lee, S. S., Yoo, J., Lee, D. G., & Lee, S. Y. (2018).*' Zn–Air Batteries: All-Hand-Drawn Zn–Air Batteries: Toward User-Customized On-the-Fly Power Sources (Adv. Sustainable Syst. 5/2018)'*. Advanced Sustainable Systems, 2(5), 1870031.

[209] Huang, S., Pei, P., & Wang, Z. (2020). *'Anode corrosion of Zn-air fuel cell: mechanism and protection.'* Journal of The Electrochemical Society, 167(9), 090538.

[210] Mainar, A. R., Iruin, E., Colmenares, L. C., Kvasha, A., De Meatza, I., Bengoechea, M., & Blazquez, J. A. (2018). *'An overview of progress in electrolytes for secondary zinc-air batteries and other storage systems based on zinc.'* Journal of Energy Storage, 15, 304-328.

[211] Davari, E., & Ivey, D. G. (2018). *'Bifunctional electrocatalysts for Zn–air batteries.'* Sustainable Energy & Fuels, 2(1), 39-67.

[212] Abbasi, A., Hosseini, S., Somwangthanaroj, A., Cheacharoen, R., Olaru, S., & Kheawhom, S. (2020). *'Discharge profile of a zinc-air flow battery at various electrolyte flow rates and discharge currents.'*Scientific data, 7(1), 196.

[213] A. Sumboja, (2017). *'All-solid-state, foldable, and rechargeable Zn-air batteries based on manganese oxide grown on graphene-coated carbon cloth air cathode',* Advanced Energy Materials, 7(20), 1700927.

[214] Masa, J., Andronescu, C., & Schuhmann, W. (2020). *'Electrocatalysis as the nexus for sustainable renewable energy: the gordian knot of activity, stability, and selectivity.'* Angewandte Chemie International Edition, 59(36), 15298-15312.

[215] Zhang, J., Zhou, Q., Tang, Y., Zhang, L., & Li, Y. (2019). '*Zinc–air batteries: are they ready for prime time?*' .Chemical Science, 10(39), 8924-8929.

[216] Chen, M., Liu, Q., Wang, S. W., Wang, E., Guo, X., & Chou, S. L. (2019). *'High-abundance and low-cost metal-based cathode materials for sodium-ion batteries: problems, progress, and key technologies.'* Advanced Energy Materials, 9(14), 1803609.

[217] Wu, X., Markir, A., Xu, Y., Zhang, C., Leonard, D. P., Shin, W., & Ji, X. (2019). *'A rechargeable battery with an iron metal anode.* 'Advanced Functional Materials, 29(20), 1900911.

[218] Fang, Y., Chen, Z., Xiao, L., Ai, X., Cao, Y., & Yang, H. (2018). *'Recent progress in iron-based electrode materials for grid-scale sodium-ion batteries.'* Small, 14(9), 1703116.

[219] He, Z., Xiong, F., Tan, S., Yao, X., Zhang, C., & An, Q. (2021). *'Iron metal anode for aqueous rechargeable batteries.'* Materials Today Advances, 11, 100156.

[220] H. Weinrich, J. Come, H. Tempel H. Kungl, R.-A. Eichel, N. Balke, (2017). *'Understanding the nanoscale redox-behavior of iron-anodes for rechargeable iron-air batteries'*, Nano Energy 41, 706-716.

[221] D.-C. Lee, D. Lei, G. Yushin, (2018). *'Morphology and phase changes in iron anodes affecting their capacity and stability in rechargeable alkaline batteries',* ACS Energy Letters 3, 794-801.

[222] H. Weinrich, M. Gehring, H. Tempel, H. Kungl, R.-A. Eichel, (2018*). 'Impact of the charging conditions on the discharge performance of rechargeable iron-anodes for alkaline irone air batteries'*, J. Appl. Electrochem. 4, 451-462.

[223] C. Han, W. Li, H.K. Liu, S. Dou, J. Wang, (2020). *'Principals and strategies for constructing a highly reversible zinc metal anode in aqueous batteries'*, Nano Energy 74,104880.

[224] Shukla, A. K., Ravikumar, M. K., & Balasubramanian, T. S. (1994). '*Nickel/iron batteries.*' Journal of power sources, 51(1-2), 29-36.

[225] Öjefors, L., & Carlsson, L. (1978).'*An iron—air vehicle battery.'* Journal of Power Sources, 2(3), 287-296.

[226] M.J. Zachman, Z. Tu, S. Choudhury, L.A. Archer, L.F. Kourkoutis, (2018). *'The Electrochemical Behavior of Alkali and Alkaline Earth Metals in Nonaqueous Battery Systems - The Solid Electrolyte Interphase Model',* Journal of the Electrochem. Soc., 126(12), 2047.

[227] W.S. LePage, Y. Chen, E. Kazyak, K.-H. Chen, A.J. Sanchez, A. Poli, E.M. Arruda, M. Thouless, N.P. Dasgupta, (2019). *'Lithium Mechanics: Roles of Strain Rate and Temperature and Implications for Lithium Metal Batteries'*, J. of the Electrochem. Soc., 166, A89–A97.

[228] H.A. Figueredo-Rodríguez, R.D. McKerracher, M. Insausti, A.G. Luis, C.P. de León, C. Alegre, V. Baglio, A.S. Arico, F.C. Walsh, (2017). *'A rechargeable, aqueous iron air battery with nanostructured electrodes capable of high energy density operation'*, J. Electrochem. Soc. 164, A1148-A1157.

[229] L. Hruska, R. Savinell, (1981),*'Investigation of factors affecting performance of the iron-redox battery'*, J. Electrochem. Soc. 128, 18.

[230] A. Dinesh, S. Olivera, K. Venkatesh, M.S. Santosh, M.G. Priya, Inamuddin A.M. Asiri, H.B. Muralidhara, (2018). *'Iron-based flow batteries to store renewable energies'*, Environ. Chem. Lett. 16, 683-694.

[231] Dinesh, A., Olivera, S., Venkatesh, K., Santosh, M. S., Priya, M. G., Asiri, A. M., & Muralidhara, H. B. (2018). '*Iron-based flow batteries to store renewable energies'*. Environmental Chemistry Letters, 16(3), 683-694.

[232] M.O. Bamgbopa, Y. Shao-Horn, R. Hashaikeh, S. Almheiri, (2018*). 'Cyclable membrane less redox flow batteries based on immiscible liquid electrolytes: demonstration with all-iron redox chemistry*', Electrochim. Acta 267, 41-50.

[233] Wu, X., Markir, A., Xu, Y., Zhang, C., Leonard, D. P., Shin, W., & Ji, X. (2019). '*A rechargeable battery with an iron metal anode.'* Advanced Functional Materials, 29(20), 1900911.

[234] Wu, X., Markir, A., Xu, Y., Hu, E. C., Dai, K. T., Zhang, C., & Ji, X. (2019). '*Rechargeable iron–sulfur battery without polysulfide shuttling'.* Advanced Energy Materials, 9(40), 1902422.

[235] C. Bai, H. Jin, Z. Gong, X. Liu, Z. Yuan, (2020). *'A high-power aqueous rechargeable Fe-I2 battery'*, Energy Storage Materials 28, 247-254

[236] Jäckle, M., Helmbrecht, K., Smits, M., Stottmeister, D., & Groß, A. (2018*). 'Self-diffusion barriers: possible descriptors for dendrite growth in batteries?'* Energy & Environmental Science, 11(12), 3400-3407.

[237] Xu, R., Cheng, X. B., Yan, C., Zhang, X. Q., Xiao, Y., Zhao, C. Z., ... & Zhang, Q. (2019). *'Artificial interphases for highly stable lithium metal anode.'* Matter, 1(2), 317-344.

[238] F. Wu, Y.-X. Yuan, X.-B. Cheng, Y. Bai, Y. Li, C. Wu, Q. Zhang,(2018). *'Perspectives for restraining harsh lithium dendrite growth: Towards robust lithium metal anodes'*, Energy Storage Mater. 15, 148-170.

[239] X.-B. Cheng, C. Yan, H.-J. Peng, J.-Q. Huang, S.-T. Yang, Q. Zhang, (2018). *'Sulfurized solid electrolyte interphases with a rapid Li+ diffusion on dendrite-free Li metal anodes'*, Energy Storage 10, 199-205.

[240] X. Xu, S. Wang, H. Wang, C. Hu, Y. Jin, J. Liu, H. Yan, (2018). *'Recent progresses in the suppression method based on the growth mechanism of lithium dendrite'*, J. Energy Chem. 27, 513-527.

[241] Zheng, J., Tang, T., Zhao, Q., Liu, X., Deng, Y., & Archer, L. A. (2019). *'Physical orphaning versus chemical instability: Is dendritic electrodeposition of Li fatal?'* ACS Energy Letters, 4(6), 1349-1355.

[242] Cheng, X. B., Yan, C., Zhang, X. Q., Liu, H., & Zhang, Q. (2018). '*Electronic and ionic channels in working interfaces of lithium metal anodes. '*ACS Energy Letters, 3(7), 1564-1570.

[243] X.-B. Cheng, C. Yan, X.-Q. Zhang, H. Liu, Q. Zhang, (2017). *'The gap between long lifespan Li-S coin and pouch cells: The importance of lithium metal anode protection,'* Energy Storage Mater. 6, 18-25.

[244] Shi, P., Cheng, X. B., Li, T., Zhang, R., Liu, H., Yan, C., & Zhang, Q. (2019). *'Electrochemical diagram of an ultrathin lithium metal anode in pouch cells.'* Advanced Materials, 31(37), 1902785.

[245] Wang, R., Cui, W., Chu, F., & Wu, F. (2020). '*Lithium metal anodes: Present and future.'* Journal of Energy Chemistry, 48, 145-159.

[246] Zhu, Y., He, X., & Mo, Y. (2017). *'Strategies based on nitride materials chemistry to stabilize Li metal anode. '*Advanced Science, 4(8), 1600517.

[247] X. Chen, T. Hou, K.A. Persson, Q. Zhang, Mater. (2019). *'Combining theory and experiment in lithium–sulfur batteries: Current progress and future perspectives'*, Today 22,142-158.

[248] Chen, X., Chen, X. R., Hou, T. Z., Li, B. Q., Cheng, X. B., Zhang, R., & Zhang, Q. (2019). '*Lithiophilicity chemistry of heteroatom-doped carbon to guide uniform lithium nucleation in lithium metal anodes.'* Science advances, 5(2), eaau7728.

[249] Zhang, R., Shen, X., Cheng, X. B., & Zhang, Q. '*Energy Storage Mater'.* 2019. V, 23, 678-683.

[250] Peled, E., & Yamin, H. (1979). *'Solid Electrolyte Interphase (SEI) Electrodes. Part 1. The Kinetics of Lithium in LiAlCl4-SOCl2'.* Israel Journal of Chemistry, 18(1-2), 131-135.

[251] Peled, E., & Menkin, S. (2017). 'SEI: past, present and future.' Journal of the Electrochemical Society, 164(7), A1703.

[252] J. Wang, W. Huang, A. Pei, Y. Li, F. Shi, X. Yu, Y. Cui, (2019*), 'Review—SEI: Past, Present and Future',* Nat. Energy 4, 664-670.

[253] C.-C. Su, M. He, R. Amine, Z. Chen, R. Sahore, N.D. Rago, K. Amine, (2019). *'A Review of Solid Electrolyte Interphases on Lithium Metal Anode'*, Energy Storage Mater. 17, 284-292.

[254] Qiao, L., Cui, Z., Chen, B., Xu, G., Zhang, Z., Ma, J., & Cui, G. (2018). *'A promising bulky anion based lithium borate salt for lithium metal batteries.'* Chemical science, 9(14), 3451-3458.

[255] F.M. Delnick, (1989). '*The kinetics of charge-transfer reactions on passive lithium electrodes,'* J. Power Sour. 26, 129-138.

[256] S. Chen, J. Zheng, L. Yu, X. Ren, M.H. Engelhard, C. Niu, H. Lee, W. Xu, J. Xiao, Liu, J.-G. Zhang, (2018). *'High-Efficiency Lithium Metal Batteries with Fire-Retardant Electrolytes',* Joule 2, 1548-1558

[257] Qiao, L., Cui, Z., Chen, B., Xu, G., Zhang, Z., Ma, J., & Cui, G. (2018). '*A promising bulky anion based lithium borate salt for lithium metal batteries.'* Chemical science, 9(14), 3451-3458.

[258] Chen, S., Zheng, J., Mei, D., Han, K. S., Engelhard, M. H., Zhao, W., & Zhang, J. G. (2018). '*High-voltage lithium-metal batteries enabled by localized high-concentration electrolytes.'* Advanced materials, 30(21), 1706102.

[259] Dong, X., Lin, Y., Li, P., Ma, Y., Huang, J., Bin, D., & Xia, Y. (2019). *'High-energy rechargeable metallic lithium battery at −70 C enabled by a cosolvent electrolyte.'* Angewandte Chemie International Edition, 58(17), 5623-5627.

[260] W. Shin, K.P. So, W.F. Stickle, C. Su, J. Lu, J. Li, X. Ji, (2019). *'High-Energy Rechargeable Metallic Lithium Battery at −70 °C Enabled by a Cosolvent Electrolyte',* Chem. Commun. 55, 3387-3389.

[261] Zhang, X. Q., Chen, X., Cheng, X. B., Li, B. Q., Shen, X., Yan, C., ... & Zhang, Q. (2018). *'Highly stable lithium metal batteries enabled by regulating the solvation of lithium ions in nonaqueous electrolytes'.* Angewandte Chemie International Edition, 57(19), 5301-5305.

[262] Cheng, X. B., Yan, C., Peng, H. J., Huang, J. Q., Yang, S. T., & Zhang, Q. (2018). *'Sulfurized solid electrolyte interphases with a rapid Li+ diffusion on dendrite-free Li metal anodes'*. Energy Storage Materials, 10, 199-205.

[263] H. Wu, Y. Cao, L. Geng, C. Wang, (2018*). 'Highly Stable Lithium Metal Batteries Enabled by Regulating the Solvation of Lithium Ions in Nonaqueous Electrolytes'*, Chem. Mater. 29

[264] Zhang, Q., Wang, K., Wang, X., Zhong, Y., Liu, M., Liu, X., & Li, W. (2019). *'Lithium Bis (oxalate) borate reinforces the interphase on Li-metal anodes.'* ACS applied materials & interfaces, 11(23), 20854-20863.

[265] Sano, H., Sakaebe, H., & Matsumoto, H. (2011).*' Effect of organic additives on electrochemical properties of Li anode in room temperature ionic liquid'.* Journal of the Electrochemical Society, 158(3), A316.

[266] Chu, F., Hu, J., Tian, J., Zhou, X., Li, Z., & Li, C. (2018). '*In situ plating of porous Mg network layer to reinforce anode dendrite suppression in Li-metal batteries.'* ACS applied materials & interfaces, 10(15), 12678-12689.

[267] H. Ye, Y.-X. Yin, S.-F. Zhang, Y. Shi, L. Liu, X.-X. Zeng, R. Wen, Y.-G. Guo, L.-J. Wan, (2017). Nano Energy 36, 411-417.

[268] Ma, L., Kim, M. S., & Archer, L. A. (2017). *'Stable artificial solid electrolyte interphases for lithium batteries.'* Chemistry of Materials, 29(10), 4181-4189.

[269] Q. Pang, X. Liang, A. Shyamsunder, L.F. Nazar, (2017*). 'Electroless Formation of Hybrid Lithium Anodes for Fast Interfacial Ion Transport'*, Joule 1, 871-886.

[270] Z. Zeng, V. Murugesan, K.S. Han, X. Jiang, Y. Cao, L. Xiao, X. Ai, H. Yang,J.-G. Zhang, M.L. Sushko, J. Liu, (2018). *'Non-flammable electrolyte enables Li-metal batteries with aggressive cathode chemistries'*, Nat. Energy 3, 674-681.

[271] X. Fan, L. Chen, X. Ji, T. Deng, S. Hou, J. Chen, J. Zheng, F. Wang, J. Jiang, K. Xu, (2018*). 'Non-flammable electrolytes with high salt-to-solvent ratios for Li-ion and Li-metal batteries',* Chem 4, 174-185.

[272] J. Alvarado, M.A. Schroeder, T.P. Pollard, X. Wang, J.Z. Lee, M. Zhang, T. Wynn, M. Ding, O. Borodin, Y.S. Meng, (2019). *'Bisalt ether electrolytes: a pathway towards lithium metal batteries with Ni-rich cathodes'*, Energy Environ. Sci. 12, 780-794.

[273] L. Suo, W. Xue, M. Gobet, S.G. Greenbaum, C. Wang, Y. Chen, W. Yang, Y. Li,J. Li, 2018,*'Fluorine-donating electrolytes enable highly reversible 5-V-class Li metal batteries',* Proc. Natl. Acad. Sci. 115, 1156.

[274] Li, Q., Yi, T., Wang, X., Pan, H., Quan, B., Liang, T., & Li, H. (2019). *'In-situ visualization of lithium plating in all-solid-state lithium-metal battery.'* Nano Energy, 63, 103895.

[275] S. Jiao, X. Ren, R. Cao, M.H. Engelhard, Y. Liu, D. Hu, D. Mei, J. Zheng, W. Zhao, Q. Li, N. Liu, B.D. Adams, C. Ma, J. Liu, J.-G. Zhang, W. Xu, (2018). *'Stable cycling of high-voltage lithium metal batteries in ether electrolytes',* Nat. Energy 3, 739-746.

[276] Zheng, J., Engelhard, M. H., Mei, D., Jiao, S., Polzin, B. J., Zhang, J. G., & Xu, W. (2017). '*Electrolyte additive enabled fast charging and stable cycling lithium metal batteries'*. Nature Energy, 2(3), 1-8.

[277] Kasemchainan, J., Zekoll, S., Spencer Jolly, D., Ning, Z., Hartley, G. O., Marrow, J., & Bruce, P. G. (2019).*'Critical stripping current leads to dendrite formation on plating in lithium anode solid electrolyte cells.'* Nature materials, 18(10), 1105-1111.

[278] M. Zhang, J. Zhang, J. Yang, X. Du, Z. Chen, K. Chen, C. Lu, H. Zhang, T. Dong, J. Li, (2019). *'Polymer Electrolyte Enlightens Wide-Temperature 4.45 V-Class LiCoO2/Li Metal Battery'*, J. Electrochem. Soc. 166, A2313–A2321.

[279] Liu, H., Tang, Y., Zhao, W., Ding, W., Xu, J., Liang, C., & Huang, F. (2018). *'Facile Synthesis of Nitrogen and Halogen Dual-Doped Porous Graphene as an Advanced Performance Anode for Lithium-Ion Batteries.'* Advanced Materials Interfaces, 5(5), 1701261.

[280] Long G.-F., Wan K., Liu M.-Y., Liang Z.-X., Piao, J.-H., and Tsiakaras, P. (2017).*'Active sites and mechanism on nitrogen-doped carbon catalyst for hydrogen evolution reaction,'* Journal of Catalysis, 348, 151-159.

[281] J. Wan, J. Xie, X. Kong, Z. Liu, K. Liu, F. Shi, A. Pei, H. Chen, W. Chen, J. Chen,X. Zhang, L. Zong, J. Wang, L.-Q. Chen, J. Qin, Y. Cui, (2019). *'Facile Synthesis of Nitrogen and Halogen Dual-Doped Porous Graphene as an Advanced Performance Anode for Lithium-Ion Batteries'*, Nat. Nanotechnol. 14, 705-711.

[282] Ma, Q., Zeng, X. X., Yue, J., Yin, Y. X., Zuo, T. T., Liang, J. Y., & Guo, Y. G. (2019). '*Viscoelastic and nonflammable interface design–enabled dendrite-free and safe solid lithium metal batteries.'* Advanced Energy Materials, 9(13), 1803854.

[283] Q. Pan, Y. Zheng, S. Kota, W. Huang, S. Wang, H. Qi, S. Kim, Y. Tu, M.W. Barsoum, C.Y. Li, (2019). *'2D MXene-containing polymer electrolytes for all-solid-state lithium metal batteries',* Nanoscale Adv. 1, 395-402.

[284] Duan, H., Fan, M., Chen, W. P., Li, J. Y., Wang, P. F., Wang, W. P., ... & Guo, Y. G. (2019). '*Extended electrochemical window of solid electrolytes via heterogeneous multilayered structure for high-voltage lithium metal batteries'.* Advanced Materials, 31(12), 1807789.

[285] H. Duan, Y.-X. Yin, X.-X. Zeng, J.-Y. Li, J.-L. Shi, Y. Shi, R. Wen, Y.-G. Guo,L.-J. Wan, (2018). *'In-situ plasticized polymer electrolyte with double-network for flexible solid-state lithium-metal batteries'*, Energy Storage Mater. 10, 85-91.

[286] Duan, H., Yin, Y. X., Zeng, X. X., Li, J. Y., Shi, J. L., Shi, Y., ... & Wan, L. J. (2018). '*In-situ plasticized polymer electrolyte with double-network for flexible solid-state lithium-metal batteries.'* Energy Storage Materials, 10, 85-91.

[287] H. Duan, Y.-X. Yin, Y. Shi, P.-F. Wang, X.-D. Zhang, C.-P. Yang, J.-L. Shi, R. Wen, Y.-G. Guo, L.-J. Wan, J. Am., (2018). *'Dendrite-Free Li-Metal Battery Enabled by a Thin Asymmetric Solid Electrolyte with Engineered Layers'*, Chem. Soc. 140, 82-85.

[288] Y. Fan, X. Chen, D. Legut, Q. Zhang, (2019). *'Effect of a novel amphipathic ionic liquid on lithium deposition in gel polymer electrolytes'*, Energy Storage Mater. 16, 169-193.

[289] Z. Zhang, Y. Shao, B. Lotsch, Y.-S. Hu, H. Li, J. Janek, L.F. Nazar, C.-W. Nan, J. Maier, M. Armand, L. Chen, (2018). *'New horizons for inorganic solid state ion conductors'*, Energy Environ. Sci. 11, 1945-1976.

[290] Meesala, Y., Jena, A., Chang, H., & Liu, R. S. (2017). '*Recent advancements in Li-ion conductors for all-solid-state Li-ion batteries.*' ACS Energy Letters, 2(12), 2734-2751.

[291] Duan, H., Zheng, H., Zhou, Y., Xu, B., & Liu, H. (2018). '*Stability of garnet-type Li ion conductors: An overview.'* Solid State Ionics, 318, 45-53.

[292] Bachman, J. C., Muy, S., Grimaud, A., Chang, H. H., Pour, N., Lux, S. F. ... & Shao-Horn, Y. (2016). *'Inorganic solid-state electrolytes for lithium batteries: mechanisms and properties governing ion conduction.'* Chemical reviews, 116(1), 140-162.

[293] R. Garcia-Mendez, F. Mizuno, R. Zhang, T.S. Arthur, J. Sakamoto, (2017), 'Electrochim Acta 237, 144-151.

[294] Fan, X., Ji, X., Han, F., Yue, J., Chen, J., Chen, L., & Wang, C. (2018). '*Fluorinated solid electrolyte interphase enables highly reversible solid-state Li metal battery'*. Science advances, 4(12), eaau9245.

[295] Ye, H., Zheng, Z. J., Yao, H. R., Liu, S. C., Zuo, T. T., Wu, X. W., & Guo, Y. G. (2019). *'Guiding uniform Li plating/stripping through lithium–aluminum alloying medium for long-life Li metal batteries'.* Angewandte Chemie International Edition, 58(4), 1094-1099.

[296] Zhao, Y., & Sun, X. (2018). '*Molecular layer deposition for energy conversion and storage.'* ACS Energy Lett 3: 899–914.

[297] Liu, Y., Sun, Q., Zhao, Y., Wang, B., Kaghazchi, P., Adair, K. R., & Sun, X. (2018). '*Stabilizing the interface of NASICON solid electrolyte against Li metal with atomic layer deposition.*' ACS applied materials & interfaces, 10(37), 31240-31248.

[298] Kazyak, E., Chen, K. H., Davis, A. L., Yu, S., Sanchez, A. J., Lasso, J., & Dasgupta, N. P. (2018). '*Atomic layer deposition and first principles modeling of glassy Li 3 BO 3–Li 2 CO 3 electrolytes for solid-state Li metal batteries'.* Journal of Materials Chemistry A, 6(40), 19425-19437.

[299] C. Wang, Y. Zhao, Q. Sun, X. Li, Y. Liu, J. Liang, X. Li, X. Lin, R. Li, K.R. Adair, L. Zhang, R. Yang, S. Lu, X. Sun, (2018). *'Stabilizing interface between Li10SnP2S12 and Li metal by molecular layer deposition',* Nano Energy 53, 168-174.

[300] Fu, K., Gong, Y., Liu, B., Zhu, Y., Xu, S., Yao, Y., & Hu, L. (2017). *'Toward garnet electrolyte–based Li metal batteries: An ultrathin, highly effective, artificial solid-state electrolyte/metallic Li interface.'* Science Advances, 3(4), e1601659.

[301] X.-B. Cheng, C.-Z. Zhao, Y.-X. Yao, H. Liu, Q. Zhang, (2019). *'Stabilizing interface between Li10SnP2S12 and Li metal by molecular layer deposition'*, Chem 5, 74-96.

[302] Chen, Y., Kang, Y., Zhao, Y., Wang, L., Liu, J., Li, Y., & Li, B. (2021). *'A review of lithium-ion battery safety concerns: The issues, strategies, and testing standards.'* Journal of Energy Chemistry, 59, 83-99.

[303] Kang, Y., Liang, Z., Zhao, Y., Xu, H., Qian, K., He, X., & Li, J. (2020). '*Large-scale synthesis of lithium-and manganese-rich materials with uniform thin-film Al2O3 coating for stable cathode cycling'*. Sci. China Mater, 63, 1683-1692.

[304] Liu, X., Ren, D., Hsu, H., Feng, X., Xu, G. L., Zhuang, M., & Ouyang, M. (2018). '*Thermal runaway of lithium-ion batteries without internal short circuit.*' Joule, 2(10), 2047-2064.

[305] Zhang, G., Shi, Y., Wang, H., Jiang, L., Yu, X., Jing, S., & Tsiakaras, P. (2019). '*A facile route to achieve ultrafine Fe2O3 nanorods anchored on graphene oxide for application in lithium-ion battery'*. Journal of Power Sources, 416, 118-124.

[306] Ozawa, (1994). *'Lithium-ion rechargeable batteries with LiCoO2 and carbon electrodes: the LiCoO2/C system'*, Solid State Ionics 69, 212-221.

[307] T. Nakajima, (2002). *'Electrochemical behavior of plasma-fluorinated graphite for lithium-ion batteries'*, J. Power Sources 104, 108-114.

[308] C. Zheng, (2019). *'Large-scale synthesis of nitrogen-rich hierarchically porous carbon as anode for lithium-ion batteries with high capacity and rate capability.'* Electrochim. Acta 306, 339-349.

[309] Choudhury, S., & Stamm, M. (2017). *'Hybrid Nanostructured Materials for Advanced Lithium Batteries*'. Hybrid Nanomaterials: Advances in Energy, Environment, and Polymer Nanocomposites, 1.

[310] J. Liu, (2019*). 'Pathways for practical high-energy long-cycling lithium metal batteries'*, Nature Energy 4, 180-186.

[311] Lai, J., Xing, Y., Chen, N., Li, L., Wu, F., & Chen, R. (2020). '*Electrolytes for rechargeable lithium–air batteries.'* Angewandte Chemie International Edition, 59(8), 2974-2997.

[312] Wang, C., Xie, Z., & Zhou, Z. (2019). '*Lithium-air batteries: Challenges coexist with opportunities'*. APL Materials, 7(4), 040701.

[313] Galbraith, A. D. (1976, August). '*The lithium-water-air battery for automotive propulsion.*' In Union Internationale des Producteurs et Distributeurs d'Energie Electrique and Electric Vehicle Council, 4th International Electric Vehicle Symposium.

[314] Chase, M. W., & National Information Standards Organization (US). (1998). 'NIST-JANAF thermochemical tables '. 9, 1-1951. Washington, DC: American Chemical Society.

[315] Imanishi, N., & Yamamoto, O. (2019). *'Perspectives and challenges of rechargeable lithium–air batteries.'* Materials Today Advances, 4, 100031.

[316] Gittleson, F. S., Jones, R. E., Ward, D. K., & Foster, M. E. (2017*). 'Oxygen solubility and transport in Li–air battery electrolytes: establishing criteria and strategies for electrolyte design'*. Energy & Environmental Science, 10(5), 1167-1179.

[317] Olabi, A. G., Onumaegbu, C., Wilberforce, T., Ramadan, M., Abdelkareem, M. A., & Al–Alami, A. H. (2021). '*Critical review of energy storage systems'*. Energy, 214, 118987.

[318] Abdelkareem, M.A.; Sayed, E.T.; Mohamed, H.O.; Obaid, M.; Rezk, H.; Chae, K.-J., (2020). *'Nonprecious anodic catalysts for low molecular-hydrocarbon fuel cells: Theoretical consideration and current progress',* 77,100805.

[319] Al-Dhaifallah, M.; Abdelkareem, M.A.; Rezk, H.; Alhumade, H.; Nassef, A.M.; Olabi, A.G., (2021*). 'Co-decorated reduced graphene/titanium nitride composite as an active oxygen reduction reaction catalyst with superior stability',* 45(2), 1587-1598.

[320] Zhao, C.; Yan, X.; Wang, G.; Jin, Y.; Du, X.; Du, W.; Sun, L.; Ji, C., (2018). *'PdCo bimetallic nano-electrocatalyst as effective air-cathode for aqueous metal-air batteries',* 43(10), 5001-5011.

[321] Zhang, L.; Huang, Q.A.; Yan, W.; Shao, Q.; Zhang, J., (2019). *'Design and fabrication of non-noble metal catalyst-based air-cathodes for metal-air battery',* 97(12), 2984-2993.

[322] Han, X.; Li, X.; White, J.; Zhong, C.; Deng, Y.; Hu, W.; Ma, T., (2018). *'Metal–air batteries: From static to flow system',* 8(7), 1801396.

[323] Tran, T.N.T.; Chung, H.-J.; Ivey, D.G., (2019). *'A study of alkaline gel polymer electrolytes for rechargeable zinc–air batteries',* 327, 135021.

[324] Jacas Biendicho, J.; Noréus, D.; Offer, C.; Svensson, G.; Smith, R.I.; Hull, S., (2018*). 'New opportunities for air cathode batteries; in-situ neutron diffraction measurements',* 12, 1-4.

[325] Teabnamang, P.; Kao-ian, W.; Nguyen, M.T.; Yonezawa, T.; Cheacharoen, R.; Kheawhom, S., (2020*). 'High-Capacity Dual-Electrolyte Aluminum–Air Battery with Circulating Methanol Anolyte', 3, 9.*

[326] Cheng, Y.; Li, D.; Shi, L.; Xiang, Z., (2018*). 'Efficient unitary oxygen electrode for air-based flow batteries',* 47, 361-367.

[327] Pan, J.; Xu, Y.Y.; Yang, H.; Dong, Z.; Liu, H.; Xia, B.Y., 2018,*'Advanced architectures and relatives of air electrodes in Zn–air batteries.',* 5(4), 1700691.

[328] Xie, Z.; Wu, Z.; An, X.; Yue, X.; Xiaokaiti, P.; Yoshida, A.; Abudula, A.; Guan, G., (2020). *'A sandwich-type composite polymer electrolyte for all-solid-state lithium metal batteries with high areal capacity and cycling stability',* 596, 117739.

[329] Chawla, (2019). *'Recent advances in air-battery chemistries',* 12, 324-331.

[330] Qu, S.; Song, Z.; Liu, J.; Li, Y.; Kou, Y.; Ma, C.; Han, X.; Deng, Y.; Zhao, N.; Hu, W.; et al., (2017). '*Electrochemical approach to prepare integrated air electrodes for highly stretchable zinc-air battery array with tunable output voltage and current for wearable electronics',* 39, 101-110.

[331] Wilberforce, T.; Olabi, A.G.; Sayed, E.T.; Elsaid, K.; Abdelkareem, M.A., (2021). *'Progress in carbon capture technologies',* 761, 143203.

[332] Abdelkareem, M.A.; Lootah, M.A.; Sayed, E.T.; Wilberforce, T.; Alawadhi, H.; Yousef, B.A.A.; Olabi, A.G., (2021*). 'Fuel cells for carbon capture applications',* 769, 144243.

[333] Sayed, E.T.; Abdelkareem, M.A.; Alawadhi, H.; Elsaid, K.; Wilberforce, T.; Olabi, A.G., (2021). *'Graphitic carbon nitride/carbon brush composite as a novel anode for yeast-based microbial fuel cells',* 221, 119849.

[334] Jiao, K.; Xuan, J.; Du, Q.; Bao, Z.; Xie, B.; Wang, B.; Zhao, Y.; Fan, L.; Wang, H.; Hou, Z., (2021). *'Designing the next generation of proton-exchange membrane fuel cells',* 595, 361-369.

[335] Gittleman, C.S.; Jia, H.; De Castro, E.S.; Chisholm, C.R.; Kim, Y.S., (2021). *'Proton conductors for heavy-duty vehicle fuel cells',* Joule, 5, 1661-1677.

[336] Rabaia, M.K.H.; Abdelkareem, M.A.; Sayed, E.T.; Elsaid, K.; Chae, K.-J.; Wilberforce, T.; Olabi, A.G., (2021*). 'Environmental impacts of solar energy systems: A review',* 754, 141989.

[337] Sebestyén, (2021*). 'Renewable and Sustainable Energy Reviews: Environmental impact networks of renewable energy power plants',* 151, 111626

[338] Dincer, I., & Rosen, M. A. (2021). '*Thermal energy storage: systems and applications'*. John Wiley & Sons.

[339] Lai, C. S., & Locatelli, G. (2021). *'Economic and financial appraisal of novel large-scale energy storage technologies.'* Energy, 214, 118954.

[340] Ahmed, S. D., Al-Ismail, F. S., Shafiullah, M., Al-Sulaiman, F. A., & El-Amin, I. M. (2020). '*Grid integration challenges of wind energy: A review'*. IEEE Access, 8, 10857-10878.

[341] Nazir, M.S.; Ali, N.; Bilal, M.; Iqbal, H.M., (2020). *'Potential environmental impacts of wind energy development: A global perspective',* 13, 85-90

[342] Zhang, Y.; Ren, J.; Pu, Y.; Wang, P, (2020). *'Solar energy potential assessment: A framework to integrate geographic, technological, and economic indices for a potential analysis.'* 149, 577-586.

[343] Iqbal, A.; Mahmoud, M.S.; Sayed, E.T.; Elsaid, K.; Abdelkareem, M.A.; Alawadhi, H.; Olabi, A.G., (2021*). 'Evaluation of the nanofluid-assisted desalination through solar stills in the last decade',* 277, 111415.

[344] Fan, X.; Liu, B.; Liu, J.; Ding, J.; Han, X.; Deng, Y.; Lv, X.; Xie, Y.; Chen, B.; Hu, W.; et al, (2020*). 'Battery technologies for grid-level large-scale electrical energy storage', 26, 92-103.*

[345] Salameh, T.; Sayed, E.T.; Abdelkareem, M.A.; Olabi, A.G.; Rezk, H., (2021). *'Optimal selection and management of hybrid renewable energy system: Neom city as a case study',* 244, 114434.

[346]Liu, Y.; Sun, Q.; Li, W.; Adair, K.R.; Li, J.; Sun, X., (2017). *'A comprehensive review on recent progress in aluminum–air batteries',* 3, 246-277.

[347] Ghahari, M.; Rashid-Nadimi, S.; Bemana, H., (2019*). 'Metal-air desalination battery: Concurrent energy generation and water desalination',* 412, 197-203.

[348] Srimuk, P.; Wang, L.; Budak, Ö. Presser, V., (2020). *'High-performance ion removal via zinc–air desalination',* 115, 106713.

[349] Clark, S.; Latz, A.; Horstmann, B., (2018). *'A review of model-based design tools for metal-air batteries',* 4(1), 5.

[350] Sun, Y., Liu, X., Jiang, Y., Li, J., Ding, J., Hu, W., & Zhong, C. (2019). '*Recent advances and challenges in divalent and multivalent metal electrodes for metal–air batteries'.* Journal of Materials Chemistry A, 7(31), 18183-18208.

[351] Wei, W., Xu, Y., Huang, J., & Zhu, J. (2019). *'Review of the application of metal-air battery principlein water treatment'.* In E3S Web of Conferences 136, 06035, EDP Sciences.

[352] Monroe, C. W. (2017). '*Does oxygen transport affect the cell voltages of metal/air batteries?*'. Journal of The Electrochemical Society, 164(11), E3547.